Branched silica precursors as additives for mineral bone cements

Verzweigte Silica-Vorläufer als Additive für mineralische Knochenzemente

Doctoral thesis for a natural science doctoral degree
at the Graduate School of Life Sciences
Julius-Maximilians-Universität Würzburg
Section Biomedicine

submitted by

Ib Holzmeister
from
Dorfprozelten

Würzburg 2022

Submitted on: …………………………………………………

Office stamp

Members of the Thesis Committee:

Chairperson: Prof. Dr. Christoph Sotriffer

Primary-Supervisor: Prof. Dr. Uwe Gbureck

Supervisor (Second): Prof. Dr. Jürgen Groll

Supervisor (Third): Prof. Dr. Torsten Blunk

Date of Public Defence: ………………………………………

Date of Receipt of Certificates: ……………………………………..

„Perfect is the enemy of good“

- Voltaire

Die vorliegende Arbeit wurde in der Abteilung für Funktionswerkstoffe der Medizin und Zahnheilkunde, Universitätsklinikum Würzburg, Deutschland in der Zeit von Juli 2017 bis Dezember 2021 unter der Leitung von Herrn Prof. Dr. Uwe Gbureck angefertigt.

Affidavit

I hereby confirm that my thesis entitled „**Branched silica precursors as additives for mineral bone cements**“ is the result of my own work. I did not receive any help or support from commercial consultants. All sources and/ or materials applied are listed and specified in the thesis.

Furthermore, I confirm that this thesis has not yet been submitted as part of another examination process neither in identical nor in similar form.

………………………….	………………………
Place, Date	Signature

Eidesstattliche Erklärung

Hiermit erkläre ich an Eides statt, die Dissertation „**Branched silica precursors as additives for mineral bone cements**“ eigenständig, d. h. insbesondere selbständig und ohne Hilfe eines kommerziellen Promotionsberaters, angefertigt und keine anderen als die von mir angegebenen Quellen und Hilfsmittel verwendet zu haben.

Ich erkläre außerdem, dass die Dissertation weder in gleicher noch in ähnlicher Form bereits in einem anderen Prüfungsverfahren vorgelegen hat.

………………………….	………………………
Ort, Datum	Unterschrift

Content

Abbreviations

3D	Three-dimensional
ACP	Amorphous calcium phosphate
ATR	Attenuated total reflection
Bag	Baghdadite
BCB	Brushite cement-baghdadite
BMCs	Bone marrow derived stromal cells
C2S	Dicalcium silicate (belite)
C3S	Tricalcium silicate (alite)
CaP	Calcium phosphates
CDHA	Calcium-deficient hydroxyapatite
CPC	Calcium phosphate cements
CSH	Calcium silicate hydrate
CT	Computed tomography
DAPI	4′,6-diamidino-2-phenylindole
DCPA	Dicalcium phosphate anhydride (monetite)
DCPD	Dicalcium phosphate dihydrate (brushite)
DTA	Differential thermal analysis
DXP	Dexamethasone disodium phosphate
e.g.	Exempli gratia (Latin) = for example.
EDX	Energy dispersive X-ray spectroscopy
Eq	Equation
et al.	Et alii (latin) = and others
FT-IR	Fourier Transform Infrared Spectroscopy
HA	Hydroxyapatite
hASC	Human adipose tissue-derived stromal cells
HEMA	2-hydroxyethyl methacrylate

HOB	Human Osteoblas
ICDD-PDF	International Centre for Diffraction Data Powder Diffraction File
ICP-MS	Inductively coupled plasma mass spectrometry
IP6	Inositol hexakiphosphate (phytic acid)
MAC	Mass attenuation coefficient
MCPA	Monocalcium phosphate anhydrate
MCPM	Monocalcium phosphate monohydrate
MG63	Human osteoblast-like cells
nBGs	Bioactive glass nanoparticles
NCO	Isocyanate
NMR	Nuclear magnetic resonance
OCP	Octacalcium phosphate
PBS	Phosphate buffered saline
PBS	Phosphate buffered saline
PCL	Polycaprolactone
PLGA	Poly (lactic-co-glycolic acid
PLR	Powder to liquid ratio
PMMA	Polymethyl methacrylate
RT	Room temperature
SBF	Simulated body fluid
SD	Standard deviation
SEM	Scanning electron microscopy
TEOS	Tetraethyl orthosilicate
TG	Thermogravimetry
TMOS	Tetramethoxyorthosilicate
TTCP	Tetracalcium phosphate
Vs	versus
wof	Work of fracture

XRD	X-ray diffraction
α-TCP	α-Tricalcium phosphate
β-TCP	β-Tricalcium phosphate

Chapter 1

Introduction

Bone is an amazing tissue with extraordinary mechanical properties and the ability to heal without scar formation. The biomechanical properties of bone are a result of its composition and architecture, where collagen fibrils mineralized with hydroxyapatite nanocrystals are arranged in a highly ordered manner on different size levels [1]. Bone is highly vital and permanently remodeled by the simultaneous activity of bone resorbing osteoclasts and bone forming osteoblasts [2, 3]. This lifelong remodeling plays a crucial role in healing microcracks in bone, which may otherwise act as starting points of larger fractures following a mechanical loading [4]. However, if larger defects exceeding a size of approx. 10 mm are present in bone (e.g. caused by trauma or disease), the healing mechanisms fails due to the slow growing nature of the tissue [5]. Here, it is important to fill such defects with a space holder to prevent fibrous tissue ingrowth and to allow bone regeneration. Autologous bone grafting remains clinically the "gold standard" for such a treatment of bone defects in terms of restoration of the osseous structure, ranging in extent from a few cm^3 of cancellous bone chips (often harvested from the iliac crest) [6], up to 15-20 cm long anastomosed fibular grafts for mandibular restoration [7]. However, due to the limited access to autologous bone grafts, alternative synthetic bone substitutes have captured increasing attention and are usually indicated for smaller defects in the absence of autologous donor bone. Here, calcium phosphates (CaP) such as hydroxyapatite or tricalcium phosphate in the form of granules, blocks, or self-setting mineral bone cements represent the vast majority of commercially available bone graft substitutes, justified by decades of clinical experience and demonstrating connective tissue-free attachment of hard tissue to these compounds [8]. The materials are usually porous in design, with macropores >100-500 µm serving for bone cell and blood vessel ingrowth, and micropores <10 µm responsible for ion exchange with the physiological electrolyte. For most calcium phosphates, this usually results in an infiltration of the porous structure by bone tissue and the formation of an osteoceramic regenerate tissue from the osteconductive calcium phosphate structure and the sprouted tissue. A complete osseous regeneration requires quantitative degradation of the biomaterial, which can occur either passively by chemical dissolution or based on cellular mechanisms due to the activity of acid-producing osteoclasts as well as particle uptaking macrophages [3, 9]. Here, the solubility product of the calcium phosphate phases is crucial: while secondary phosphates such as brushite ($CaHPO_4 \cdot 2H_2O$) or monetite ($CaHPO_4$) are soluble at about 40-80 mg/l to the extent that both processes can contribute to material degradation [10], tertiary CaPs such as hydroxyapatite or tricalcium phosphate are less soluble at 0.2-5 mg/l, which is below the concentration of Ca^{2+} and HPO_4^{2-} present in the electrolyte. Due to this supersaturation, such compounds can practically only be degraded by cellular mechanisms. Even here, processing conditions of calcium phosphates with further influence their degradation potential: sintered hydroxyapatite is practically insoluble under *in vivo* conditions due to the microcrystalline texture, such that even after years the implant is still present leading to the above mentioned osteoceramic regenerate [11]. The process of material degradation is accelerated by using low-temperature nanocrystalline HA prepared by a precipitation reaction. Such nanocrystals are somewhere similar to the bone mineral in terms of material parameters such as specific surface area, crystal structure and solubility.

However, even with a similar structure and composition to native bone mineral, such crystals are not directly used as a building blocks for newly formed hard tissue after implantation, but must be - similar to other materials - primarily be degraded by the processes described above. The extent to which the calcium and phosphate ions released during degradation of the material are directly involved in the formation of new bone mineral has not been conclusively determined. Studies by Den Hollander et al. [12] using ^{45}Ca labeled β-tricalcium phosphate and hydroxyapatite revealed that the Ca^{2+} ions released from the implant are used only in trace amounts to build up the new bone mineral. Instead, the authors concluded that after dissolution, the ions are distributed in the extracellular body fluid and excreted via calcium metabolism. Following this mechanism, a synthetic bone substitute does not necessarily have to be based on calcium phosphate minerals to show good bone healing in the defect. Rather, moderate degradation of the material is of great importance, which should occur slowly enough to prevent ingrowth of connective tissue, while at the same time the surface of the ceramic provides a good osteoconductive substrate for the growth of bone-forming osteoblasts. In case of an overfalling hydrolytic degradation as in the case of calcium sulfate dihydrate (gypsum), this is however counterproductive and leads to dissolution of the implant, often associated with ingrowth of connective tissue into the defect and the absence of a quantitative bone regeneration [13, 14]. Possible alternative materials for bone replacement are magnesium phosphate minerals [15] or calcium magnesium silicates [16]. The latter would be advantageous for a further modification with bioactive metal ions (e.g. Cu^{2+}, Sr^{2+}, Cr^{3+}) to direct biological functions by bioinorganics [17] after *in vivo* release. Especially due to the lack of phosphate, there is no formation of poorly soluble phosphates of the doping ions, which would in turn result in only a low release tendency as known for calcium phosphates [18].

An improvement of the mechanical properties of bone replacement materials can be based on various intrinsic or extrinsic mechanisms [19]. Similar to high performance concretes from civil engineering applications [20], a minimization of cement porosity will result in a reinforcement of the implant due to the well-known inverse relationship between strength and total porosity of brittle materials [21]. This was demonstrated by a study of Barralet et al. [22], in which the authors demonstrated a strength improvement of a calcium phosphate biocement by a factor of three when reducing cement porosity from ~34% to ~16 % by using both sodium citrate as liquefier and a pre-compaction regime to remove parts of the cement liquid after paste formation [23]. A second reinforcement strategy uses polymeric fibers, which can bridge defects to prevent a catastrophic failure of the implant at low strain [24]. Although this works well for a large number of fiber – cement combinations, some further issues remain, e.g. the often non-degradable nature of the fiber as well as the difficulty to apply such fiber – cement composites by minimal invasive techniques.

More recently, an alternative approach to reduce the brittleness of biocements has been shown by pioneering works of DosSantos et al. [25] and Christel et al. [26]. Here, a hydrogel matrix is initially formed within the cement paste by polymerization of 2-hydroxyethyl methacrylate (HEMA) dissolved in the cement liquid. Afterwards, the cement setting reaction subsequently mineralizes this gel with hydroxyapatite nanocrystals formed by the hydrolysis of α-tricalcium phosphate. This not only resulted in an increase of the bending strength at a HEMA content of 50 wt.%, but also increased the work of fracture by an order of magnitude. This concept of dual-setting cements was further explored by others, whereas hydrogel formation can be achieved by cross-linking of water soluble isocyanates [27], pH induced gelation of silk fibroin solution [28] or a controlled condensation of silica gels during cement setting [29].

Building on these preliminary works on dual-setting silica-brushite cements, the current thesis aimed to further improve the mechanical properties of silica modified biocements. It is hypothesized that using a silicate based cement matrix will help to improve bonding between the silica gel and cement. Here, the bioceramic baghdadite was chosen, whose biocompatibility and osteogenic regeneration capacity are already known. In a first step, this requires to convert baghdadite ceramics into self-setting cement formulations. This was investigated in a first approach by subsequently replacing the β-TCP component in a brushite cement by baghdadite. In a second step, baghdadite was mechanically activated by prolonged grinding in order to completely eliminate the phosphate component, such that a cement reaction will take place only by using baghdadite powder without further cement ingredients. It is further hypothesized that the use of multi-arm silica precursors should result in a higher crosslinking density of the silica matrix with improved mechanical performance, as well as smaller pore sizes. The latter would be of interest, for example, with regard to a delayed release profile of incorporated drugs. After synthesis of hydrophilic silica precursors by coupling multivalent alcohols such as ethylene glycol, glycerol or pentaerythrit with an NCO-modified silica precursor, these modified silica matrices were combined with baghdadite cement to demonstrate the principal feasibility of this approach.

Chapter 2

State of the art

Parts of the section 2.3 are reused from the review article I. Holzmeister[1], M. Schamel[1], J. Groll, U. Gbureck, E. Vorndran Artificial inorganic biohybrids: The functional combination of microorganisms and cells with inorganic materials Acta Biomaterialia 2018, 74, 17-35.

[1] Equal first authorship.

2.1 Mineral bone cements

Traditional bone cements are usually based on polymethyl methacrylate (PMMA), whereas the term “cement” for this material class is somewhere misleading as it does not set via a typical cement setting reaction. PMMA is a polymer of organic methyl methacrylate monomer units and it is named as cement due to the mixing process of MMA monomer with PMMA particles forming a kneadable or injectable paste. Although PMMA cements have very good mechanical properties and are therefore used in knee or hip replacement surgery, major disadvantages are related to their strong exothermic setting reaction, release of unreacted monomer and their non-biodegradable nature [30, 31]. In comparison, mineral bone cements have the possibility of being degraded and replaced by an ingrowth of newly formed bone tissue, whereas the degradation kinetics of such mineral cements strongly depend on various parameters such as chemical composition, total porosity and pore size distribution [10, 32]. Mineral bone cements can have a wide variety of chemical compositions depending on the raw materials used, e.g. calcium phosphate [33, 34], magnesium phosphate [15, 35], calcium sulfate [36, 37], calcium silicate [38, 39], or mixtures thereof [40].

When developing and improving bone cements, some material criteria must be considered. The setting time of such cements must be adapted such that they can be used in clinical applications within a reasonable time frame (5-15 min) and neither set too quickly during surgery (which may inhibit a transfer of the paste into the defect), nor too slow which can lead to a paste disintegration and subsequent particle release into the surrounding tissue. In addition, it is important that no strong exothermic reaction takes place during setting, as this increased temperature may damage adjacent tissues and cause tissue necrosis. The mechanical properties must be sufficient to ensure clinical handling and should be at least in the range of trabecular bone after setting even for non-load bearing defects [41]. When implanting bone cements in the patient, it is important to ensure that there is a good connection to bone (osteoconductivity) and that bone in-growth can occur. This prevents an initial loosening of the bone graft, what would lead in any case to a crucial failure. Following degradation of the cement implant, the formation of new bone will then result in a complete defect regeneration. A further requirement is to some extend radiopacity of the material to allow monitoring of the implant after surgery by non-invasive X-ray radiography.

These criteria can be used to evaluate existing and new cement systems, e.g. to determine which characteristics still need to be improved and in which areas the material already has sufficient properties for an application. The necessary criteria can also vary depending on the application site, e.g. non-load bearing sites in craniomaxillofacial areas will have different mechanical requirements compared to partial load bearing application in vertebroplasty or kyphoplasty [42]. The design of new bone cements can be done in many ways. It depends mostly on the material composition itself, but also by varying the particle size distribution of the cement raw powder, cement properties such as solubility, reactivity, setting times and strength can be modified. Furthermore, it also depends on processing parameters for the cement paste, e.g. the ratio in which the powder is mixed with the liquid (PLR) or the modification with further cement additives to adjust paste rheology [43] or setting time. Composites can also be used to handle with the requirements for a certain application. Here, as an example the mechanical properties of mineral bone cements can be vastly improved by the addition of fibers [44] or creating dual-setting cement systems, whereas a dissolved monomer is polymerized during setting to obtain a hydrogel, which is then subsequently mineralized due to the cement setting reaction [19]. Such approaches not necessarily improve the overall strength of the hardened cement, but more importantly reduce their brittle fracture behavior. This leads to a highly improved work of fracture (wof) for such cement composites, which opens the way for an application under somewhere load-bearing conditions. This also enables completely new properties, e.g. a self-healing capacity of the cement matrix [45]. Here, surface modified fibers have been shown to bridge opened cracks, while the release of phosphate ions from embedded capsules resulted in a subsequent remineralization and closing of the crack.

2.1.1 Calcium phosphate cements

Calcium orthophosphate minerals

In the early 20th century, especially the work of F.K.Cameron and H. Bassett brought fundamental knowledge about these CP compounds.[46-53] All calcium orthophosphates consist of the elements calcium, phosphorus and oxygen and in combination they occur in the oxidation states Ca = +2, P = +5 and O= -2.[54] Crystalline calcium phosphate minerals are of white color in the absence of other metal ion impurities and have medium hardness. The color changes when the minerals are impure, e.g. by doping with rare earth elements in naturally occurring calcium orthophosphates.[55, 56]

Formulations without ion substitution are the best studied, and for calcium orthophosphate compounds eleven different ones are known to have Ca/P molar ratios in the range of 0.5 to 2.0. All are obtained from orthophosphoric acid H_3PO_4 by subsequent replacement of hydrogen ions by calcium forming three different groups of primary, secondary and tertiary phosphate salts. They differ significantly in terms of their solubility and the pH value that occurs in the equilibrium of dissociation. With higher Ca/P ratios, basicity increases and water solubility decreases. [57, 58] Primary calcium phosphates, for example, have a good solubility in water of about 17 g/l, whereas secondary calcium phosphates have a solubility of only about 40-80 mg/l. These include compounds such as brushite and monetite. With complete phosphoric acid dissociation, tertiary calcium phosphates are formed which have the worst solubility in comparison with each other with less than 0.2 mg/l. The solubility of the calcium phosphate compounds varies by several orders of magnitude depending on the pH of the solution with a strong increase of solubility in the acidic region. The dissociation constants of phosphoric acid and calcium hydroxide form the basis for the calculation of the solubility isotherms. In addition, the stability constants and activation coefficients of the ions involved have an influence from this and must be taken into account for the calculation. Selected isotherms are displayed in **Figure 1**. The mineral phase of bones and teeth consists mainly of hydroxyapatites, as this is the least soluble calcium phosphate in the non-acidic pH range. The solubility of hydroxyapatite is increased in acidic conditions, which is mechanistically the basis how osteoclasts lead to bone resorption and are also able to degrade CaP materials by locally lowering the pH. Calcium phosphates which are least soluble at low pH values < 4.2 are brushite and monetite.

Primary monocalcium phosphate monohydrate (MCPM, $Ca(H_2PO_4)_2 \cdot H_2O$) is soluble in water and acidic and is therefore not found in calcified tissues. As such, MCPM is not biocompatible, but is used for CaP cements as a starting material.[59-63] With thermal treatment of MCPM above 100°C, crystal water can be removed to obtain the anhydride monocalcium phosphate anhydrous (MCPA, $Ca(H_2PO_4)_2$). Chemical and biological properties are mainly the same as for MCPM and both compounds can be used mostly by proxy.[64] In contrast, a material of important biological significance is dicalcium phosphate dihydrate, (brushite, DCPD, $CaHPO_4 \cdot 2H_2O$), which crystallizes from aqueous solutions at $pH < 6.5$. These acidic conditions can be generated by different reactants such as MCPM or phosphoric acid, which is shown in Eq. 1 and Eq. 2. *In vivo*, brushite occurs as pathological calcification or carious lesions and is therefore particularly interesting as a biomaterial. It is used in biomedicine in calcium orthophosphate cements for bones replacement.[57, 60, 65-71] DCPD can also rearrange into the corresponding anhydride monetite (DCPA, $CaHPO_4$). This material is more insoluble in aqueous environments than DCPD due to the lack of water intercalation. DPCA can be obtained under the same conditions as DCPD by precipitation from aqueous solution, except that the temperature must be elevated to 100°C. Monetite is also used for the fabrication of calcium phosphate cements. [70, 72-76]

$$\beta\text{-}Ca_3(PO_4)_2 + Ca(H_2PO_4)_2 \cdot H_2O + 7\ H_2O \rightarrow 4\ CaHPO_4 \cdot 2\ H_2O \qquad \text{Eq. 1}$$

$$\beta\text{-}Ca_3(PO_4)_2 + H_3PO_4 + 6\ H_2O \rightarrow 3\ CaHPO_4 \cdot 2\ H_2O \qquad \text{Eq. 2}$$

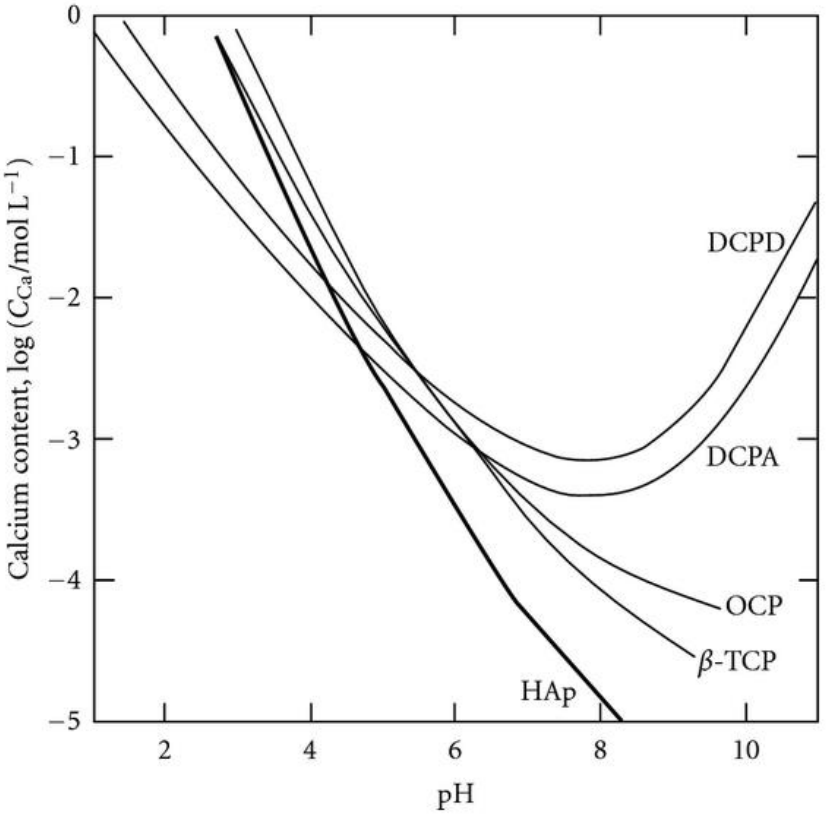

Figure 1: Solubility phase diagram of different calcium orthophosphates at 37°C, depending on pH in aqueous solution. HAp: hydroxyapatite ($Ca_{10}(PO_4)_6(OH)_2$), TCP: calcium phosphate ($Ca_3(PO_4)_2$), OCP: octacalcium phosphate ($Ca_8H_2(PO_4)_6$ $5H_2O$), DCPA: dicalcium phosphate anhydrous ($CaHPO_4$), DCPD: dicalcium phosphate dihydrate ($CaHPO_4$ $2H_2O$). Reprinted from [77] with permission Copy-right (2012), K. Kuroda and M. Okido.

Tricalcium phosphate ($Ca_3(PO_4)_2$) can exist in two different crystalline variants. A distinction is made between α-TCP and β-TCP, where α-TCP is the high temperature phase and is obtained from β-TCP by thermal treatment above 1125°C. Despite having the same chemical compositions, they differ in their crystal structure and solubility. As a result, β-TCP is more stable and has inferior solubility in aqueous systems.[78] α-TCP, on the other hand, is more reactive due to its higher specific energy and hydrolyzes faster when dissolved in aqueous solutions. Both variants do not occur in pure form in biological calcification but still find application in medicine. Because of their good reactivity, α-TCP and β-TCP are used as starting materials for calcium phosphate cements.[60, 68-71, 74, 76, 79, 80] For example, in biomedicine β-TCP is used for calcium orthophosphate bone cements [81-84] or together with hydroxyapatite (HA) for sintered biphasic calcium phosphates [85-94]. Monoclinic tetracalcium phosphate (hilgenstockit, TTCP, $Ca_4(PO_4)_2O$) is formed in the ($CaO–P_2O_5$) system at temperatures >1300°C, whereas it is the only calcium phosphate with a Ca/P ratio greater than hydroxyapatite (HA) [95]. TTCP is therefore a common raw material for calcium phosphate cements in combination with secondary phosphates such as monetite or brushite according to Eq. 3 .

HA has the chemical formula $Ca_5(PO_4)_3(OH)$ and is one of the compounds with the lowest solubility and highest stability among the calcium orthophosphates.[96] This compound can be made by precipitation from aqueous solution to obtain nanocrystalline HA crystals or by solid state synthesis similar to TTCP or TCP from monetite – calcium carbonate mixtures. Calcium-deficient HA can be prepared via a single component system according to Eq. 4 by hydrolysis of α-TCP.

$$Ca_4(PO_4)_2O + CaHPO_4 \rightarrow Ca_5(PO_4)_3OH \qquad \text{Eq. 3}$$

$$3\ \alpha\text{-}Ca_3(PO_4)_2 + H_2O \rightarrow Ca_9(PO_4)_5(HPO_4)(OH) \qquad \text{Eq. 4}$$

Setting reaction of calcium phosphate cements

Calcium phosphate cements were firstly reported by Kingery (1950) [97], later LeGeros 1982 [98] described their use for orthopedic and dental applications and these cements were then developed further by Brown and Chow [99] and subsequently several others, such that today there are several products licensed for use in the body with some more in clinical trials. Essentially there are two types of cement, which can be classified according to their products, namely apatite, and brushite, which is a more soluble hydrated dicalcium phosphate. The nanocrystalline structure of such cements enables resorption by either cellular mechanisms (hydroxyapatite) or simple dissolution (brushite).

The thermodynamic driving force for a cement setting reaction is the different solubility of cement raw material and the setting product. The reaction is a continuous solution-precipitation reaction, in which the reactants partially dissolve in the cement liquid forming a supersaturated solution with respect to the setting product. The latter precipitates from the solution and hardening of the pastes occurs by an entanglement of such crystals within the narrow space of the cement implant. The type of product which is formed is determined by the pH of the paste as well as the stoichiometry of the raw powder. Usually, hydroxyapatite is formed at neutral or alkaline pH conditions, whereas acidic conditions result in the formation of brushite or monetite as these have the highest stability at low pH. Despite the fact that monetite is actually less soluble than brushite, the latter is often the setting product, since it has a faster crystal growth rate than monetite. However, at either highly acidic conditions, elevated temperature or a high ionic strength (e.g. by the addition of NaCl), monetite is precipitated in CPC [100]. In some cases octacalcium phosphate can be obtained under neutral conditions, if setting regulators like carbonic acids are added to the cement paste [101].

The reactivity of calcium phosphates in cements and the setting speed depends on several factors. The thermodynamic solubility (solubility product) of cement reactants determines the degree of supersaturation of the cement liquid with respect to the reaction product. In practice, the degree of supersaturation has to reach about several times the solubility product of HA before the nucleation and crystal growth will start. This explains, why for example crystalline β-TCP will not form a setting cement system because the lower solubility compared to α-TCP does not form a sufficient supersaturated environment for HA precipitation. The solubility product is a material constant for crystalline compounds, however it can be increased by high energy ball milling of the materials due to a mechanically induced amorphization as demonstrated for various calcium phosphate compounds [102-104].

Factors influencing the speed of reaction of CPC are both the kinetic solubility (rate of dissolution) of cement reactants and the crystal growth rate of the reaction product. The rate of dissolution depends on the specific surface area of cement particles, which is usually adjusted by dry or wet ball-milling of the materials [105]. Multicomponent powder mixtures require a congruent dissolution of all components for a setting reaction, such that precise particle sizes must be prepared by grinding. For example, the cement reaction according to Eq. 4 requires an aspect ratio d_{50}(TTCP) : d_{50}(DCPA) of about 10 : 1 to obtain a mostly similar rate of dissolution of both compounds and a setting cement system [106]. A further parameter which controls the speed of reaction is related to the crystal growth rate of the reaction product; while hydroxyapatite is a slowly growing system (2.7 x 10-7 mol $Ca_5(PO_4)_3OH$ $min^{-1}m^{-2}$ [107]) which usually requires setting accelerators (Na-phosphates or H_3PO_4) to adjust clinically required setting times, brushite crystals grow at a rate of two orders of magnitude higher (3.32 x 10-4 mol DCPD $min^{-1}m^{-2}$ [108]). This makes clear why brushite cements set often fast and need setting retarders (e.g. phytic acid or citrates [109, 110]) for clinically acceptable setting times.

2.1.2 Magnesium phosphate cements

The setting reaction for the formation of magnesium phosphate cements is somewhere similar to that of calcium phosphate cements. It is based on the principle of dissolution of raw materials in the cement liquid followed by a subsequent precipitation of the setting product. The precipitation causes growth of magnesium phosphate crystals, which interlock and thus advance the setting process.[111] Suitable reactants for the magnesium source are magnesium oxide (MgO), trimagnesium phosphate (farringtonite, $Mg_3(PO_4)_2$) and magnesium hydroxide ($Mg(OH)_2$).[112-124] These crystalline reactants can react together with phosphate-containing reactants to form a variety of magnesium phosphate cements. Useful compounds are diammonium hydrogen phosphate ($(NH_4)_2HPO_4$), ammonium dihydrogen phosphate ($NH_4H_2PO_4$), sodium dihydrogen phosphate (NaH_2PO_4), potassium dihydrogen phosphate (KH_2PO_4) or phosphoric acid (H_3PO_4). [112-126] The phosphate reactants can be added either to the solid phase or can be dissolved in the cement liquid. The latter has the advantage that there is little effect of PLR on strength and porosity, since phosphate and water are mostly consumed during the reaction.

Magnesium ammonium phosphate hexahydrate (struvite, NH_4MgPO_4-$6H_2O$) has the lowest solubility at near neutral pH and is therefore preferentially formed during the setting reaction in the system Mg^{2+} - NH^{4+} - PO_4^{3-} [111, 114-124, 127, 128]. Other compounds that can be formed are dittmarite (NH_4MgPO_4-H_2O) [127], schertelite ($(NH_4)_2Mg(HPO_4)_2$-$4H_2O$) [114, 116, 117], and more rarely hannayite ($(NH_4)_2Mg_3(HPO_4)_4$-$8H_2O$)[113, 127]. In many studies, it was observed in the course of the reaction that these phases appear as intermediate products in the reaction to struvite or the phases were further transformed in the process depending on the parameters applied. [128-131] The complex interrelationship of these different phases and how they transform into each other with the corresponding parameters is shown in **Figure 2**. Since potassium ions have in similar ionic radius as ammonium ions, the latter can be substituted in the crystal lattice to form K-struvite cements ($KMgPO_4$-$6H_2O$).[112, 125, 126, 132]

In general, the setting process of magnesium phosphate cements proceeds in a short time frame, with a good manageability of the paste until solidification. The setting kinetics can be influenced and adjusted by various parameters. Composition and stoichiometry of reaction raw materials as well as the PLR and the composition of the setting solution are known to be rate determining parameters during setting. According to Ostrowski et al [133], the rate determining step is the dissociation of the crystalline reactants. For better reactivity, the magnesium powders can be treated with high temperature before the reaction.

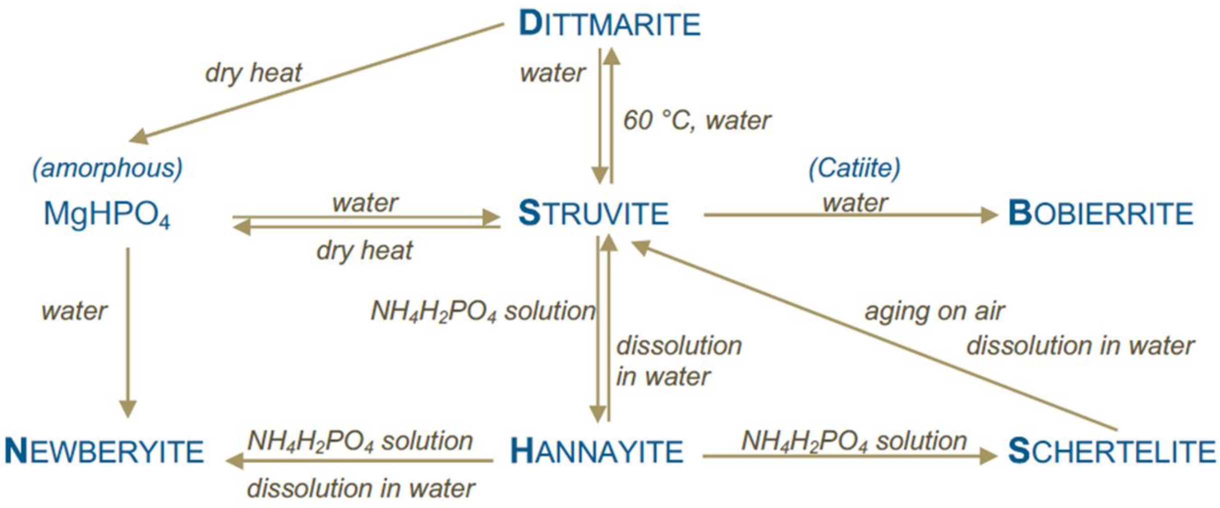

Figure 2: The correlation of the different magnesium phosphates and how they can be converted into each other with the relevant parameters. Reprinted from [15] with permission.

As with previous cement systems, various magnesium phosphates are suitable as biomaterials for bone replacement and regeneration. MgP cements generally set quite fast and achieve strengths that are higher than calcium phosphate cements [112, 114, 116, 117, 132, 134-138] Magnesium phosphate cements have been shown to initially bridge critical bone defects in rabbits, with complete bone regeneration and biodegradation of the implant after 6 months.[139] With nano-magnesium phosphates, a bridging with newly formed bone of over 85% can be observed even in such defects after only 3 months.[140] Due to the degradation of the material, further surgical interventions can be dispensed, which completely prevents unnecessary risks. In addition, Mg^{2+} ions are released, which have been shown to have a positive effect on osteogenesis and bone regeneration.[141-146] The ingrowth of new bone is also favored by the porous structure of about 10%.[117, 147] All this leads to a good bond between implant and bone.

These advantages can be used in combination with calcium phosphate cements. Composites showed improved bone regeneration compared to pure calcium phosphates [115] because of the above mentioned points such as faster degradation and the stimulating influence of the ions on osteogenesis.[148]

2.1.3 Calcium(magnesium)silicates

As already described in section 2.1.1 calcium phosphate cements are an essential component as biomaterial for bone replacement tissue as they have a similar mineral structure as bone tissue. An approach to enhance the biological performance of CPC is doping with bioactive metal ions such as Sr^{2+}, Zn^{2+}, Si^{4+} or Cu^{2+}.[17] During the degradation of implants, the resulting ions have an influence on biological behavior. The effect of the ions Si^{4+}, Mg^{2+}, Zr^{4+} and Ca^{2+} in the body is shown in **Figure 3**.

For a higher silicon content in self-setting cements, calcium silicates were investigated in addition to calcium phosphates. Known representatives for this class are dicalcium silicate (Ca_2SiO_4)[149, 150] and tricalcium silicate [150, 151] both of which are the major components in civil engineering Portland cement. It is known that hydraulic reactivity emanates from these compounds due to hydration of silicate ions, resulting in strength enhancement and the formation of calcium silicate hydrate gel with nanoporous character.[152-154] This is one reason why these materials are considered to be suitable for drug release. Studies have observed a long release profile for gentamicin, although other drugs are also conceivable.[149, 155]Tricalcium silicate paste is injectable and thus can be used in a minimally invasive manner. Bioactive properties have been demonstrated for the hydration product.[149, 151, 156]Other calcium silicate materials such as pseudo wollastonite ($CaSiO_3$) [157-160] and calcium silicate gel (CSH) [161] have been investigated as well as compounds with additional doping elements such as strontium and magnesium.[162, 163]

The class of calcium magnesium silicates includes several materials that have been well studied. The first representative is Bredigite with a chemical composition of $Ca_7MgSi_4O_{16}$. As already postulated for silicon containing materials, this material was shown *in vitro* to enhance osteoblast proliferation by dissolution into the ionic components at concentrations in the range of 6.25-50 mg/ml. Concentrations above 100 mg/ml had the opposite effect.[164, 165] Scaffolds of bredigite are more suitable for proliferation of osteoblast-like cells compared to β-TCP after coating with an apatite layer by precipitation into SBF. The differentiation level was higher and a better proliferation rate was observed.[166] An antibacterial effect may be exerted by bredigite when it is present in appropriate doses at elevated pH values of aqueous solution.[167]

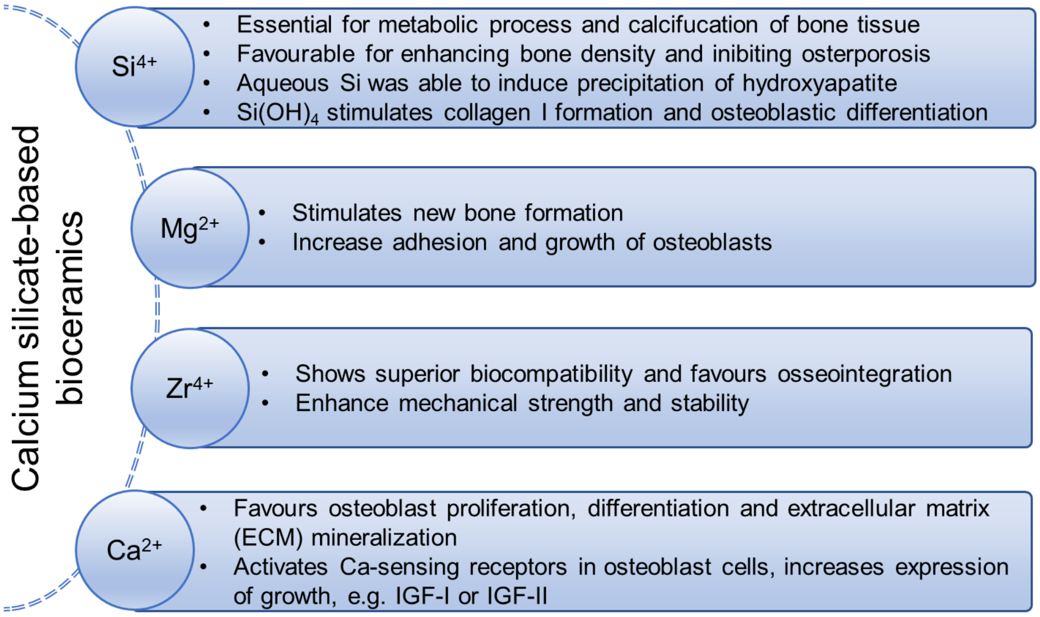

Figure 3: Effects of Si^{4+}, Mg^{2+}, Zr^{4+} and Ca^{2+} ions of dissolved calcium silicate implants on biological response, adapted from [168] with copyright permission.

Diopside ($CaMgSi_2O_6$) also exhibits good bioactivity.[169-171] It has a very low degradation rate and can generate a direct bond between scaffold and bone.[170, 172-175] Because of these properties, diopside has been investigated as a coating because it is a good bonding ability between the substrate and bone.[176, 177] Advantages such as deposition of apatite on diopside are as relevant [169, 178-180], as antibacterial activity and good osteogenic differentiation.[181, 182] The material is also suitable for drug release. This was investigated by Wu et al. with porous diopside microspheres and dexamethasone. PLGA modification of the microspheres changed their porosity, resulting in controlled release of the drug. [183]

Merwinite has the composition $Ca_3MgSi_2O_8$ and like the other calcium magnesium silicates is capable of forming apatite layers on the surface.[184, 185] The material is also bioactive and has the potential to be used for bone replacement, as *in vivo* studies have shown good bone regeneration for the Lewis rat femoral defect model. After 2 and 8 weeks of implantation, more new bone formation was observed in the defects treated with merwinite than in the defects treated with HA and the untreated defects. [186]

Akermanite ($Ca_2MgSi_2O_7$), like the other compounds in the same group, has good bioactive properties. Studies have observed increased cell proliferation in various cell types. The positive effect occurs in stem cells derived from human adipose tissue (hASC) [187, 188] as well as in bone marrow derived stromal cells (BMCs)[189, 190] and periodontal cells[191]. In these studies, β-TCP was used as the reference material. The superficial deposition of apatite layers enhances osteoblast proliferation. As a result, new bone can be formed within akermanite scaffolds.[192, 193] This osteoinducing property is supported by angiogenesis and akermanite scaffolds showed a better vascular ingrowth, as compared to β-TCP.[194]

Apatite can also be deposited on the surface of monticellite ($CaMgSiO_4$) by treatment with SBF. This layer leads to better conditions for osteoblasts, promoting an enhanced cell proliferation.[195] In general, the bioactivity of this material is similar to that of akermanite and bredigite .[195, 196]

Hardystonite with the formula $Ca_2ZnSi_2O_7$ has good chemical stability, and due to the zinc content, no affinity for apatite formation. This is a significant difference to the previously described calcium magnesium silicates. Nevertheless, hardystonite is biocompatible, and the Zn content in the material supports human bone osteoblast-like cell proliferation and differentiation. This was the conclusion of a study on Zn-containing Ca-Si system ceramics, in which the effecs of Zn additives (0%, 10%, 20%, 50%) to $CaSiO_3$ were investigated. At the highest level, a new crystal phase was formed: Hardystonite. [197] Another study verified the osteoconductivity of this material by treating tibial bone defects in rats with hardystonite and implanting the scaffolds for up to 6 weeks. After 3 and 6 weeks, the new bone formation was observed with histological staining.[198]

A summary of some important key properties of calcium silicate-based ceramics in comparison to cortical bone and cancellous bone as references are listed in **Table 1**.

Table 1: Mechanical properties, apatite mineralization, and dissolution behavior of calcium silicate-based bioceramics, adapted from [168] with copyright permission.

Compound	**Bending strength (MPa)**	**Bending strength (MPa)**	**Apatite Mineral-ization**	**Dissolution behavior**	**Ref.**
Wollastonite ($CaSiO_3$)	95.03 ± 7.1	<1.0	Excellent	Rapid	[199]
Diopside ($CaMgSi_2O_6$)	300	3.5	Moderate	Slow	[170, 200]
Akermanite ($Ca_2MgSi_2O_7$)	176.2 ± 9.8	1.83 ± 0.1	Good	Moderate	[201]
Bredigite ($Ca_7MgSi_4O_{16}$)	151.2 ± 5.7	1.57 ± 0.12	Excellent	Rapid	[164]
Merwinite ($Ca_3MgSi_2O_8$)	151.2 ± 5.7	1.72 ± 0.11	Good	Moderate	[196]
Monticellite ($CaMgSiO_4$)	159.7	1.63	Moderate	Slow	[195]
Hardystonite ($Ca_2ZnSi_2O_7$)	136.4 ± 3.9	1.24 ± 0.03	Poor	Very slow	[202, 203]
Baghdadite ($Ca_3ZrSi_2O_9$)	83-98	1.1-1.3	Moderate	Slow	[204]
Human cortical bone	50-150	2-12	N/A	N/A	[205-207]
Human cancellous bone	10-20	0.1-0.5	N/A	N/A	[206-208]

2.2 Baghdadite as bioceramic

Baghdadite ($Ca_3ZrSi_2O_9$) was discovered in Qala-Dizeh, Iraq, in 1986 as a naturally occurring mineral.[209] Other natural occurrences of the mineral were later found in Norway, Japan, and Russia.[210] It is a white solid material, has a monoclinic crystal system and is assigned to the $P2_1/c$ space group.[211] With the increasing interest in calcium silicates due to their potential use as biomaterials for bone replacement applications, baghdadite has also become a focus of research. *In vitro* tests have shown no cytotoxicity of baghdadite-based scaffolds to human bone osteosarcoma cells (Saos-2) and MG63 osteoblast cells.[212, 213] The material is cytocompatible and this has been demonstrated in studies using cultured baghdadite scaffolds with MG63 and bone marrow stem cells. In addition, even improved cell viability and proliferation was observed.[214, 215]

As a result, the material finds particular application as a bioceramic. After the first studies on promising and successful applications of baghdadite for bone regeneration were published [216], further *in vivo* studies on baghdadite tissue scaffold basis followed. Roohani et al [217] studied critical size bone defects in rabbits treated with porous Baghdadite scaffolds. Highly porous baghdadite scaffolds were used for the study with β-tricalcium phosphate/ hydroxyapatite (TCP/HA) scaffolds as the control group. To circumvent the brittleness of baghdadite, the scaffolds and reference scaffolds were coated with a thin layer (400 nm) of polycaprolactone (PCL)/bioactive glass nanoparticles (nBGs). Scaffolds measuring 4mm x 4mm x 15mm were implanted for 12 weeks into radial segmental defects in rabbits. As shown in the radiographic images of **Figure 4**, little new bone formation was detected for TCP/HA and coated TCP/HA. the baghdadite scaffolds had an exceptionally improved ingrowth of new bone. Both the uncoated specimens and the baghdadite scaffolds with PCL-nBG coating showed complete bridging of the defect after 12 weeks.

Baghdadite scaffolds were used in other studies to induce bone regeneration in tibial segmental defects of sheep.[218] No TCP/HA control group was used in this series of tests. The reference to the PCL-nBG coated baghdadite scaffolds was untreated baghdadite as hollow cylinders of 30mm length and 22mm diameter with a rim thickness of 6.5mm. After 26 weeks, complete bridging was observed for both baghdadite and baghdadite PCL-nBG. The new bone formation can be seen in **Figure 5**.

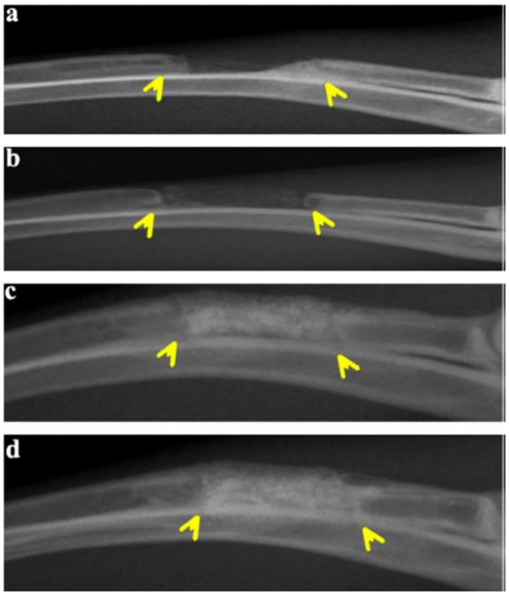

Figure 4: Radiographical images 12 weeks after implantation of a)TCP/HA, b)TCP/HA PCL-nBG, c)Baghdadite and d) Baghdadite PCL-nBG. Reprinted from [217] with permission.

In addition to these promising observations, the interaction of the material with the host tissue in the long term was also investigated. Li et al.[219] confirmed with their study the high bioactivity of baghdadite by implanting tubular baghdadite scaffolds into critical sized segmental bone defects in sheep tibia (3 cm) and their favorable *in vivo* interaction with bone tissue was demonstrated. Defect healing was observed long-term (26 weeks) and no chronic inflammation or fibrous capsule formation was detected. Bone regeneration was induced by the baghdadite scaffolds, and because of this ability to heal defects, the use of baghdadite as a new bone graft substitute is reasonable.

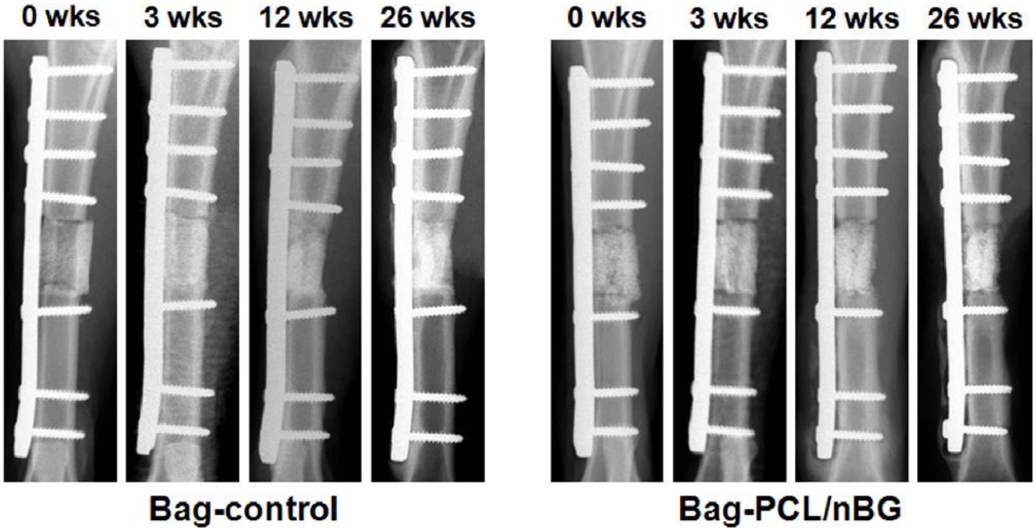

Figure 5: X-ray images over the duration of the *in vivo* experiment for baghdadite scaffolds (Bag-control, left) and coated baghdadite scaffolds (Bag-PCL/nBG, right). Reprinted from [218] with permission.

The drug release and antibacterial properties of baghdadite were studied on porous structures prepared by the sponge-elongated method. In the study, the antibacterial activity of vancomycin loaded baghdadite scaffolds against *Staphylococcus aureus* was demonstrated by Bakhsheshi-Rad et al.[213]. The *in vitro* release results showed that the samples released 45-75% of the drug after the first 36 hours immersed in PBS. In another study, baghdadite scaffold was loaded with dexamethasone disodium phosphate (DXP) as osteoinductive agent. The scaffolds were dialyzed against PBS (37°C, 126h) to simulate the release *in vitro*. For baghdadite scaffolds the release of 92 ±8 % DXP in 1h was observed. This bust release was then inhibited by modifying the material with gellan and xanthan hydrogel to achieve a sustained drug release for 5 days with a total release of 78±6%. Thereafter, a significant increase in osteogenic differentiation of MG63 cells on the baghdadite scaffold was observed due to the drug release.[220]

The bioactivity of baghdadite was already postulated in several studies [214, 215, 221, 222], but also the apatite binding ability of baghdadite is an *in vitro* indicator for the *in vivo* bioactivity of baghdadite. [204, 216, 223-225] The rate of apatite deposition and consequently bone regeneration must be in reasonable proportion to the biodegradation of the baghdadite implant to prevent implant failure.[226, 227] Methodologically, this is demonstrated by weight loss of specimens immersed in buffer solutions in a time-dependent manner. Various studies have demonstrated a high degradation rate of baghdadite scaffolds (~ 15% weight loss after 28 days).[214, 215] In one case, a weight loss of 51% was measured after 28 d of aging. [228] This rapid weight loss is in contradiction to the slower bone regeneration. To slow down the degradation, polymer coatings can be used. These modified scaffolds coated with poly(caprolactone fumarate) had about 91% less weight loss after 7 days.

Baghdadite is not only used as a scaffold, but can also be used in the form of microspheres for bone filling material. Luo et al.[229] implanted baghdadite spheres with the size of ~1mm diameter in Wistar rats femur defects for 4 weeks and a high rate of osteogenesis and new bone formation was achieved compared to materials such as β-TCP or Mg^{2+}-modified diopside. Another approach by No et al. [230] was the development of polycaprolactone PCL with baghdadite microspheres as an injectable composite material. The amount of baghdadite is limited to a maximum of 10% by volume, since a higher baghdadite content requires too high pressures during injection. In this process, an injection needle at 75°C is also required, and after extrusion the material has temperatures in the range of 55-60°C and solidifies after 2.5-

3.5 min. These composites result in higher compressive strength (26-47 MPa) and promote osteogenic expression compared to the reference material of pure PCL.

Since the polymer content has a great influence on the composite, in another approach by Pahlevanzadeh et al. [225] PCL was used together with PMMA as the polymer phase, to form bio-composite cements with a baghdadite filler content of 20-60% by weight. Many changes in the properties of the composites could be observed, e.g. the implementation of baghdadite results in an increased compressive strength and a larger E-modulus. A higher baghdadite content results not only in improved material properties, it also leads to an increased bioactivity, because after the incubation in SBF, noticeably more apatite was deposited on the surface than in cements without baghdadite content as shown in **Figure 6** .

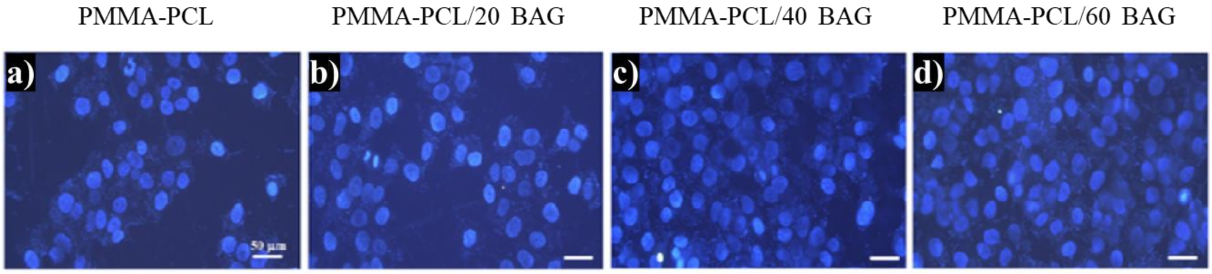

Figure 6: MG63 cells stained with DAPI on the cements containing various baghdadite content. Scale bars are 50µm. Reprinted from [225] with permission.

2.3 Sol-Gel-Processing of silica ceramics

The sol-gel synthesis allows the formation of materials from molecular precursors by subsequent hydrolysis and condensation of mainly silica alkoxides. Sol-gel-processing is an important tool to produce silica-cement composites. There are different approaches to transform the silica precursors into a sol that will crosslinks to a gel. A distinction is made between the alkoxide pathway and the aqueous pathway, which are described in more detail below.

2.3.1 Alkoxide pathway

For the alkoxide pathway, precursors of the form $Si(OR)_4$ are used, wherein R is preferably an alkyl group. The gold standard of this synthetic route is tetraethoxyorthosilicate (TEOS, $R = C_2H_5$) and tetramethoxyorthosilicate (TMOS, $R = CH_3$) as precursors [231-233]. The mechanism (Eq. 5, Eq. 6) for initiation of the sol-gel process is dependent on the prevailing pH, whereby both an acidic or basic pH are favoring hydrolysis of the alkoxide groups to form silanols (Si-OH) in the first step. Silanols are unstable and tend to form Si-O-Si bonds in a condensation reaction [233-235]. This condensation can take place by either the reaction of two silanol groups (dehydration) or by the reaction of the silanol with an alkoxide group (dealcoholation). As the reaction / condensation progresses, nanometer sized silica particles are initially formed, which further grow and finally interlink until a 3D network is formed [236]. For immobilization of microorganisms via such a system, the biological systems can be mixed into the pre-hydrolyzed precursor solution [233, 237]. The external conditions in this step are mild regarding pressure and temperature [236], however, great care must be taken to have control over pH and alcohol development, as this can have cytotoxic effects and proteins can be denatured [238, 239].

2.3.2 Aqueous pathway

As an alternative to the alkoxide pathway, there is also the option of using an aqueous route to produce silica matrices, which avoids the release of toxic alcohols by using sodium silicate as a precursor [236]. This route also takes place in two steps, whereas in a first step silanols are produced by acidifying a solution of sodium silicate (Eq. 7). A suitable acid is hydrochloric acid, whereby the resulting by-product is NaCl and a buffer can be used to control the pH [234]. Optionally, a cation exchanger may also be used to initiate the first reaction step [240-242]. In a second step (Eq. 8), the neutralized silanols react in a polycondensation reaction to form a 3D network analogous to the alkoxide synthesis route

$$\mathrm{Si(OR)_4 + n\ H_2O \rightarrow Si(OR)_{4-n}(OH)_n + n\ ROH} \qquad \text{Eq. 5}$$

$$\left.\begin{array}{l} \mathrm{X_3Si\text{-}OH} \\ \textit{or} \\ \mathrm{X_3Si\text{-}OR} \end{array}\right\} \mathrm{+ HO\text{-}SiX_3 \rightarrow X_3Si\text{-}O\text{-}SiX_3 + H_2O/ROH} \qquad \text{Eq. 6}$$

$$\mathrm{Si(O^-Na^+)_4 + 4\ HCl \rightarrow Si(OH)_4 + 4\ NaCl} \qquad \text{Eq. 7}$$

$$\mathrm{2\ Si(OH)_4 \rightarrow Si(OH)_3OSi(OH)_3 + H_2O} \qquad \text{Eq. 8}$$

2.3.3 Variation of precursors

The sol-gel process with TEOS or TMOS results in the formation of a SiO_2 network, in which ideally all silicon atoms are fourfold linked to other Si-atoms. However, it is also possible to use modified precursors, which contain at least one covalently bound spacer with functional moieties such as amines, carboxylic acids, thiols or oxiranes (**Figure 7**). In this way, properties of the 3D structures can be specifically changed and adjusted depending on the intended use. Siloxane derivatives with functional groups such as aminoalkyl and carboxyalkyl have great influence on ionic interactions by forming networks with either brittle, transparent or soft hydrogel-like properties, which can be used to immobilize biologicals, improve wettability, and extend biocompatibility [237, 243].

Alkyl and aryl siloxanes are capable of forming meso- and microporous glasses with the ability to adjust mechanical and optical properties over a broad range by varying precursor composition. Since hydrophobic properties and porosity are well controllable in such glasses, these materials are suitable as surface biosensors [244-246], stimulating matrixes for enzymes like lipases [247] and porous foam scaffolds for cells [237]. In contrast, hydroxyalkyl siloxanes are used for the synthesis of hydrophilic materials. These may have properties similar to soft hydrogels, which are particularly well suited for the immobilization of labile proteins and cells.

Modified siloxanes used in combination with the standard silica and silicate precursors can act as catalyst or redox systems. The resulting networks are transparent glasses, which have either semi-hard or a brittle fracture behavior. In particular, they are used in conjunction with biosensors and enzymes. Further research in this field could have much impact on the used sol-gel matrices and it remains interesting how siloxanes could be differently modified and used [237, 248, 249], e.g. by using branched precursors [250]. Surprisingly, most of the described precursor modifications are not yet applied for the encapsulation of microorganisms, although these would offer the possibility to adjust crucial properties (mechanics, optics, chemical resistance, surface properties) in a much broader range than pure TEOS.

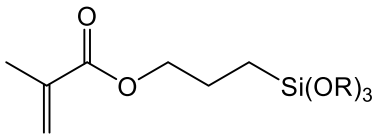

Methacryloxypropyl-[251]

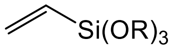

Vinyl-[252, 253]

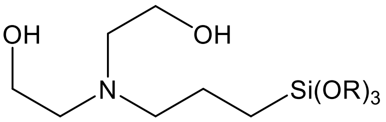

Bis(2-hydroxyethyl)-3-aminopropyl-[254]

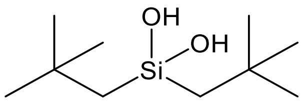

Di-isobutylsilanediol[251]

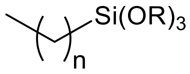

Alkyl-[237, 255, 256]

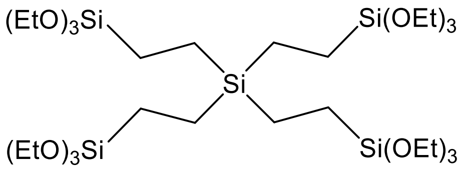

3,11-Dioxa-4,7,10-trisilatridecane, 4,4,10,10-tetraethoxy-7,7-bis[2-(triethoxysilyl)ethyl][250, 257]

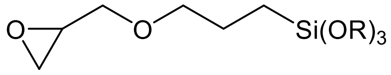

Gycidoxypropyl-[253, 255]

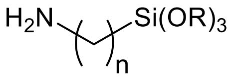

Aminoalkyl-[237, 258]

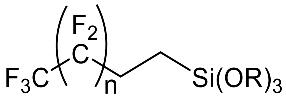

Perfluoroalkyl-[253, 259]

Figure 7: A selection of modified siloxane precursors with R = alky groups. Dialkoxysilanes having two functional groups are also possible.

2.4 Cement – silica composites for bone replacement

In addition to basic material research on mineral biocements, further modifications are investigated to improve the biological performance by inorganic substitution. Silicon substitution adds another bioactive factor to these materials besides calcium, which is thought to promote bone growth leading to strong bone bonding after implantation.[260-265] The bioactivity depends on the amount of silicon released. Osteoblast proliferation will be activated by small concentrations of silicon, whereas concentrations of 9.95mM and higher will have an opposite effect.[164, 169, 266-268].Compared to non-substituted calcium phosphate cements, the frameworks are also more rapidly degraded by the body which clearly indicates an improvement as a bioactive material.[269-273]

Silicon substitution can be generated by various synthesis methods (solid state reaction, hydrothermal synthesis, sol-gel)[274-278] with a strong focus in this context on TCP and HA as calcium phosphate phases.[272, 273, 277-282] As an example, sodium silicate solution was proved by several studies as additive for an improved hardening of CaP cements or was used right away as a liquid phase for the cement reaction which leads to changes in material properties.[283-285] For example, Komlev et al. [283] was able to obtain a setting time of 15 min for dicalcium phosphate dihydrate powder when combined in PLR = 1 g/ml with sodium polysilicate solution as hardening liquid.

The effect of mixing α-tricalcium phosphate and tricalcium silicate to obtain a composite cement resulted in an improved bioactivity, leading to the formation of bone-like apatite on the cement surface, while at the same time the mechanical cement performance was not altered by silicate modification.[286]

Calcium phosphate cements was also modified with zinc silicate together with poly (lactic-co-glycolic acid) (PLGA) microspheres. Qian et al.[287] were able to demonstrate improved new bone formation in the resulting composite. The released zinc ions can also be of benefit as they have anti-inflammatory properties.

Core-shell nanorods are another interesting approach for composites with silica content. The deposition of a uniform silica layer on a core of rod-shaped nano-hydroxyapatite crystals improves bioactivity. The properties of good biocompatibility, osteogenic differentiation, vascularization and bone regeneration potential have also been successfully demonstrated with studies in chicken chorioallantoic membrane and rat models. The *in vivo* study was done on critical-sized femoral segmental defects in rats and the scaffolds were implanted for 4 months.[288] Composites consisting of apatite cement reinforced with 5 wt.% calcium silicate fibers showed an increase in strength of 250% with the same setting reaction. With such an enormous change in mechanical properties, these composites are options for novel materials for bone repair treatment even in somewhere load-bearing applications.[289] The combination of silanized nanosilica with amorphous calcium phosphate (ACP) combined with resin represents a new composite used for tooth remineralization and has improved mechanical properties. The material with silica content shows an enhanced ion release behavior of Ca^{2+} and PO_4^{3-} in both static and dynamic release systems. For ACP resin composites without silanization, the ion release in the static system after 28 d was 0.38 mmol/l for Ca^{2+} and 0.45 mmol/l for PO_4^{3-}, whereas the silanized composites released 0.65 mmol/l ions and 0.79 mmol/l ions for Ca^{2+} and PO_4^{3-}, respectively. In the dynamic system, the cumulative release of ions was measured, with silicon-free composites releasing 0.84 mmol/l Ca^{2+} ions and 0.93 mmol/l PO_4^{3-} ions after 28 d, and silicon-containing composites releasing 1.17 mmol/l Ca^{2+} and 1.15 mmol/l PO_4^{3-} ions.[290]

Chapter 3

Challenges of baghdadite synthesis

A common synthetic route for baghdadite ceramics is the sol-gel method, in which TEOS, calcium acetate and tetraethoxyzirconate are used as precursors. As described in Chapter 2.3, the sol-gel processing involves dissolution of the precursors in an inert organic solvent, followed by controlled hydrolysis with an excess of water under acidic conditions to form a sol. Finally, ageing of the sol results in the growth of nanosized particles leading to a subsequent gelation reaction. The gels are finally dried and calcined at a temperature of 1150°C for 3 hours to obtain nanocrystalline baghdadite ceramics.[217] In a modified version, temperatures of up to 800°C for 3 hours are also suitable for calcination. [291]While sol-gel-processing of baghdadite has the advantage of a homogeneous mixing of all components on a molecular level and is known to lead to a high phase purity after calcination, disadvantages occur due to the high amount of solvent necessary for the synthesis of a sufficient amount of material for further experiment. For example, the synthesis of a 1 kg baghdadite batch according to the synthesis protocol of the sol-gel method [217] requires approx. 6 l of ethanol, which has to be removed prior sintering. In contrast, a direct solid-state synthesis route by using solid raw materials such as nanosilica, calcium carbonate and zirconia is much more powerful in terms of large-scale production as shown by previous works of as Schumacher et al. [204] However, the solid state synthesis from a three-component powder mixture may cause other problems, e.g. a homogeneous mixing of the powders as well as controlled sintering conditions are crucial to obtain baghdadite batches with high purity. Here, any deviations from powder mixture homogeneity may cause local deviation in the stoichiometry of the mixture, which will in turn result in an impurity of the sintered baghdadite batch. In addition, an inappropriate sintering regime may either results in an incomplete reaction (if the temperature is too low) or a thermal decomposition of the material. During the course of this study, a lot of baghdadite batches were produced, while varying parameters such as the mixing conditions of the powder as well as the sintering regime. The obtained batches were primarily characterized regarding their phase composition by XRD, while a sufficient purity was considered to be > 95 % baghdadite with minor amounts of unreacted zirconia and dicalcium silicate side products. The optimized material was not only used for the experiments in this thesis, but also provided to the cooperation partner Prof. Hala Zreiqat and used for different applications such as plasma spraying of baghdadite coatings on metallic implants.[292]

In a first step of baghdadite solid state synthesis, nanosilica is mixed with isopropanol, 30 min homogenized in a ball mill and then mixed with the remaining reactant powders by further milling for 90 min. This resulted in a macroscopically homogeneous slurry, which was subsequently dried in air in a fume hood. The next step was sintering of the powder mixture in order to induce the solid state reaction to baghdadite, however, no phase pure baghdadite was obtained after the sintering process. The result from an X-ray diffraction analysis (**Figure 8**) showed the presence of both cubic and monoclinic ZrO2 phases as well dicalcium silicate. Quantification of the diffraction pattern by Rietveld analysis revealed only 75% of baghdadite within this initially produced batch. The reason behind this was thought to be an inhomogeneous mixture of the raw materials. To overcome this problem, the impure baghdadite powder was milled again for 15 min, followed by a second sintering regime at 1300°C. As this only marginally improved phase purity, the process was repeated twice, which helped to increase purity up to ~88%. In a second attempt, also the sintering temperature was increased to 1400°C to accelerate the solid state diffusion processes during heat treatment. Here, subsequently phase purity improved and exceed the demanded value of >95% after an additional sintering step at this temperature. A repetition of the synthesis of the raw powders revealed that double sintering at 1400°C with a 15 min grinding regime in between again showed the requested purity >95%. A full list of all sinter steps and variations are shown in **Table 2**.

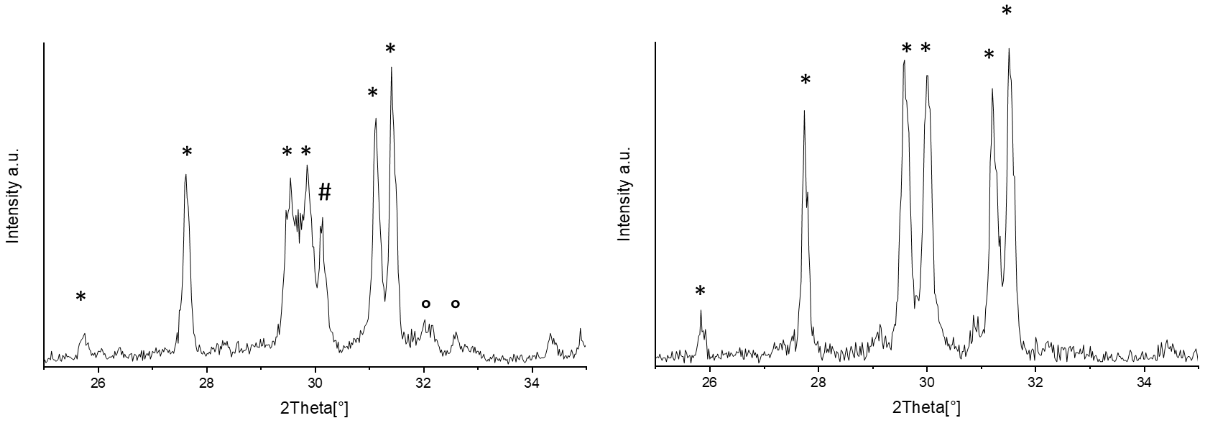

Figure 8: XRD analysis of different baghdadite sintering batches, left: sintered once at 1300 ° C, right sintered twice at 1400 ° C with a 15 min grinding process in between. * = baghdadite, # = zirconium dioxide, ° = C2S.

In an attempt to further purify the material, a salicylic acid extract with a split amount of impure baghdadite was carried out for purification from the C2S phase. For this purpose, 40 g salicylic acid was dissolved in 400 ml methanol and 10 g cement powder was added. The suspension was stirred for one hour at 60°C and then filtered off with a Büchner funnel and dried overnight at 60°C. A scheme of this full process is shown in **Figure 9**. As described in the literature, this process reliably removes the C2S phase, but the other impurities still remain. This purification method was subsequently not pursued further, since it shows the purification effect too specifically only for one minor phase and the problem has become invalid due to the choice of a higher sintering temperature.

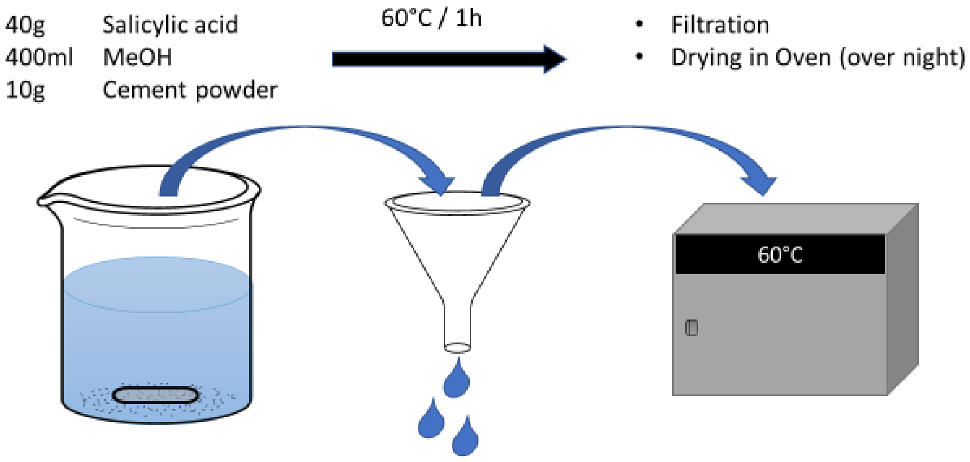

Figure 9: Salicylic acid extraction scheme. Process to selectively extract C2S phases.

It was further observed during the synthesis of baghdadite, that the type of furnace seemed to play a crucial role for the final phase purity of the obtained batches. While there were nearly no impurities in the synthesis with the sintering furnace from Oyten Thermotechnik System Vectra, the use of another device (Schröder; TYP: ASM 30/H) resulted in impure batches. This was surprising as the new sintering unit ran the set sintering regime very accurately and reliably as proved by measuring the temperature inside the furnace during the process. This was done with furnace temperature control disks, also known as "bullers rings". These rings are placed in the oven together with the material and, depending on the temperature, they shrink a certain amount. This shrinking is an independent indicator to monitor the heat work of the sinter process and can be measured afterwards to determine the exact maximum temperature. For big furnace chambers more than one buller ring is used to identify the temperature distribution as there may be slight temperature differences in various positions. Further measurements revealed, that the previously used devise had somewhere deviations from the set temperatures and the oven exceeds the set temperature by about 100°C.

Even though it turned out that the attempt to optimize the synthesis again resulted in the same conditions as already described by Schumacher et al.[9], a deeper understanding of the whole process and the analysis could be gained. Because of the equipment error, additional phases such as ZrO_2 or the C2S phase are now included in the XRD evaluation. Since these phases have such small signals, or can be determined only computationally, they were not noticed with an evaluation before and the baghdadite was considered to be phase pure. The diffractograms of Schumacher et al.[204] look very similar to these measurements and are declared as phase pure. It is possible that these phases also tend to be only >95% baghdadite. Nevertheless, it is astonishing how simple this synthesis route is compared to the much more complex production process via a sol-gel route. For the production of baghdadites by the sol-gel process, TEOS is first stirred with ethanol and 2M nitric acid in the ratio 1:8:0.16 for 45 min. Zirconium(IV) nitrate hexahydrate and calcium nitrate tetrahydrate are then added and stirred for 5h at room temperature. The solution is then stored at 75°C for 24h and then heated to 120°C for 48h. The sintering process is then identical to that described above. Najafinezhad et al. [223] describe the baghdadite obtained in this manner phase-pure. With the corresponding XRD images in those publications it is not possible to confirm these statements, because after this deeper examination of the possible phases within the baghdadite synthesis, the other phases can not really be observed in the diffractogram and need to be calculated via Rietveld refinement analysis.

Table 2: Phase composition of manufactured baghdadite and all steps of the purification process.

Sintering 1300°C	1400°C	**Baghdadite %**	**ZrO_2 cubic %**	**ZrO_2 monoclinic %**	**C2S beta %**
1x		78.67	4.82	1.56	14.95
2x		87.32	3.73	3.62	5.33
3x		88.09	3.36	2.92	5.63
1x	1x	92.63	1.25	1.96	4.17
3x	1x	96.62	0.27	0.94	2.17
1x	2x	93.88	0.82	1.10	4.20
3x	2x	95.98	0.64	1.55	1.83
3x	3x	97.71	0.07	0.13	2.10
	1x	92.41	2.27	1.20	4.13
	2x	95.19	1.16	1.48	2.17
Salicylic acid extraction		75.34	16.92	7.44	0.29

Chapter 4

Baghdadite as filler in brushite cements

Parts of the following chapter 4 is reused from the research article:

No, Y.J.; Holzmeister, I.; Lu, Z.; Prajapati, S.; Shi, J.; Gbureck, U.; Zreiqat, H. Effect of Baghdadite Substitution on the Physicochemical Properties of Brushite Cements. Materials 2019, 12, 1719

Y.J. No holds first authorship; I. Holzmeister carried out all experiments excluding µ-CT and *in vitro* cytocompatibility.

4.1 Introduction

While hydroxyapatite has only a low solubility *in vivo* and can be only degraded by osteoclastic cells [293], brushite cements for bone defect filling applications have gathered increasing research attention recently due to their ability to partially resorb *in vivo* and support surrounding bone tissue growth [294, 295]. In addition, strategies to overcome inherent issues of brushite cement such as injectability, rapid reaction, and lack of initial strength have been extensively investigated [296-308]. There is however limited literature on strategies addressing the issues regarding exothermicity of the cement reaction, acidity, and low radiopacity of brushite cements. The reaction between β-tricalcium phosphate (β-TCP) and primary calcium phosphates in equimolar ratios to produce stoichiometric brushite is an exothermic acid-base reaction [309, 310], and the cement paste causes the surrounding aqueous environment to become acidic [294, 311]. Subsequently, the acidic reaction can detrimentally impact host bone tissue response [312, 313] especially upon injection. In addition, the use of certain setting retardants and modifiers to control injectability, setting time, and strength have been shown to detrimentally impact cytocompatibility [302, 314] and the ability to be resorbed *in vivo* [119].

Radiopacity of bone cements is also an important property to consider when monitoring the cement and the surrounding bone tissue during and after surgery. The radiopacity of a material is a function of the x-ray mass attenuation coefficients of the elements in its composition, with generally higher values with heavier elements, and density of the material, given that the x-ray mass attenuation coefficient of water is negligible in the context of inorganic materials such as cements and ceramics [315]. The elemental composition of calcium phosphate-based cements such as brushite is similar to human bone, hence the ability to adequately distinguish both under conventional x-ray imaging is difficult. Current strategies to enhance radiopacity of bone cements, both acrylic-based and calcium phosphate-based, use hard bioinert particles with high radiopacity such as barium sulfate and zirconia that are simply embedded into the brittle cement structure [316, 317]. These embedded radiopaque particles have been found to act as stress concentration points and subsequently weaken the mechanical properties of the cement [316, 318].

The presence of the heavy element zirconium results in baghdadite possessing a higher X-ray mass attenuation coefficient compared to other ceramics for bone repair such as calcium phosphate, calcium sulfate, and calcium silicate. Baghdadite microparticles have previously been incorporated into polymer composites to enhance their strength, radiopacity and bioactivity [230]. Similar to tricalcium phosphate, baghdadite is also slightly soluble in aqueous physiologically-relevant media [216, 217], and has hence the potential to release calcium ions which are also thought to form brushite in the presence of an acidic phosphate source. Here, we hypothesize that through the novel approach of substituting of β-tricalcium phosphate with baghdadite in a brushite cement formulation, we would be able to synthesize brushite cements with enhanced radiopacity, while maintaining biocompatibility of the cement samples. This approach is novel, since the baghdadite is not simply a radiopaque filler in the cement matrix, but acts as further cement reactant due to its calcium ion release. This will likely overcome the above-described limitations of weakening the mechanical performance of the cement by chemically binding the particles within the cement matrix. This study investigates the effect of the substitution of β-TCP with baghdadite at various concentrations (0, 5, 10, 20, 30, 50, 100 wt% of β-TCP) on the brushite cement reaction and the physicochemical properties of set brushite cement.

4.2 Cement setting reaction and phase composition

The XRD profiles between 2-theta angles of 10° and 50° for brushite and baghdadite-substituted brushite cements (BCB) after 1 day setting in deionized water at 37 °C are shown in **Figure 10**. The XRD profiles for all cements showed distinct crystalline peaks corresponding to brushite (ICDD-PDF #09-0077) and a smaller fraction of monetite ($CaHPO_4$, ICDD-PDF #09-0080). The crystalline peaks corresponding to baghdadite (ICDD-PDF #54-0710) were not reliably detected in the XRD profiles of brushite cements with less than 30wt% substitution of baghdadite. The major crystalline peaks corresponding to baghdadite appeared in the XRD profile of BCB30 at very low relative intensities with respect to the crystalline peak of brushite corresponding to plane (020). For the BCB100 both the formation of brushite and monetite as well as a larger amount of unreacted baghdadite could be detected. To further analyse whether the substitution with baghdadite influences the lattice parameter of the precipitated brushite crystals, a diffraction pattern of the BCB50 sample with an added internal corundum standard was collected and the peak shift for different lattice planes was analysed (**Table 3**). The results showed that the peak shift is overall marginal, which indicates that the further ions present in baghdadite (SiO_4^{4-}, Zr^{4+}) are most likely not incorporated into the crystalline brushite phase and must have formed an amorphous fraction within the cement matrix due to the absence of further reflection peaks.

Table 3: Brushite lattice plane reflex positions adjusted to the corundum reference for sample BCB50%.

Lattice plane	Lattice parameter: diffraction angle in °2θ, (distance d in nm)	
	theoretical	measured
0 2 0	11.65 (7.59)	11.62 (7.61)
1 2 -1	20.95 (4.24)	20.95 (4.24)
1 1 -2	29.28 (3.05)	29.28 (3.05)
1 2 1	30.53 (2.93)	30.52 (2.93)
2 0 0	34.15 (2.62)	34.13 (2.62)

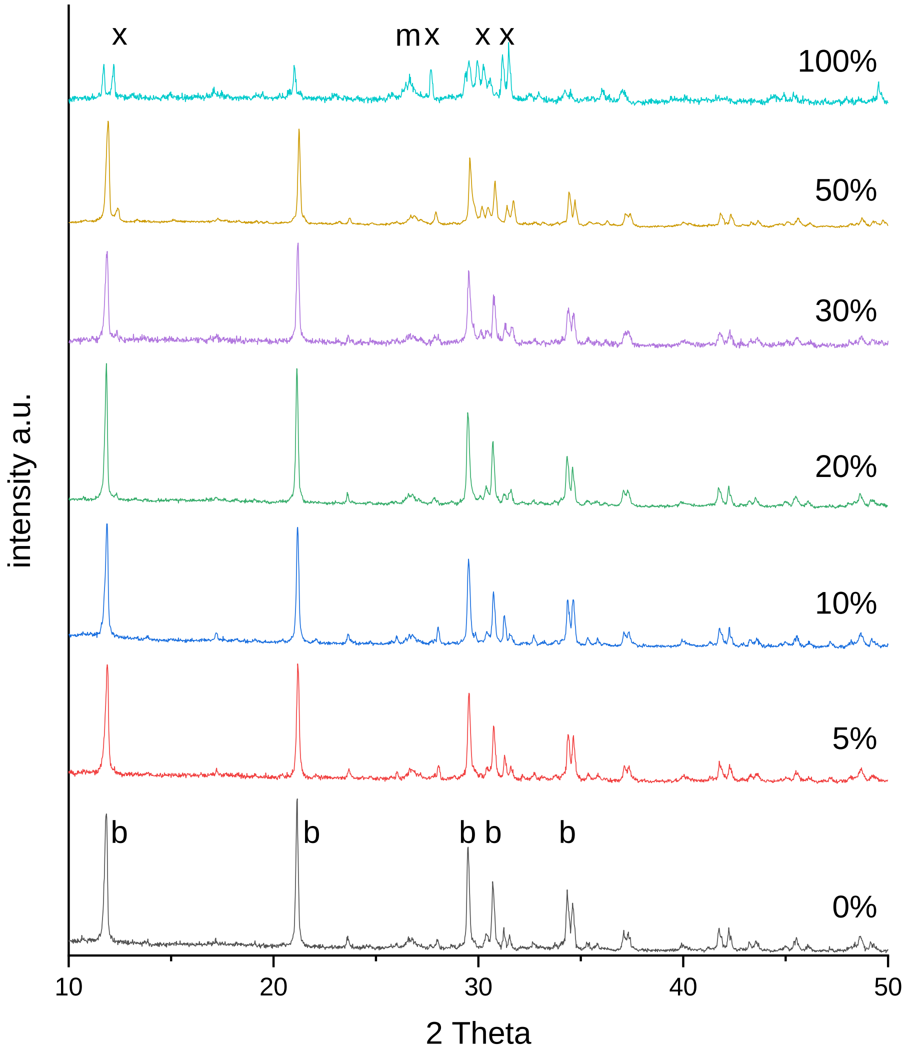

Figure 10: X-ray diffraction patterns of BCB samples with 0%, 10%, 20%, 30%, 50% and 100% ß-TCP substitution by baghdadite after 1 day setting in deionized water at 37°C with marked peaks of brushite (b, ICDD-PDF #09-0077)), monetite (m, ICDD-PDF #09-0080), baghdadite (x, ICDD-PDF #54-0710).

4.3 Compressive strength and modulus

Unmodified set brushite cement exhibited an average compressive strength of 12.9 ± 3.1 MPa (**Figure 11**) and an E-modulus of 1.00 ± 0.21 GPa (**Figure 12**). Increased baghdadite substitution into brushite was shown to increase the compressive strength and modulus of the cement with statistical significance, with BCB10 exhibiting a compressive strength and modulus of 21.1 ± 4.1 MPa and 1.18 ± 0.38 GPa respectively, and BCB100 exhibiting a compressive strength and modulus of 7.7 ± 1.9 MPa and 0.39 ± 0.1 GPa respectively. The change in properties depending on the baghdadite content is shown in **Figure 11** and **Figure 12**.

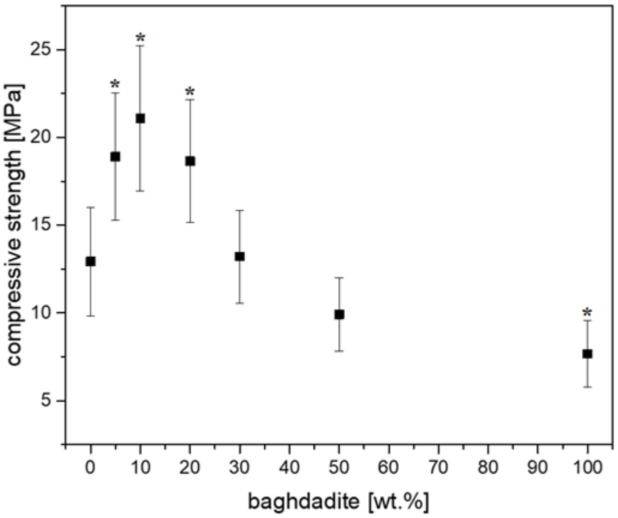

Figure 11: Compressive strength with different amount of baghdadite substitution of β-TCP in brushite cement formulations. *: $p < 0.05$ versus pure set brushite cement.

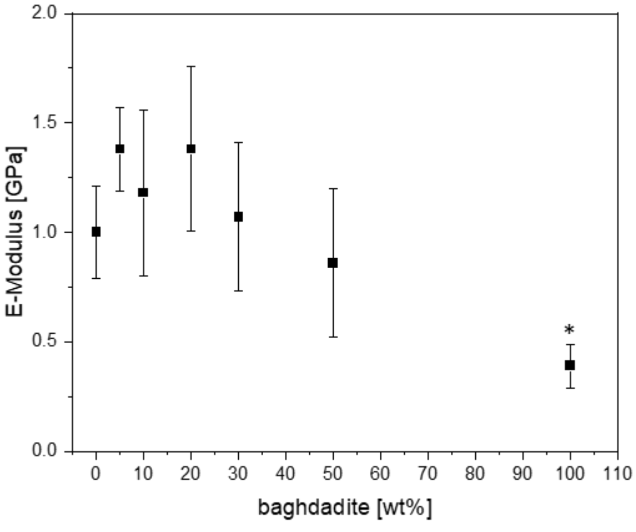

Figure 12: E-modulus with different amount of baghdadite substitution of β-TCP in brushite cement formulations. *: $p < 0.05$ versus pure set brushite cement.

4.4 Microstructure under scanning electron microscopy and computed tomography

Figure 13 shows the representative scanning electron microscopy images of BC, BCB10, BCB20, and BCB50. Irregular plate-like crystal structures can be observed for all cement groups throughout the cement fracture surface when observed using secondary electron detectors. With increasing baghdadite content, areas with agglomerates of sub-micron sized particles can be observed. When measuring the distribution of elements within the cement structure, it appears that calcium is homogeneously distributed within the matrix, while zirconium and silicon form cluster-like aggregates with sizes ranging from few microns to more than 50 µm. Within these structures, phosphorous seems to be depleted (**Figure 14**). Micro-CT image analysis of the set cements indicate a gradual increase in measured average greyscale values with increased concentration of baghdadite in the cement. Increased substitution of β-TCP with baghdadite in the brushite cement formulation resulted in increased radiopacity of the set cements, with the radiopacity HU values increasing linearly with increased baghdadite substitution ($R^2 > 0.99$) as shown in **Figure 15**. BC, BCB5, BCB10, and BCB20 showed 2610 ± 130 HU, 2930 ± 50 HU, 3160 ± 80 HU, and 3910 ± 130 HU respectively when scanned at 70 keV x-ray energy. All cement groups showed statistically significant difference from one another. X-ray images comparing the brushite and baghdadite-substituted brushite cements with various thicknesses of aluminium (**Figure 15** b) also demonstrated increased radiopacity with increased baghdadite concentration. BC, BCB10, BCB20, and BCB50 showed equivalent aluminium thicknesses of 1.24 ± 0.2 mm, 1.53 ± 0.2 mm, 1.56 ± 0.1 mm, and 2.19 ± 0.1 mm respectively. This higher radiopacity also leads to an improved visibility of cement implants within a bony structure as demonstrated by filling bore-holes in a porcine mandible with cement (**Figure 16**).

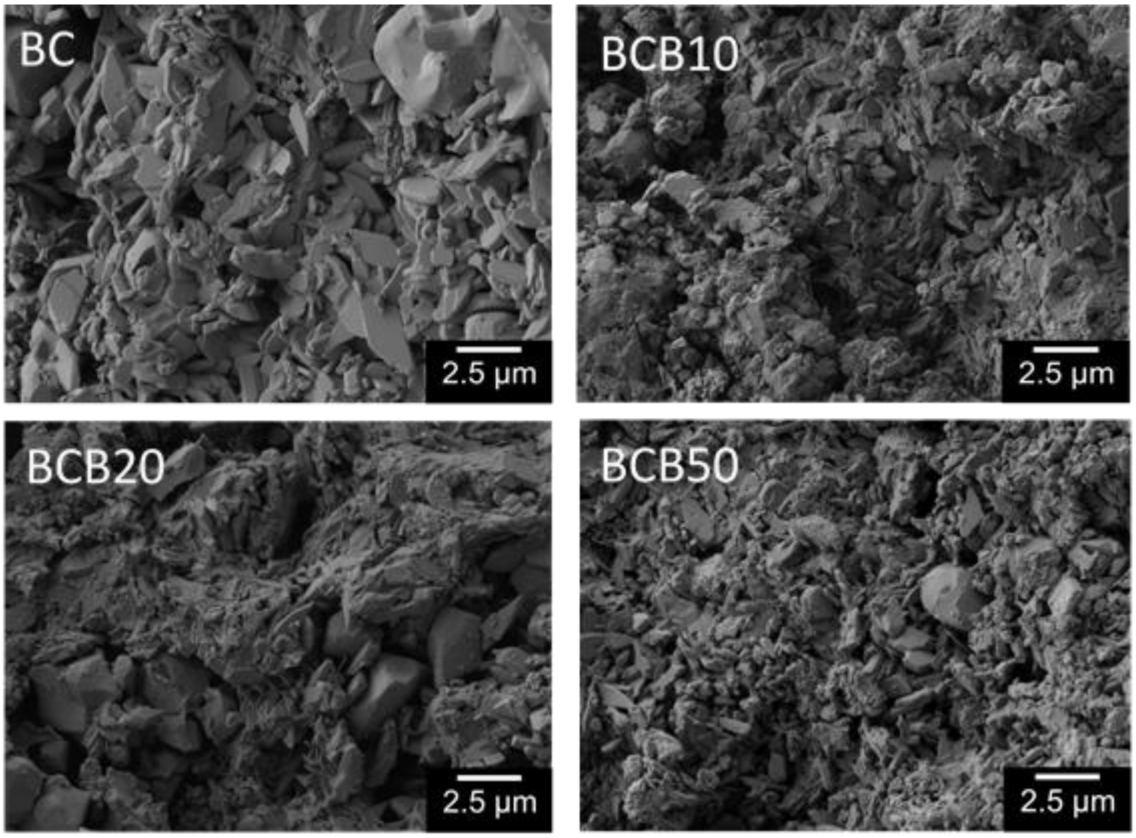

Figure 13: Scanning electron microscopy images of the cement fracture surfaces.

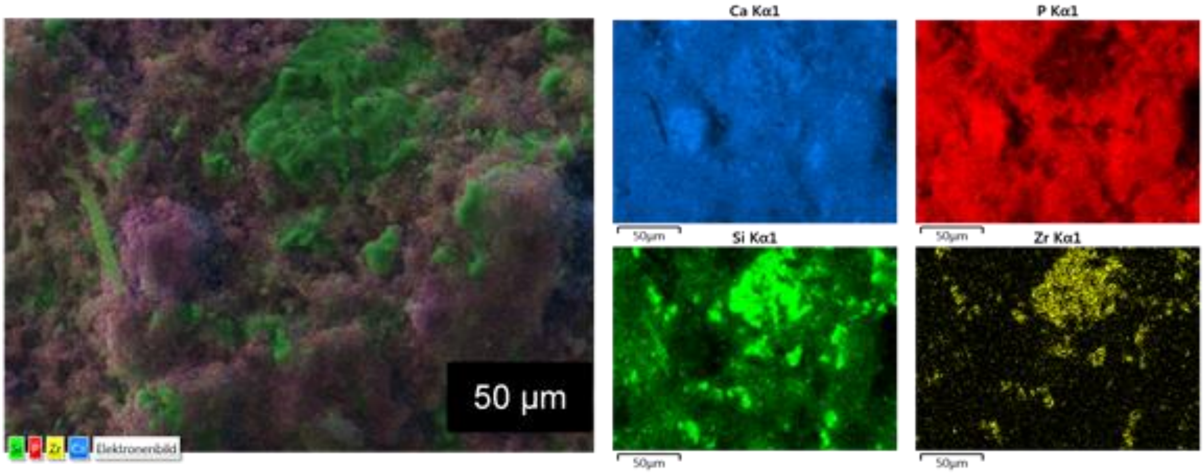

Figure 14: Distribution of calcium, zirconium, phosphorous and silicon within the BCB50 cement microstructure determined by EDX analysis.

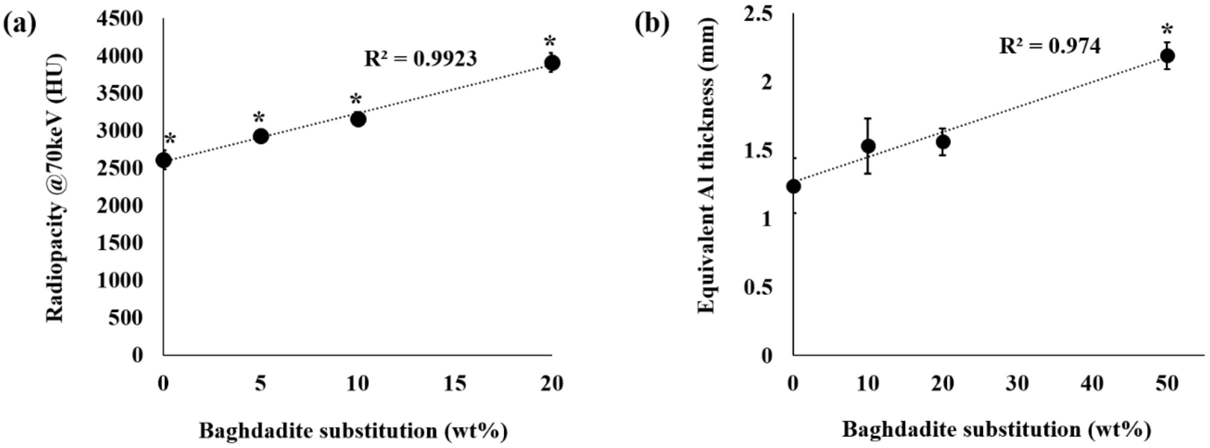

Figure 15: Graphs of the (a) micro-CT measured and (b) X-ray measured radiopacity of the brushite cement samples with increased baghdadite substitution; *: $p < 0.05$ vs all other groups.

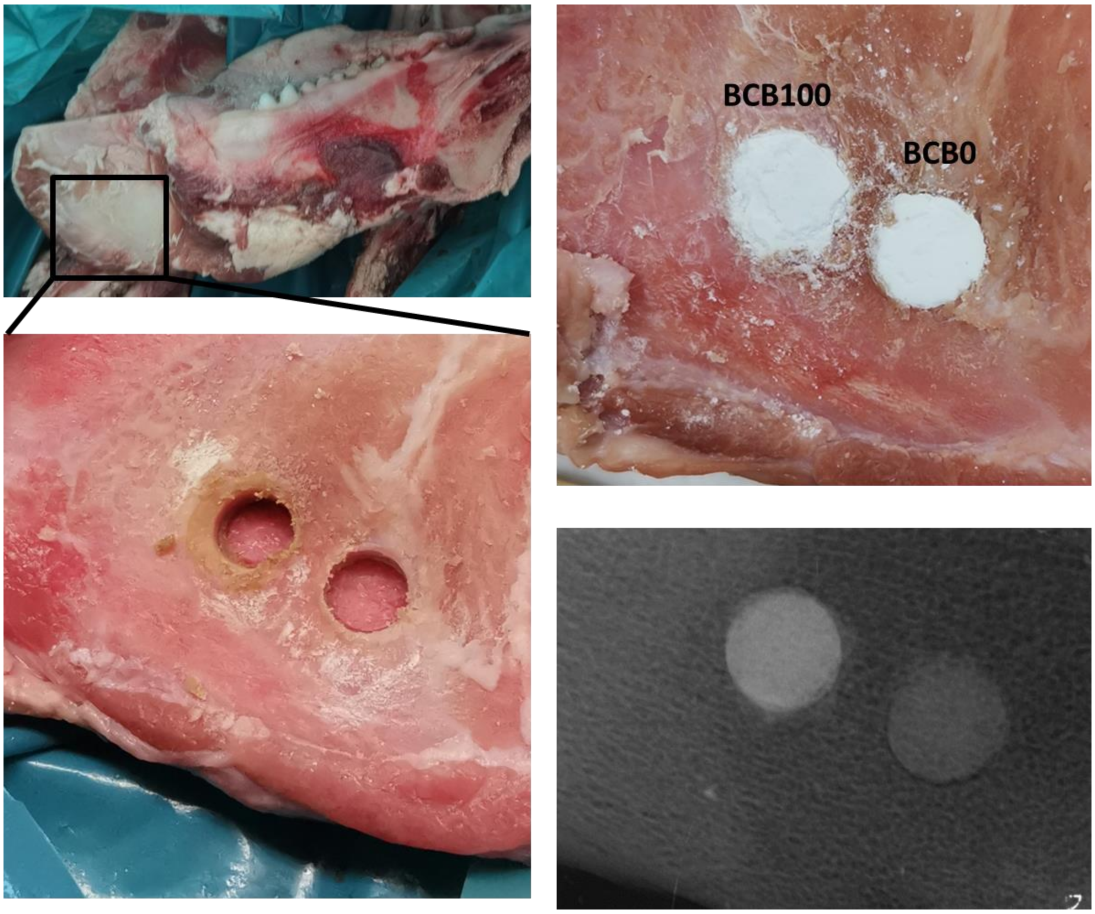

Figure 16: Porcine cadaver mandible with 6 x 3.5 mm bore holes generated with a trepan drill and filled with either BC or BCB100 cement. An X-ray image of the cement implants demonstrates an improved visibility due to the higher radiopacity of the BCB100 cement.

4.5 *In vitro* cytocompatibility

The pH and ion content of each of the culture media conditioned with BC, BCB5, BCB10, and BCB20 are listed in **Table 4**. The pH of the culture media conditioned with BC, BCB5, BCB10, and BCB20 were measured to be 6.47, 6.57, 6.73, and 7.02 respectively. The media conditioned with BCB5, BCB10, and BCB20 indicate presence of silicon ions ranging from 64.7 to 69.9 ppm, whereas no silicon ions were detected in BC-conditioned media. Culture media conditioned BCB10 and BCB20 showed almost half the phosphorus ion levels (362.9 ppm and 349.1 ppm respectively) compared to those conditioned with BC (709.5 ppm). No zirconium ions were detected in any of the culture medium solutions. Culture medium conditioned with BCB10 showed the highest calcium concentration out of the groups tested and showed calcium levels of 34.4 ppm. **Figure 17** shows all cement-conditioned media samples showed statistically significant increase in absorbance values between day 1 and day 7 within the respective cement groups. The absorbance at 490 nm for BCB10 samples were significantly higher than BC and BCB5 samples for both the day 1 and day 7 time points of primary HOB culture. Similarly, the absorbance values recorded for BCB20 samples were significantly higher than BC and BCB5 for days 1 and 7. No statistically significant differences were observed for all time points between BC and BCB5, and no statistically significant differences were observed between BCB10 and BCB20 after 1 and 7 days of HOB culture.

Table 4: pH and ion content of culture media conditioned with BC, BCB5, BCB10, and BCB20. All ion concentration measurements in parts per million (ppm). n.d.: not detectable.

	BC	**BCB5**	**BCB10**	**BCB20**
pH	6.47	6.57	6.73	7.02
Calcium	27.9	29.7	34.4	27.2
Sodium	3429.9	3325.8	3207.5	3220.6
Phosphorus	709.5	560.9	362.9	349.1
Silicon	n.d.	64.7	69.9	65.9
Zirconium	n.d	n.d.	n.d.	n.d

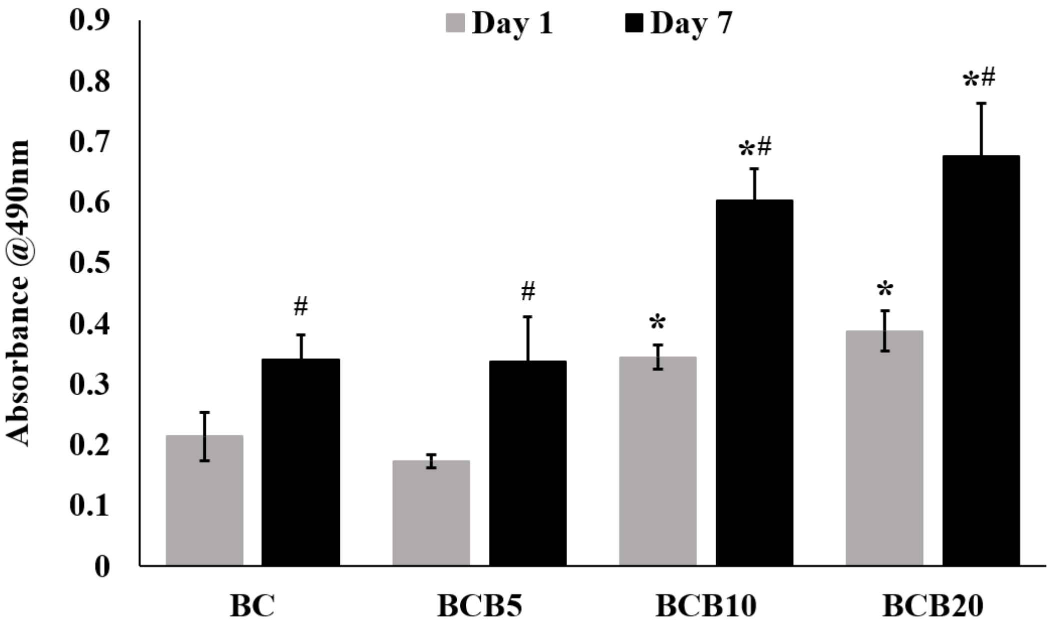

Figure 17: MTS assay absorbance values recorded for primary human osteoblasts cultured in media conditioned with 200 mg/mL of BC, BCB5, BCB10, and BCB20 after 1 day and 7 days of cell culture. #: $p < 0.05$ vs day 1 absorbance values of the corresponding material; *: $p < 0.05$ vs BC and BCB5 at the corresponding cell culture time point.

4.6 Formation of baghdadite granules

Calcium phosphates are often applied in granular form in the field of mineral bone replacement materials, especially in dentistry for the filling of alveolar pockets after tooth extraction. This is usually performed prior to the insertion of dental implants for bone augmentation to achieve a mechanically stable implant anchoring. The advantage of using granules instead of a rigidly shaped material block is the flexibility to adapt the granules to any defect geometry as well as the packing of granules into the defect provides additional intergranular space to achieve an osteoconductive environment for hard tissue ingrowth. Thus, specimen preparation remains independent of the shape and size of the defect. In addition, the material with a carrier fluid can then be introduced minimally invasively by injection to form a dense granular packing in the defect.[319] [320] Especially with granules in the range of 425 to 1000 µm sphere diameter, clinical studies have already been demonstrated a successful bone regeneration with TCP based granules.[321] Granules can fabricated by crushing larger blocks of the material followed by sieving, however, this usually produces granules with sharp edges as well as a certain amount of fine sized particles. An alternative approach of granule fabrication is based on an emulsion technique[322] with the advantage of producing spherical granules with a narrow size distribution.

In this process (**Figure 18**), a cement paste is mixed with aqueous phase and added to lipophilic liquid, i.e. oils, with vigorous stirring. It is important to add a surfactant such as Tween80 to stabilize the entire system. It can be added initially to the cement paste or directly into the oil phase. This creates a water-in-oil emulsion while the cement reaction takes place and spherical granules of different sizes are formed and subsequently harden due to the setting reaction. The size (distribution) is influenced by all the factors involved. The obvious parameters such as cement composition, setting kinetics, choice of oil and agitation speed are as relevant as the paste-oil ratio, surfactant concentration and shape of the agitator.[323, 324]

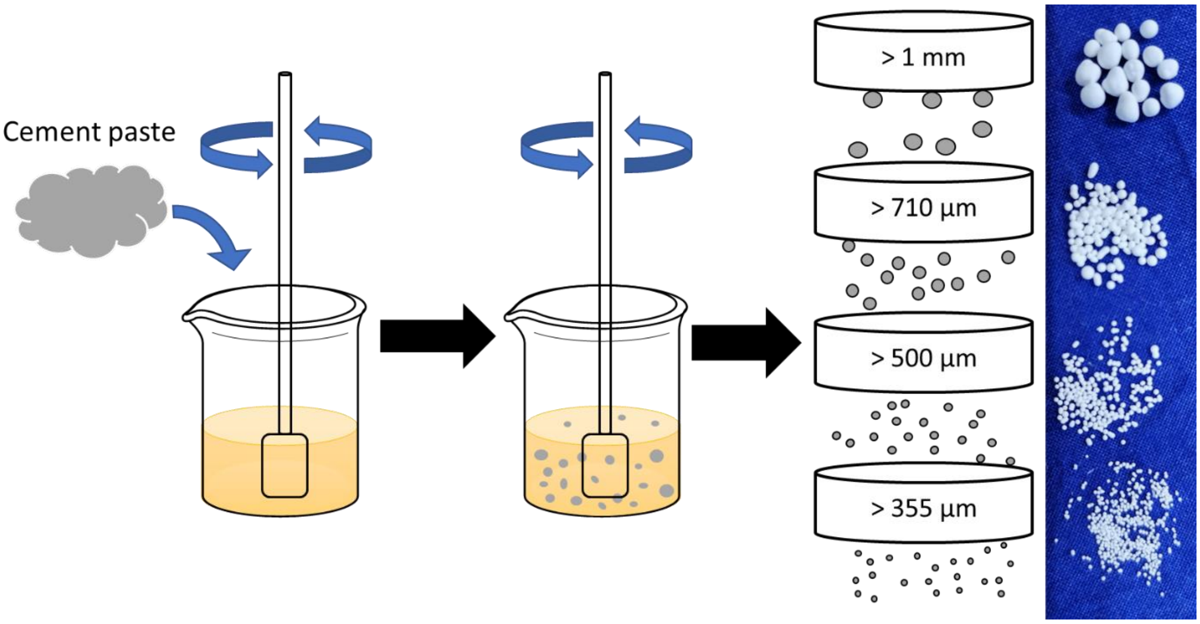

Figure 18: Schematic process of how granules are produced from cement paste. After suspension in oil and hardening, the granules are washed with isopropanol and separated by sieving.

The use of baghdadite as a filler material in brushite cement does not interfere with the granulation process. Highly spherical granules could be produced for BCB formulations with various baghdadite content, as shown in **Figure 19**. Granules without baghdadite content resulted in a smaller size distribution at the same process parameters (1% citric acid, PLR = 2 g/ml, 5% Tween80, RT). The materials with calcium silicate filler resulted in slightly larger granules during processing, but regardless of the content the BCBs formed granules in the same size range.

The influence of the process parameters temperature, tween80 content, PLR and setting retarder concentration (citric acid) on the granule size was discussed in the literature by Moseke et al.[323] The study was about the preparation of brushite granules in specific sizes that may be relevant for clinical applications(100-1000 µm). It was shown that, for example, granulation at 5°C preferentially produces >1 mm spheres, but granulation at higher temperatures of 40°C results in granules with size in the range of 500-710 µm. A similar effect was obtained by using higher concentrations of citric acid, so the granule size changes at 0.05 M from main granule diameters >710 µm to a preferred granule size of 500-710 µm with 0.20 M setting retarder. The concentration of the surfactant (Tween80), on the other hand, had no major influence. Concentrations of 5 mg/ml, 10 mg/ml and 100 mg/ml were investigated and each time primarily granules in the size range of 500-710 µm were produced. only at the highest concentration was there a marginal trend towards slightly larger granules (>710 µm). The PLR has a decisive influence, as it significantly affects the consistency of the cement paste. At PLR=1 g/ml, almost exclusively spheres of >1 mm were produced. With larger PLR's, the average granule size decreases. Thus, for PLR= 1.5 g/ml, mainly granules in the range of 710 µm-1 mm were obtained, and for PLR= 2 g/ml, most granules with the size of 500-710 µm were produced. Regarding the results with baghdadite modified brushite cements, the results demonstrated an overall increase of the granule sizes for the same synthesis conditions. This is likely correlated to the (macroscopically observed) higher viscosity of such cement pastes, which result in the formation of larger cement paste droplets at the same stirring speed.

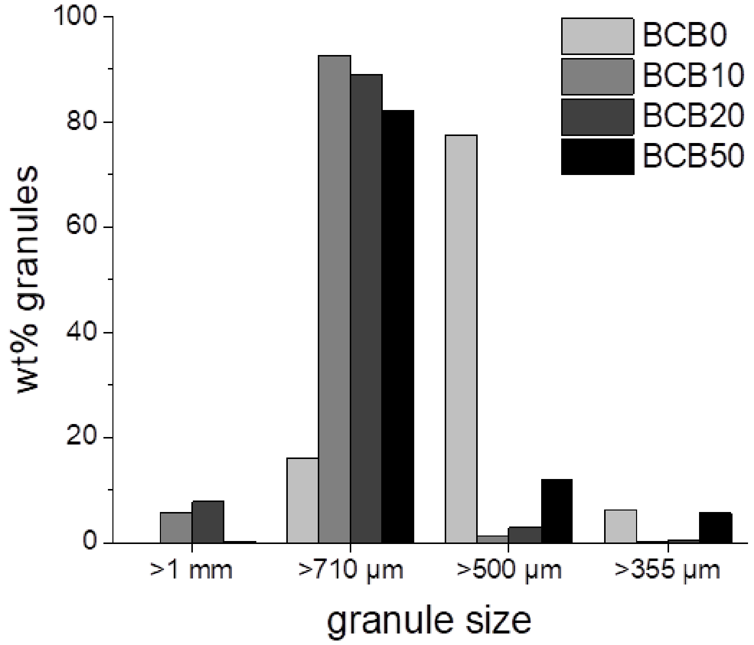

Figure 19 : Distribution of granule size of BCB cements with different calcium silicate content. Process parameters: PLR = 2 g/ml, retarding agent = 1% citric acid, surfactant = 5% Tween80, RT, oil phase= mygliol, stir/setting time= 1h

The use of granules as bone void fillers is particularly advantageous because of their spherical nature (**Figure 20**). Without sharp edges, there is a reduced risk of tissue inflammation and therefore increased potential for use in the medical field. Such spherical granules were obtained for cement formulations with a baghdadite content ≤ 20 wt.%. For a higher BCB content (BCB50), the granules are no longer spherically round. SEM images suggest a possible mechanism for this. It seems that due to rapid setting, the highly viscous cement paste initially formed very large granules. These collide with each other in the emulsion process, and these crashes cause them to break and grind against each other. This is why the edges on the broken granules are not sharp at all. (**Figure 20**). Although not explicitly tested in this study, this problem might be overcome by reducing the PLR of the paste for a lower viscosity as well as by increasing the amount of setting retarder to increase the setting time.

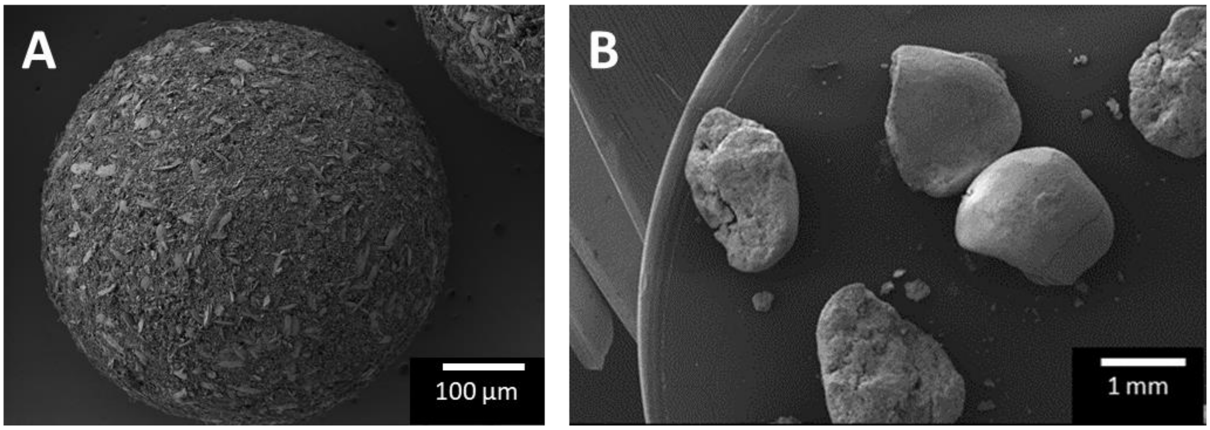

Figure 20: SEM images with different magnification of A) BCB10 granules and B) Fractured BCB50 (>710µm) granules with ground-off edges.

4.7 Discussion

Conventional brushite cements are formed via a dissolution-precipitation mechanism of the slightly basic β-tricalcium phosphate particles and acidic monocalcium phosphate monobasic in equimolar amounts. Previous studies have developed and characterized modified brushite cements, by using Mg-, Zn-, and Sr- substituted β-TCP as the primary reactant, resulting in improved biological activity of the materials [325-327]. Other studies have reported the effect on the brushite cements upon additional incorporation of calcium silicate reactants [63, 328]. This is the first study to modify the brushite reaction by way of substituting the β-TCP phase with baghdadite, a calcium silicate ceramic with zirconium incorporated into its stoichiometry, recently shown to possess excellent bone regeneration properties *in vitro* and *in vivo*, in comparison to calcium phosphate ceramics. Similar to β-TCP, baghdadite powder is also slightly basic, and is shown in this study to dissolve in the cement reaction and become actively incorporated into the brushite structure, rather than acting as a passive non-reacting additive. The stoichiometry of the setting reactions for cements with pure β-TCP and pure baghdadite are shown in Eq. 9, Eq. 10 and Eq. 11:

$$Ca_3(PO_4)_2 + Ca(H_2PO_4)_2 + 8\,H_2O \rightarrow 4\,CaHPO_4 \cdot 2H_2O \qquad \text{Eq. 9}$$

$$Ca_3ZrSi_2O_9 + Ca(H_2PO_4)_2 + 3\,H_2O \rightarrow 2\,CaHPO_4 \cdot 2H_2O + Ca_2ZrSi_2O_8 \qquad \text{Eq. 10}$$

$$Ca_3ZrSi_2O_9 + 3\,Ca(H_2PO_4)_2 + 9\,H_2O \rightarrow 6\,CaHPO_4 \cdot 2H_2O + ZrSi_2O_6 \qquad \text{Eq. 11}$$

While the reaction of cement BC with pure β-TCP results in the quantitative formation of brushite due to an equimolar ratio of both reactants, the reaction of baghdadite with MCPA forms both brushite and a calcium depleted ceramic composed of calcium, zirconium and silicate or a zirconium silicate, depending on the baghdadite: MCPA ratio. Since XRD analysis indicated even for the highest baghdadite content in BCP100 only small diffraction peaks for the baghdadite raw powder, it can be assumed that baghdadite reacts practically in quantitative manner according to Eq. 10 and Eq. 11. Since also no further diffraction peaks could be found, it is also likely that the byproducts formed must have an amorphous nature. As the elemental mapping in EDX analysis (**Figure 14**) showed the presence of zirconium, silicon and calcium within the same local area, it is also likely that only a partial depletion of baghdadite has occurred according to Eq. 10 rather than the formation of a pure zirconium silicate compound. The simultaneously formed brushite phase showed no crystallographic changes due to the addition of baghdadite as cement reactant as demonstrated by analyzing the crystal lattice parameters by Rietveld refinement analysis. The microstructure of the set cements with increased baghdadite substitution also still shows the characteristic plate-like structures of brushite crystals, however with a reduced crystal size and a second phase of closely packed particles sub-micron particles.

The reduction in β-TCP + MCPM reaction due to increased baghdadite substitution of β-TCP did not negatively affect the mechanical integrity of the final set brushite cements, but rather enhanced its mechanical properties for a baghdadite substitution of up to 10-20 wt.%, further suggesting the active role of baghdadite in the cement reaction. The final cement compressive strength attained in the brushite and baghdadite-modified brushite is lower than those reported elsewhere [304], primarily due to the use of a lower powder-to-liquid ratio of 3.0 g/ml. In this study, this lower PLR to sufficiently investigate the effect of baghdadite substitution in the final brushite cement production, as opposed to other studies which typically use ratios higher than 3.3 g/ml was used intentionally. For example, mixing the BCB20 formulation at 3.3g/ml did not allow enough time for sufficient mixing of the components and subsequent transfer into molds, and that a PLR of 3.0 g/ml was optimal for the preparation of all the cements investigated in this study, and was maintained for all groups for scientific validity for observing the effect of baghdadite in the brushite cement reaction. Although lower PLR typically results in lower mechanical strength of set cements [307, 309, 329], lower PLR also allows for good homogenous mixing of the powder components and reduces the potential effect of manual mixing on the final obtained results. The baghdadite-substituted brushite cements still achieve compressive strengths of up to 21 MPa, which is within range of the compressive strengths reported for cancellous bone. In addition, baghdadite substitution can readily be incorporated into previously published strategies that have successfully enhanced the strength of brushite cement through other means such as controlling particle size and use of alternate additives into the cement reaction [304, 330].

The central hypothesis of this study was an enhancement of radiopacity of the cements due to baghdadite substitution. Radiopacity of bone cements is an important property to consider when monitoring the cement and the surrounding bone during and after surgery. This was clearly verified by measuring X-ray absorption of samples and determining the aluminum equivalent thickness according to ISO4049, which nearly doubles for 50wt.% substitution. In addition, micro-CT images also indicate approximately 50% increase in the measured radiopacity in Hounsfield units when exposed to X-ray at 70 keV energy. Though the Hounsfield units obtained depends on the x-ray energy, the values obtained from CT scans is a useful quantitative tool in comparing the radiopacity of materials under clinically relevant conditions [331]. An advantage of this approach compared to current strategies to enhance radiopacity of bone cements by using hard bioinert particles such as barium sulfate and zirconia is that these inert particles are simply embedded into the brittle cement structure and subsequently can weaken its mechanical properties. In this study, simultaneous increases in radiopacity and mechanical strength through baghdadite-substitution into brushite cement due to the cementitious reactivity of the baghdadite component under acidic conditions was achieved

Regarding cytocompatibility issues, baghdadite substitution positively influenced the proliferation activity of primary human osteoblast. Such increased proliferation effect is most likely a function of both the increased bioactivity of baghdadite when compared to calcium phosphate-based materials as reported previously [217], as well as the increased starting pH of the culture media conditioned with baghdadite-substituted brushite compared to that conditioned with unmodified brushite cement. The pH of the culture media used was affected by the amount of baghdadite substituted into the brushite, with culture media conditioned with BCB20 showing pH of ~7 compared to ~6.5 for pure brushite. It is reported in literature that brushite cement is acidic in aqueous environments [294, 311], and though brushite cements have been shown to demonstrate good *in vivo* bone regeneration [294, 295], there is very little *in vitro* analysis done on brushite cements due to the inherent inability to continuously ‘flush out’ the acidity in a typical *in vitro* experiment. Low pH has been shown detrimentally affect osteoblasts [313], and so by incorporating baghdadite into brushite cements the effect of acidity in the implant region for bone cement applications especially during the early setting phase when the bodily fluids are closely interacting with the applied cement was reduced. A second effect is related to the reduced phosphate content of the culture medium. Here, previous studies have revealed that brushite cements can increase the phosphate concentration of cell culture medium by the factor of 20-30 during cell culture [332], whereas phosphate concentrations exceeding a certain level have a detrimental effect on cell viability *in vitro*. Baghdadite substitution in brushite cements showed a strong reduction in phosphate release and may hence also be responsible for the observed better cytocompatibility of the materials.

4.8 Conclusion

This study has demonstrated that baghdadite substitution of β-TCP is a useful strategy to improve the properties of brushite cements for bone defect filling applications by its radiopacity and *in vitro* HOB proliferation, without significantly compromising its mechanical properties for up to 50wt% substitution. This strategy may be used concurrently with other reported protocols to further optimize the formulation of brushite-based cements, as well as potentially other mineral based cements such as apatite- and calcium sulfate-based cements.

Chapter 5

Hydraulic reactivity and cement formation of baghdadite

Parts of Chapter 5 were published as original research article: Holzmeister, I., Weichhold, J., Groll, J., Zreiqat, H. and Gbureck, U. (2021), Hydraulic reactivity and cement formation of baghdadite. J. Am. Ceram. Soc., 104: 3554-3561.

The article is based on the work of the author of this dissertation thesis Ib Holzmeister, who developed and characterized the composite material, designed and performed all experiments, interpreted (excluding XRD) and graded the data and wrote the manuscript.

5.1 Introduction

As previously mentioned, in most studies, baghdadite was applied as sintered porous ceramic block [204, 213], or partially as a highly porous scaffold in combination with polycaprolactone/ nano-bioglas coatings to reduce the brittle behavior of the bone graft and minimize the risk of inflammation. [220]. More recently, it was shown that baghdadite can act as a reactive filler compound in acidic setting brushite cement formulations. Here, baghdadite can substitute the β-tricalcium phosphate compound and participate in the setting reaction by delivering Ca^{2+} ions, whereas a calcium depleted ceramic composed of calcium, zirconium, and silicate is formed [333]. At low baghdadite concentrations, this resulted in a mechanical reinforcement of the cement, while at higher concentrations ≥ 50% a significant increase in radiopacity was achieved.

While the previous study used a 3-component system of baghdadite, β-TCP and acidic monocalcium phosphate for cement formation with associated problems such as the need of a homogeneous mixing of all compounds, the current study aimed to produce single-component baghdadite cements. Due to the fact that calcium silicates usually show a hydraulic activity and are widely used in civil engineering Portland cements, it was hypothesized that baghdadite may also possess such a hydraulic reactivity and will be able to form self-setting cements. This was investigated in this study by grinding baghdadite for up to 24 h, followed by mixing the resulting powders with water. The setting reaction was analyzed by X-ray diffraction regarding changes of the phase composition as well as mechanical tests to determine the performance under compressive loading.

5.2 Mechanical activation of baghdadite by grinding

The synthesis of baghdadite followed the stoichiometric mixture of calcium carbonate, silicon dioxide and zirconium dioxide according to the corresponding ratio of Eq. 12. According to Rietveld refinement analysis, the material consisted mainly of baghdadite (95.2%) with minor phases such as zirconium oxide in cubic (1.16%) and monoclinic (1.48%) structure, as well as dicalcium silicate (2.17%). These side phases either stem from remaining raw powder or abrasion of the zirconium oxide milling beaker or may be formed by a side reaction (Eq. 13).

$$3\ CaCO_3 + 2\ SiO_2 + ZrO_2 \rightarrow Ca_3ZrSi_2O_9 + 3\ CO_2 \qquad \text{Eq. 12}$$

$$4\ CaCO_3 + 2\ SiO_2 \rightarrow 2\ Ca_2SiO_4 + 4\ CO_2 \qquad \text{Eq. 13}$$

Prolonged grinding of baghdadite was thought to produce a higher amorphous content in the cement powder, which in turn should increase the hydraulic reactivity towards self-setting cement formulations. Such a mechanical activation regime for cement powders is known for a range of different cement types based on calcium silicates [334], calcium phosphates [104, 335] or magnesium phosphate [336] compounds. Mechanistically, the activation is usually based on a decrease in particle and crystal size, increase in specific surface and increase of the amorphous fraction of the cement powder. All effects result in both a higher rate of dissolution and higher solubility product, which increases the supersaturation level in the cement liquid and hence accelerates cement setting.

As expected, grinding of baghdadite not only resulted in a reduction of particle size D_{50} from 2.68 ± 0.9 µm to 0.59 ± 0.01 µm after 24 h, but also lead to decrease of peak intensity and peak broadening in XRD patterns (**Figure 21**). The latter is a result of a decrease in crystal size from 150 nm to 20 nm after 24 h grinding as well as the formation of amorphous domains in the material (**Figure 22** A). The crystalline and amorphous parts were calculated from XRD measurements using Rietveld refinement combined with an external standard (corundum) method (G-factor). This was done by calculating G with Eq. 14, where S_{cor} is the Rietveld scale factor of corundum, ρ_{cor} is the corundum density, V_{cor} as unit-cell volume, μ_{cor}^* is the mass attenuation coefficient (MAC) of the corundum and c_{cor} is the weight fraction of corundum. With Eq. 15 and this G-factor it was possible to calculate the amount of crystallinity for each different phase j and additionally the amorphous content in the sample.[337, 338] For each phase of the independent XRD-measurements the standard deviation was calculated in the range of 0-3%. After combing the crystalline calculations of the single phases for each material, the deviation for the amorphous content was 0,00%.

$$\mathrm{G} = S_{cor}\frac{\rho_{cor}V_{cor}^{2}\mu_{cor}^{*}}{c_{cor}} \qquad \text{Eq. 14}$$

$$C_j = S_j\frac{\rho_j V_j^{2}\mu_{sample}^{*}}{G} \qquad \text{Eq. 15}$$

While the reduction in crystal size is somewhere following the same trend as for other bioceramics such as α-tricalcium phosphate, the overall amorphization is much less pronounced and reached only 10 % after 24 h compared to 71 % for α-TCP after a 15x15 min grinding regime [338]. This is probably due to the different grinding parameters as well as varying material properties. Hurle et al. [338] used 100 balls with a diameter of approx. 10 mm for grinding of 100 g powder, while grinding in the current study was performed with 165 balls of 6 mm diameter for 24 h and a change of rotation direction each minute. This likely resulted in a less efficient amorphization as baghdadite particles seemed to have a more brittle character and were predominantly splitted into smaller parts rather than plastically deformed. A similar behavior was found for the calcium magnesium phosphate merwinite [339], which could be efficiently amorphized by using a ten times higher rotation speed of the ball mill.

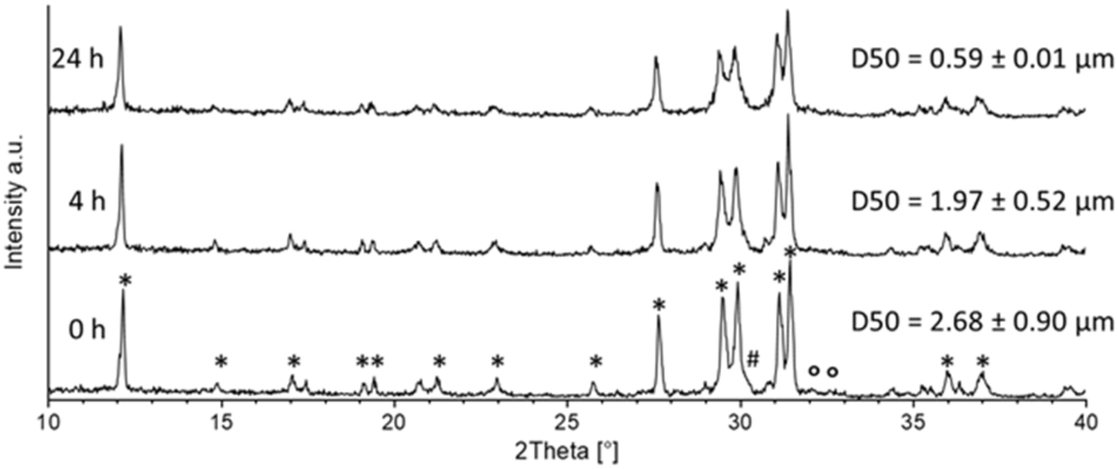

Figure 21: Influence of the grinding time on X-ray diffractograms (* = Baghdadite, # = Zirconoxide, ° = C2S) including medium particle sizes of the individual samples.

The mechanical activation process could be also seen in DTA -TG measurements (**Figure 22** B). The slight loss in mass of the mechanically activated powder is most likely due to the adsorption of isopropanol on the particle surface since the materials were wet milled and afterwards only dried at ambient conditions.

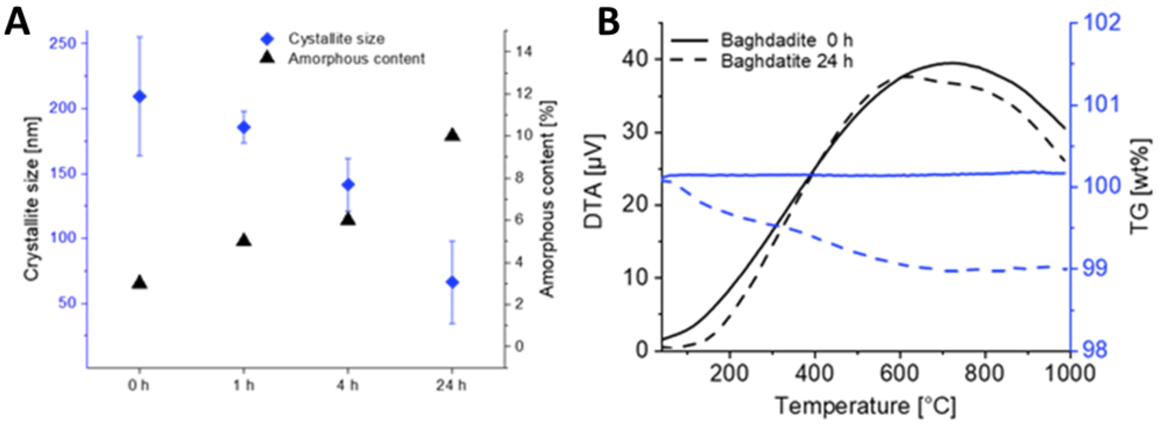

Figure 22: Influence of the grinding time on A) crystal sizes and amorphous content and B) differential thermogravimetry and calorimetry of the individual samples.

5.3 Solubility and cement formation

Activation also influences the solubility of the baghdadite powders as demonstrated by ICP measurements (**Figure 23** A). The ground powder as well as the set cement was stored in MiliQ water. Practically all powder showed an incongruent dissolution with an access of dissolved calcium and less released zirconium ions. While a complete dissolution is expected to lead to a mass ratio of calcium, zircon and silicon of 2.06 : 2.56 : 1.0 in water, solutions with the cement powders were usually depleted regarding Zr and enriched with Ca. The solubility profile of the cement powder showed an increase of Ca and Zr and a decrease of Si in solution. Trends can be determined after 24 h of grinding. The amount of calcium ions in solution increases from ~225 mg/l to 325.6 ± 5.01 mg/l (24 h). In a different manner the concentration of zirconium increases. After no change in solubility until 4 h of milling (~0.1 mg/l), a higher zirconium concentration can be measured for 24 h (1.30 ± 1.64 mg/l). An incongruent trend can be monitored for the silicon release. The solubility of ~4 mg/l without grinding decreases to 3.08 ± 1.61 mg/l after 24 h ball milling. Over the whole grinding time, the Ca : Si ratio increased from 52.8 : 1 (not ground) to 105.7 :1 (24 h ground) (**Table 5**).

In contrast, there is no clear trend for the measurements of the cement samples (**Figure 23** B) but slight fluctuations can be seen in the different samples. In comparison to the powder samples, it is noticeable that less calcium ions are released, but higher concentrations of silicon ion can be measured. For the zircon ions no notable changes occur. Noteworthy is the lower Ca/Si ratio, which is in the range of < 2 : 1, which is much nearer to the expected theoretical range.

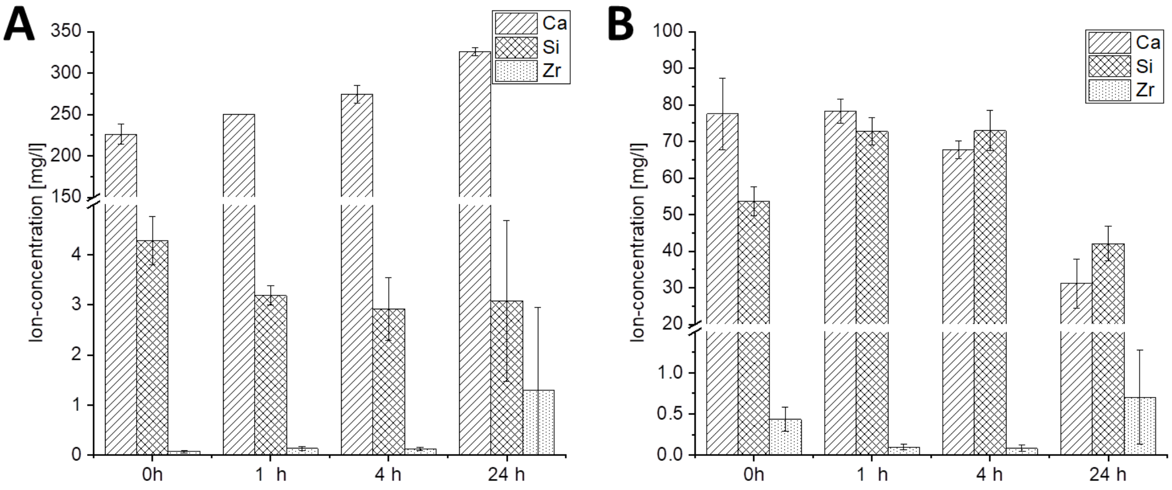

Figure 23: Ca, Si and Zr ion concentrations after 1d exposure of (A) ground powder in MilliQ water and (B) set cement in MilliQ water.

Table 5: Ratios of Ca/Si/Zr ion concentration for solubility testing power and cement in water.

	Powder in milliQ water			**Cement in milliQ water**		
	Calcium	Silicone	Zircon	Calcium	Silicone	Zircon
0h	52.80299	1	0.017509	1.443318	1	0.008096
1h	78.36963	1	0.041697	1.075463	1	0.001323
4h	94.03676	1	0.042163	0.928582	1	0.001113
24h	105.7285	1	0.42242	0.742081	1	0.016675

This increase in solubility also affects the pH value of the cement setting reaction (**Figure 24**). While the unground baghdadite powder reached a pH plateau of 11.9 after 2-3 min, cement pastes made from the ground cement powders resulted in pH ~ 12.3 after 45 min setting. This corresponds to an increase in [OH$^-$] by a factor of 2.5 from ~0.0079 mol l^{-1} to ~0.02 mol l^{-1} after 24 h grinding. This increase in pH is somewhere similar to biocements based on tetracalcium phosphate [340] or calcium alkali phosphates [341], which have been proved to have antimicrobial properties due to their alkaline pH. Hence it can be speculated that the baghdadite cements from this study could have a similar biological performance regarding their antimicrobial activity.

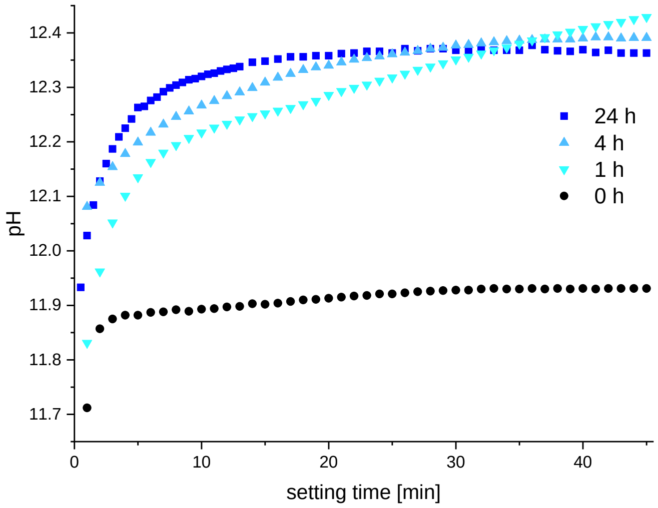

Figure 24: Initial pH changes of the cement setting reaction after mixing the different powders with water.

Mixing of the baghdadite powders with MiliQ water resulted in a hardening of the cement pastes with compressive strengths of up to 1.93 ± 0.46 MPa for 24 h ground powder after 3 d setting (**Figure 25**). This clearly demonstrated both an inherent hydraulic activity of baghdadite as well as an effect of the grinding regime on the mechanical performance of the cements. How the strength changes over a period of 3 weeks is shown in **Figure 26**. The selected sample was the 24 hours milled powder. The initial strength value measured after one day was only 0.38 ± 0.07 MPa, which increased after a setting time of 3d. to 1.93 ± 0.46 MPa could be found and later on decreased continuously to ~1 MPa.

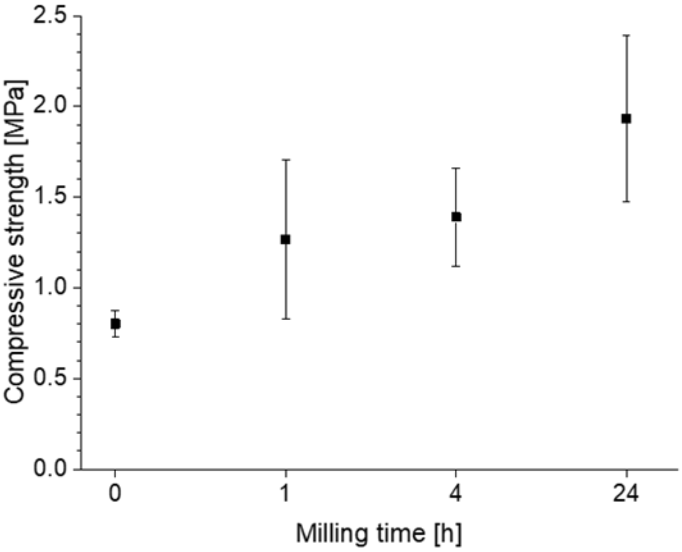

Figure 25: Compressive strength measurements of cement samples with different milling time.

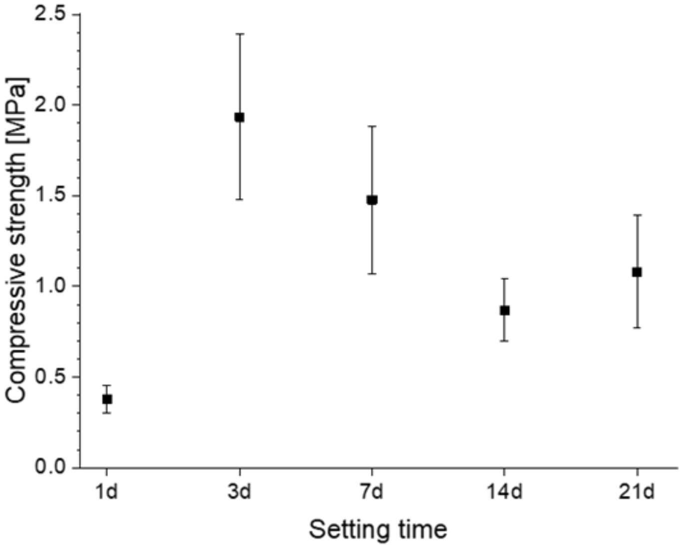

Figure 26: 3 weeks time depending study for hydraulic activity of activated cement.

These findings were further confirmed by SEM images (**Figure 27** A), where much larger particles can be seen in the non-ground cement, whereas the cement texture becomes more homogeneous with increasing grinding time. In addition, the elemental distribution was affected by grinding as shown for zirconium (**Figure 27** B), showing a less homogeneous appearance of this element for non-ground cements in contrast to a homogeneous distribution for the 24 h ground cement powder.

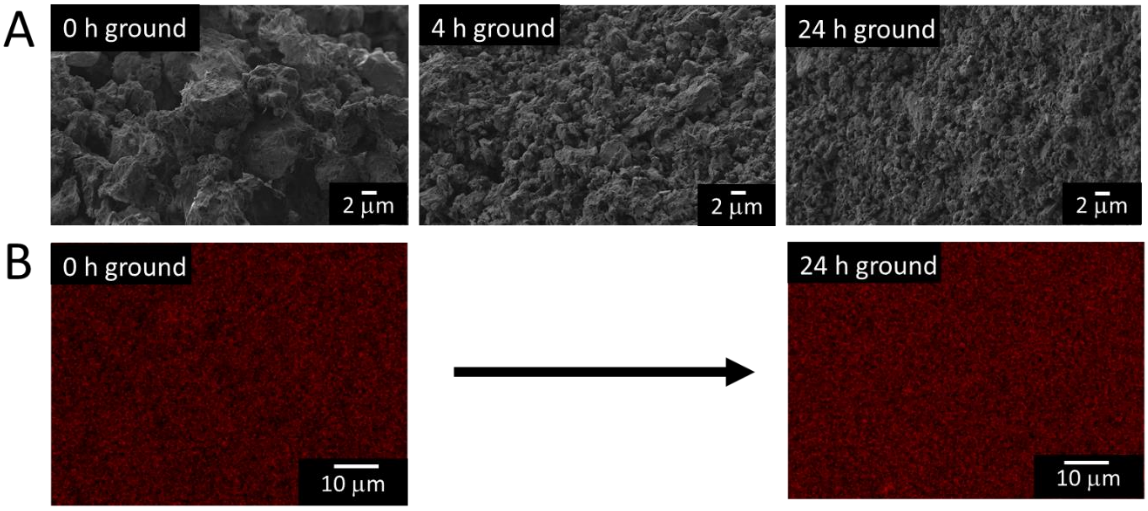

Figure 27: A) morphology of baghdadite cements and B) element mappings for zirconium for baghdadite cements from either unground and 24 h ground cement powders.

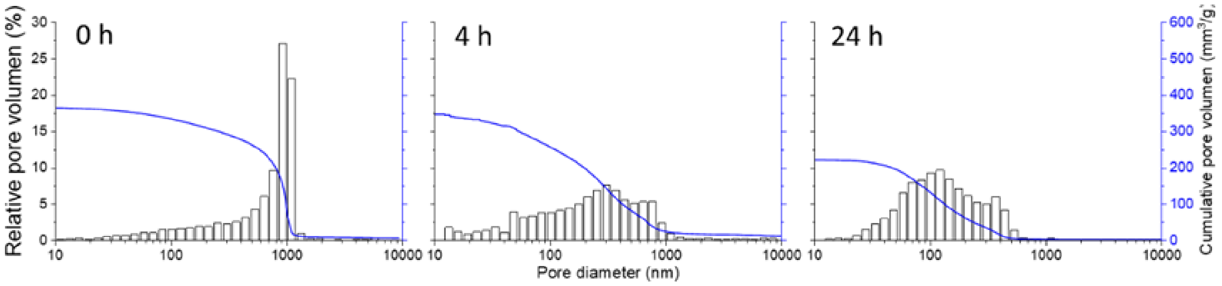

Figure 28: Relative pore volume and cumulative pore volume for baghdadite cements from either unground, 4 h and 24 h ground cement powders.

Mercury porosity measurements **Figure 28** showed that the cumulative pore volume decreased from approx. 364.7 mm^3/ g (unground) to approx. 220.9 mm^3/ g for the 24h ground powder. While for the non-ground cements pores are predominantly found in the µm-size range, the main peak shifts to smaller pore sizes in the nm-range for long-term ground cement. This corresponds to a porosity of 60.55% at 0h, 59.09% for 4 h ground and the smallest porosity with 41.18% corresponds to the 24h ground powder after setting. The fact that a short initial grinding process has little or no influence on the porosity and that it changes only after longer grinding was also observed for mechanically activated β-TCP cements. The porosity at 1h and 4h grinding time are identical and a value of 45% was measured. After grinding for 24h, however, the porosity decreases to 40%. [102] The inverse effect was observed for tetracalcium phosphate cements, where the porosity for cements consisting of short milled starting powder is ~ 40%, but cements with powder milled for 24 h had a porosity of 45%.[340]

In comparison, a cumulative pore volume of ~250 mm^3/g could be measured with PLR = 2 g/ml using the same measurement method for brushite, but at higher PLRs such as PLR = 3 g/ml, the volume decreases to approx. 180 mm^3/g. A similar tendency can be observed with struvite cements from literature, where the cumulative pore volume decreases with increasing PLR. For example, a value of ~55 mm^3/g was determined for PLR = 2 g/ml, but only ~45mm^3/g for PLR = 3 g/ml. Hydroxyapatite cement differs slightly in this comparison, since it has a larger pore volume. with approx. 275 mm^3/g at the PLR = 3 g/ml. These results were published by Kanter et al.[119] and were placed in the context of the development of the values after 10 months of orthopedic implantation. It was observed that the porosity of struvite cements increases from 5-7% to 19-26% and brushite cements show a similar tendency for PLR = 2 g/ml (porosity increase from 38% to 59%). However, the cumulative pore volume changed only marginally for PLR = 3 g/ml. For hydroxyapatite, an opposite effect occurred and the material decreased porosity from 42% to 33%.

Surprisingly, XRD measurements of set cements appeared quite similar to the raw powder and did not show the formation of new crystalline phases Figure 29). However, the increase of the amorphous content (**Figure 30**) reveals the formation of a non-crystalline setting product, which might consist of hydrated calcium silicates from released Ca^{2+} and SiO_4^{4-} ions: Eq. 16

$$3\ Ca^{2+} + 2\ SiO_4^{4-} + 4\ H_2O \rightarrow Ca_3Si_2O_6 \cdot 3H_2O + 2\ OH^- \qquad \text{Eq. 16}$$

These CSH phases have usually no signals in the XRD due to their amorphous or very weak crystalline character. The reaction of precursors such as C3S (alite) or C2S (belite) with water to CSH leads to its substantial material properties, such as greater mechanical strength [342]. The important aspect for the formation of these phases is the Ca / Si ratio. This can range from 1.2 to 2.1. Baghdadite with a Ca / Si ratio of 1.5 is therefore a potential candidate for the formation of these corresponding CSH phases, even if the value differs a bit from the peculiar optimal ratio of 1.75 [342].

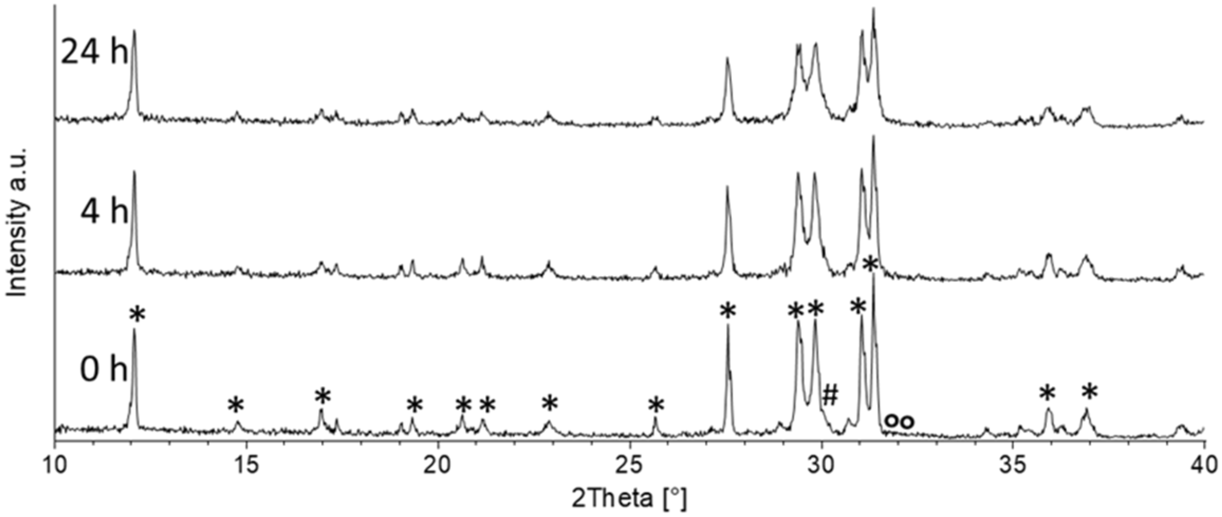

Figure 29: X-ray diffraction patterns (* = Baghdadite, # = Zirconoxide, ° = C2S) of baghdadite cements depending on grinding time and setting for 3 days at 37°C.

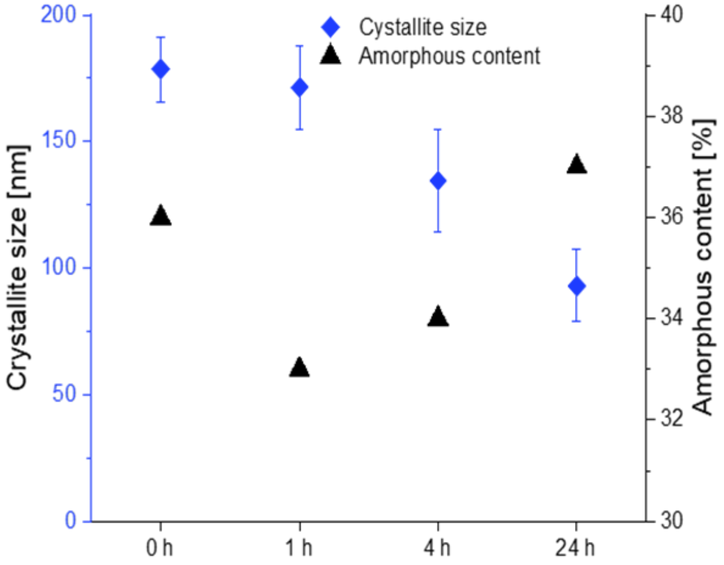

Figure 30: Crystal size and calculated amorphous content of baghdadite cements depending on grinding time and setting for 3 days at 37°C.

5.4 ^{29}Si NMR measurements

For a further investigation of the material, ^{29}Si NMR was carried out to gain an insight into the bonding type of the silicate groups. While monomeric orthosilicate anions have the highest chemical shift Q^0 at about – (71—73) ppm, silica peaks with a higher negative shift (-(78—82) ppm) can be assigned in the position as end group (Q^1) or with two binding partners as middle group of a chain (– (83—85) ppm; Q^2). For higher crosslinked silicates such as branching site silicates the signals belong to Q^3 (-100 ppm) and for fully crosslinked groups Q^4 (-110 ppm) [339, 343, 344]. **Figure 31** shows that depending on the grinding stage, different numbers of signals can be measured. The deconvolution of spectrum A shows signals at -71.0 ppm for Q^0 and at -80.2 ppm and -80.89 ppm for Q^1. As it can be seen in Table 6, Q^0: Q^1 is in a ratio of 1: 13.7, such that most silicate ions are bound to calcium after synthesis. These signals are similar to other studies on calcium silicate hydrate phases [345, 346]. After grinding for 4 h (**Figure 31** B), more signals appear, whereas the peaks at -70.9 ppm and -74.1ppm can be assigned to the Q^0 and the signals with a chemical shift of -79.5 ppm, -80.2 ppm and -80.9 ppm are assigned to Q^1. In this spectrum, also a very weak Q^2 signal occurs with a chemical shift of -81.4 ppm. Table 6 shows a Q^0 : Q^1 : Q^2 ratio of 1 : 4.78 : 0.68, which means that in this material the proportion of unbound silicate ions is increased. Further grinding for up to 24 h (**Figure 31** C) results in peaks at -71.2 ppm (Q^0), -80.6 ppm and -80.9 ppm (Q^1) and at -82.0 ppm and -83.2 ppm (Q^2). The ratio of those Q^0 : Q^1 : Q^2 signal integrals are 1 : 3.49 : 1.34 demonstrating an increasing amount of Q^0 signal and also a small increase of Q^2. Only the Q^1 signals lose intensity because of the milling process. Hence, the high energy impact during prolonged grinding not only reduces crystal size of baghdadite and forms an amorphous material fraction, but also leads to a partial condensation of silicate. Compared to a study by Kriskova et al. [339] on the mechanochemical activation of merwinite, more signals appear for both not activated and mechanically activated baghdadite. It is possible that the material generates several signals due to the formation of amorphous domains such that slight changes in the chemical shift occur. This assumption also matches with the observations by Rejmak et al. Their work has shown that the chemical shift of these signals strongly depends on the phase and near surroundings in which they are located [347]. Chen et al also points out that with ^{29}Si-NMR measurements small broad shoulders may be observed with the Q^2 signals [344]. This phenomenon has occurred in many other studies [348-352] and the origin of this shoulder could not be clearly determined yet. Furthermore, Chen et al. describes how the chemical shift changes due to different Ca/Si ratios. At high ratios, the signals show higher chemical shifts [344].

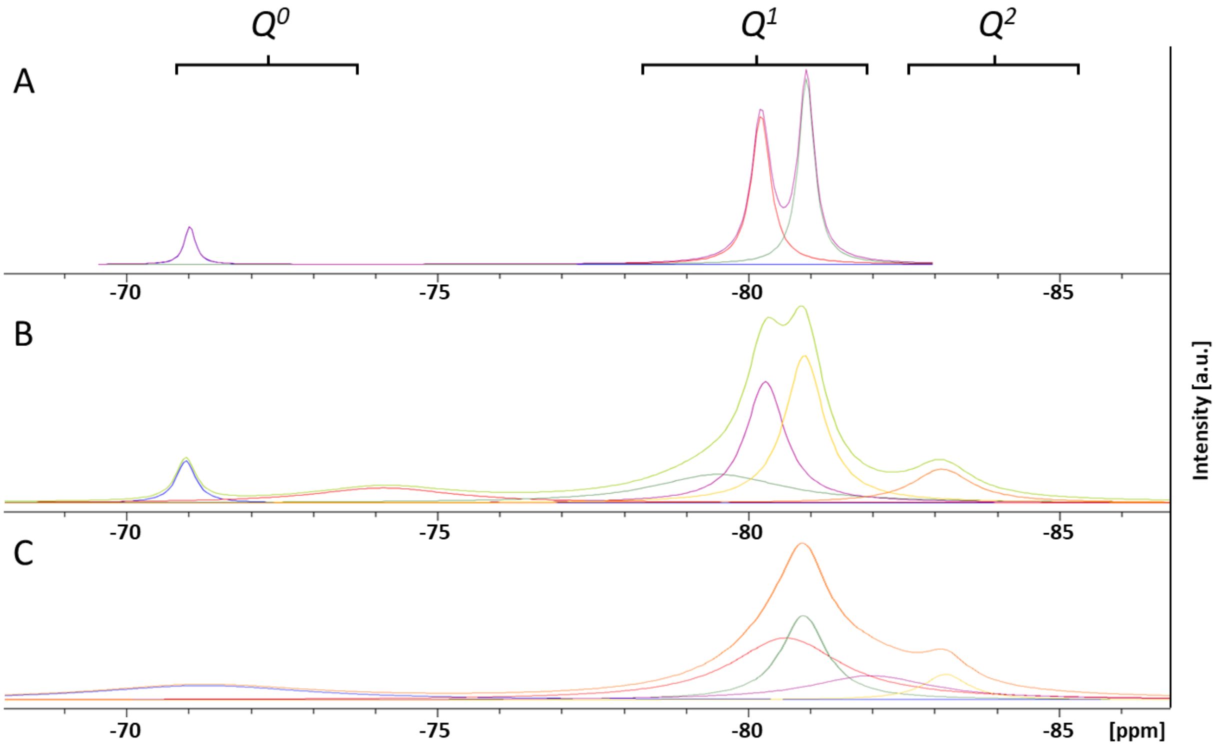

Figure 31: Deconvoluted 29Si solid-state NMR measurements for A) unmilled powder B) 8h ground powder and C) 24h ground powder.

Table 6: Ratios of the 29Si-NMR signal integrals (Q^0, Q^1, Q^2) from **Figure 31** normalized to the signal of Q^0.

	Q^0	Q^1	Q^2
0h ground (A)	1	13.7	
8h ground (B)	1	4.78	0.68
24h ground (C)	1	3.49	1.34

5.5 Cryostructuring to produce microporous baghdadite scaffolds

Another possible form of processing baghdadite is cryo-structuring. In this process, lamellar structures can be created in the cement slurry under controlled process conditions. Important for the process is an external temperature gradient, which is applied to the sample via two peltier elements. A schematic setup is shown in **Figure 32** .In order for the structuring process to run in a controlled manner, it is essential to keep the system in thermal equilibrium during the process and to conduct heat away efficiently. This is achieved by a complex cooling system, which is described in more detail in the literature.[353, 354]

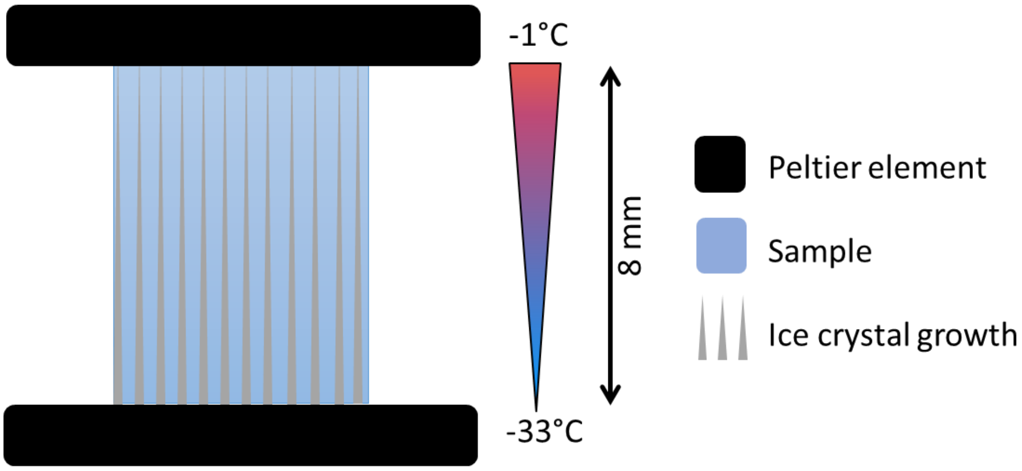

Figure 32: Schematic of the cryostructuring process the sample is placed between two Peltier elements that generate an external temperature gradient.

As proof of principle, baghdadite powder was mixed with a solution of dextran with the concentration of 2.5 wt%. The polymer serves as a supporting structure and does not react with the calcium silicate. The slurry was then placed in the cryostructuring device and after the was frozen, the water is removed by lyophilization. As a final step to obtain a structured monolith, the samples were sintered. This removed the dextran from the system resulting in a porous as structure with parallely aligned pores.

The samples were viewed under the microscope and already on a macroscopic level the structure in the sample can be visualized. The SEM analyses in **Figure 33** showed that the cryo structuring has indeed created a highly porous baghdadite scaffold with a lamellar structure parallel and pores a width of ~15-20 µm that extend completely through the sample. On the basis that baghdadite is suitable as a biomaterial and shows bioactivity, it can be postulated that this treatment will have a positive effect on cell proliferation. Such an effect of improved cell activity has already been demonstrated in other materials with structured surfaces.[355-358] However, this needs to be verified by further testing because some other studies claim that there is no correlation/effect on cell proliferation by a structured environment.[359-361] In addition, due to the similar structure to lamellar bone, this method can lay the foundation for hierarchically structured bone substitute materials to come close to and optimally imitate the natural structure of human bone.

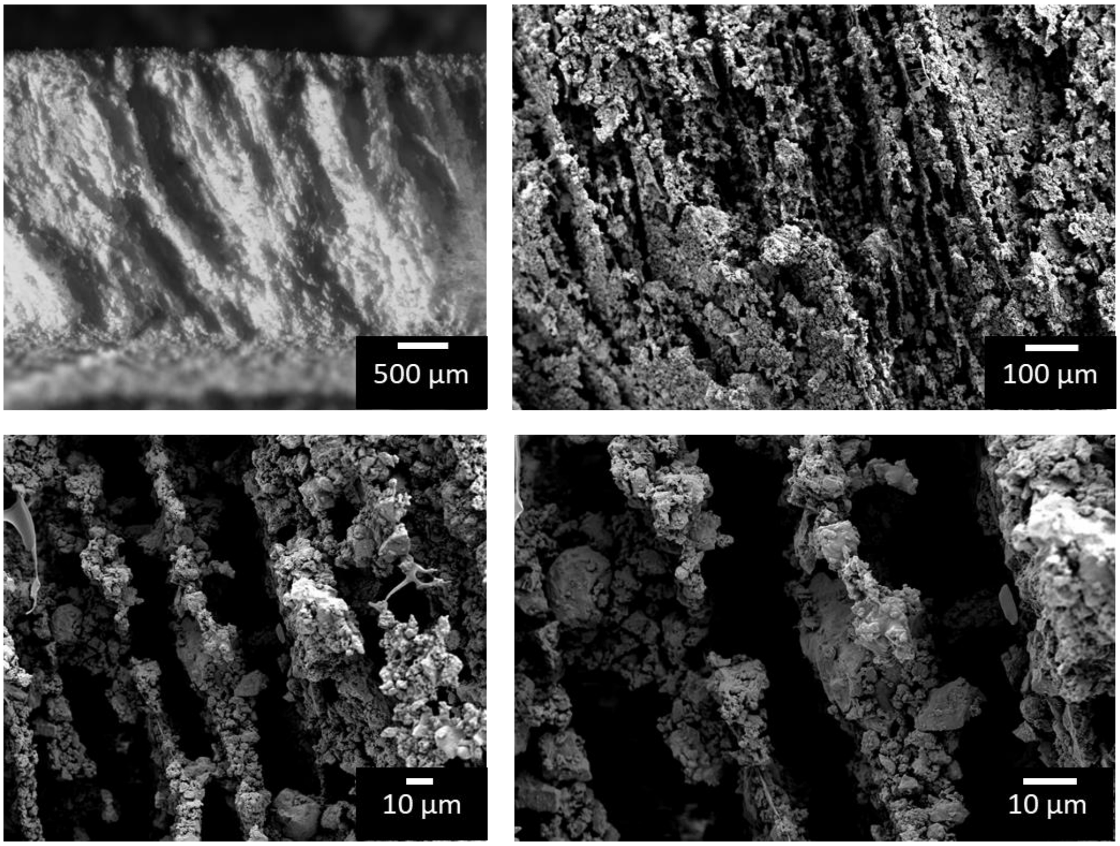

Figure 33: Microscopy and SEM images with various magnifications of the structured baghdadite sample.

The method of cryostructuring offers many further possibilities in the design of structured pores. In a study by Seifert et al. [354] using α-TCP and alginate as polymeric support structure, pores dimensions of ~23µm could be generated. These are in the same range as the freeze-structured baghdadite with dextran as supporting structure (~15-20µm). In another work with the same freezing device using material without cement, aligned pores ranging in size between (50 ± 22) µm and (144 ± 56) µm were obtained for freeze structured alginate.[353] This shows which pore range can be covered with this method, but the parameters (e.g. temperature gradient) must always be adapted to the used materials.

5.6 Conclusion

Baghdadite appears to have an intrinsic hydraulic activity, which can be further enhanced by mechanical activation due to prolonged grinding. This changes the material properties and leads to the formation of amorphous material, which reacts with water to form X-ray amorphous hydrated phases. Although the cements have currently a comparable low mechanical performance of ~2 MPa under compressive loading, strength might be further increased by optimization of the grinding regime leading to an improved activation process as well as by adjusting a bimodal particle size distribution to increase packing density and reduce cement porosity. Setting of baghdadite occurred without further additives, and baghdadite cements have a clear potential for a biomedical application either in bone replacement or – due to the inherent X-ray opacity [333] – as endodontic filler.

Chapter 6

Dual setting silica-cement composites

The following Chapter 6 consists of some parts, which are written in form of a research paper manuscript. This manuscript is neither submitted or published by the time of the submission of the thesis.

6.1 Introduction

Strategies to improve the mechanical properties of inorganic biocements include the reduction of inherent cement porosity, the addition of fibers or – more recently – a dual setting cement approach by an additional hydrogel phase in the cement matrix. This was previously achieved by gels based on poly-hydroxyethyl methacrylate [362], cross-linked NCO-star-PEG [363] or silica [364]. The latter was described by Geffers et al. [364] for a brushite cement, in which a silica phase was generated by hydrolysis and condensation of tetraethoxysilane (TEOS). This not only successful in term of higher mechanical performance, but also improved cytocompatibility and prolonged drug release due to the nano porous silica matrix.

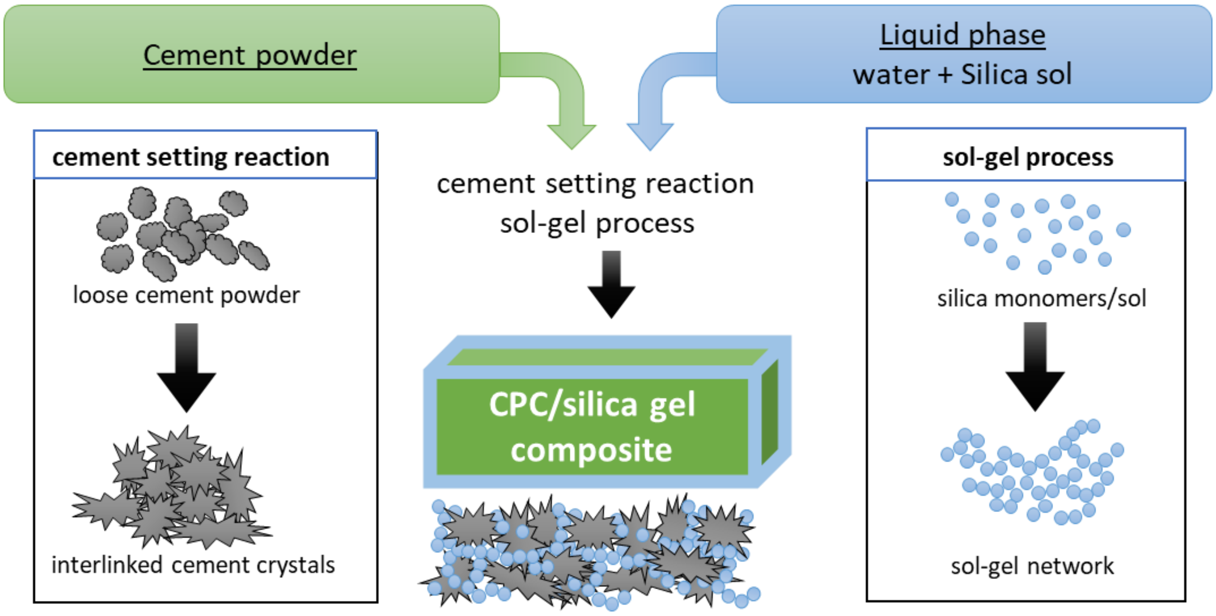

Figure 34: Schematic of dual-setting silica-cement composites in which the cement reaction proceeds simultaneously with the formation of the sol network.

The current study aims to improve the mechanical performance of cements by a dual-setting approach with various silica gels (**Figure 34**). The silica precursors used in this thesis are shown in **Figure 35**, being designed as spacers of different lengths and chemical structures. 1,2-Bis(triethoxysilyl)ethane and 1,2-Bis(triethoxysilyl)octane were commercially available and precursors P1, P2 and P3 were selectively synthesized. While a modification of the cement pastes with a TEOS derived sol is already thought to improve strength, it is further hypothesized that using multi-arm silica precursors can further enhance their mechanical performance due to a higher network density. In addition, this should also reduce pore size of both gels and cement and hence will be able to adjust the release kinetics of incorporated drugs.

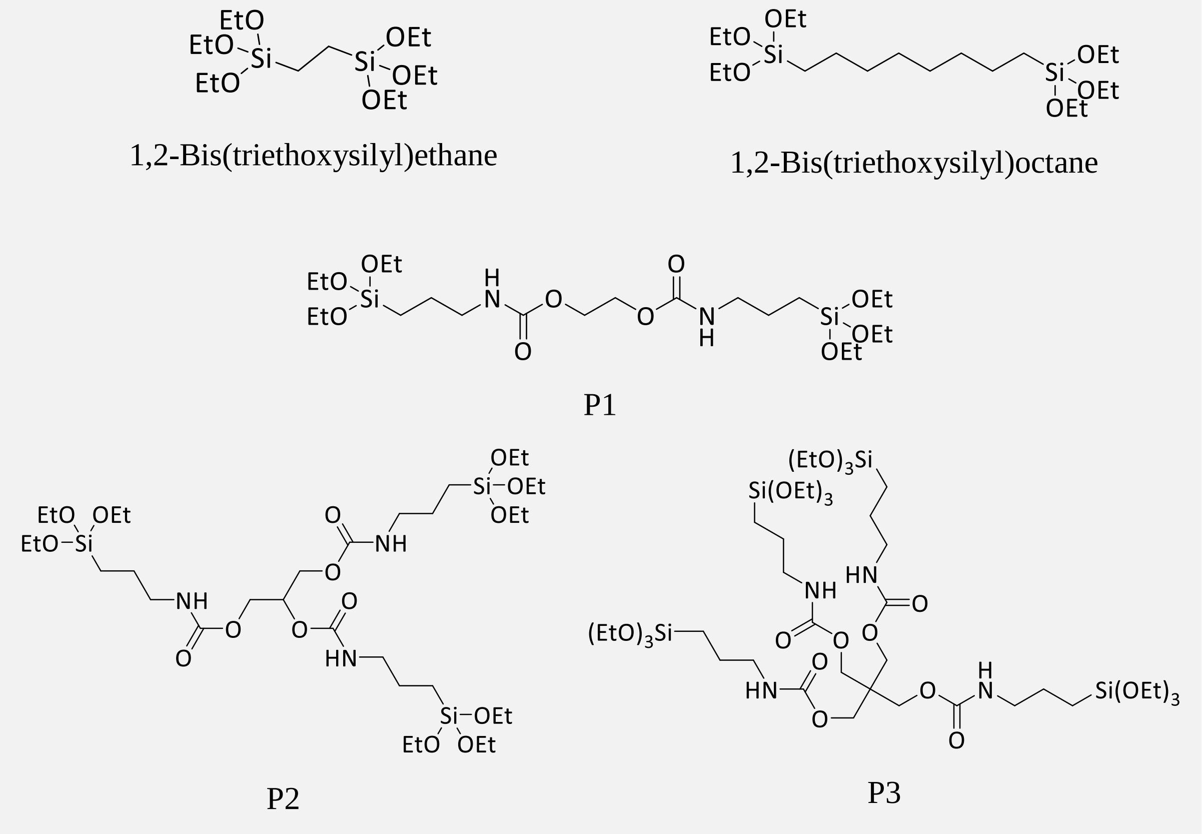

Figure 35: Chemical structure of the various silica precursors used for generating new composites.

In a first attempt, composites were prepared with brushite cements, because these have already been investigated in the literature with TEOS as precursor and the influence of precursor variation can be observed better. Based on the newly gained knowledge, a following study on dual-setting silica baghdadite composites was carried out. For this, the precursors P1, P2 and P3 were synthesized by the reaction of various multivalent alcohols (ethylene glycol, glycerine, pentaerythrit) with an isocyanate modified silica precursor (**Figure 36**). The carbamate groups contained in the precursors can have an additional positive effect on the composites due to their hydrophilicity. After hydrolysis under acidic conditions, the sols were mixed with baghdadite cement powders in order to allow a simultaneous gel formation and cement setting. The resulting composites were then analyzed by X-ray diffraction for changes in the phase composition as well as mechanical tests and porosity to determine basic material properties. In addition, vancomycin-loaded composites were examined according to their release profile and their antimicrobial potency was investigated by an agar diffusion test against *S. aureus*.

Figure 36: Isocyanate modified silica precursor (3-(triethoxysilyl)-propylisocyanat)

6.2 Silica sol variations combined with brushite cements

Silica networks with TEOS as precursor have already been investigated as composites together with brushite forming cements. Initially, tests were carried out in which the composition of the silica sol varied, but brushite was chosen as the cement system. This allowed to study the influence of this parameter as a preliminary test for composites with baghdadite as cement and branched precursors. **Figure 37** and **Figure 38** show reference measurements of brushite cement and brushite cement with TEOS as precursor. It can be observed that for higher powder to liquid ratios, higher strength values were achieved. One limitation is, that it was impossible to produce suitable test specimens with a PLR≥2.5 g/ml for composite with silica sol, because no moldable cement paste could be produced during mixing due to the lack of water. When mixing the solid and liquid phases, only very crumbly lumps are formed, which cannot be further processed. This was also observed with all other dual-setting silica systems at PLR 2.5 g/ml, and only the PLRs of 1 g/ml, 1.5 g/ml and 2 g/ml could be investigated.

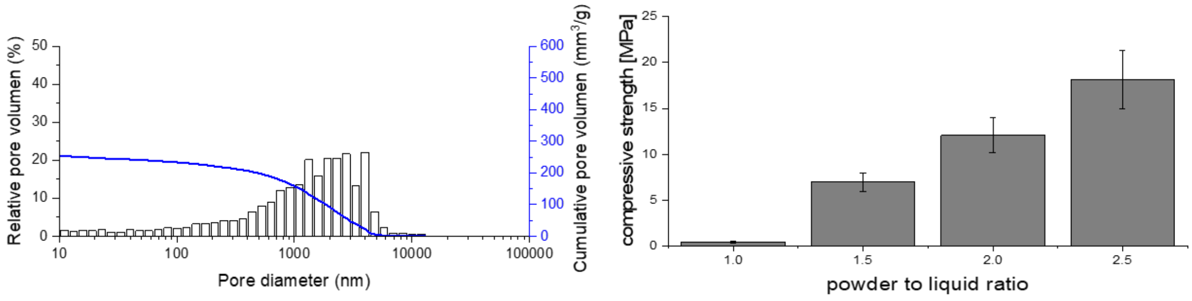

Figure 37: Pore size distribution (left, PLR=1 g/ml) and compressive strength (right) of brushite as a reference for brushite-based silica composites.

The results of mercury porosimetry show a monomodal pore size distribution for the Brushite cement, and a bimodal pore size distribution for the TEOS composite reference, with a tendency towards increased smaller pores in the material.

The attempt to replace TEOS completely by other precursors could not be implemented, because the sol cross-linked too quickly, making it impossible to mix it with the cement powder. As a consequence, the compositions of the silica sols were still based on TEOS, but corresponding mol% are substituted by precursors from **Figure 35**. This leads to a higher crosslinking density, since the selected precursors have two to eight more linking sites compared to TEOS.

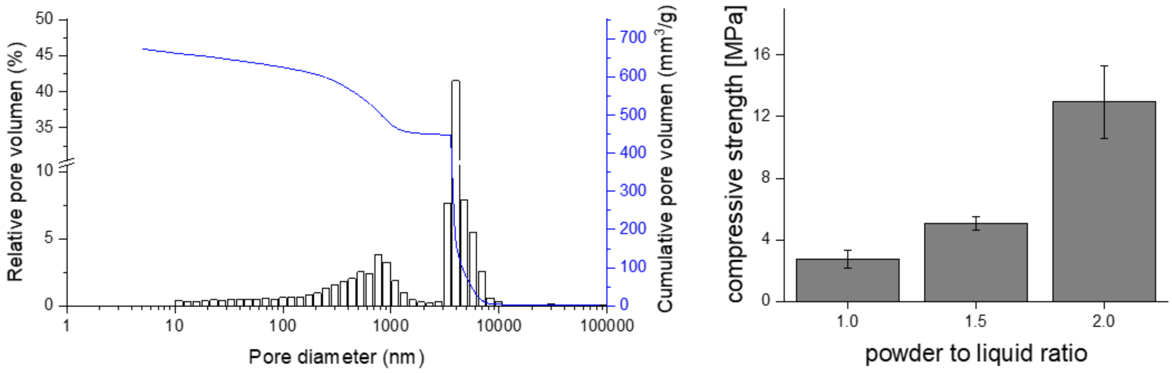

Figure 38: Pore size distribution (left, PLR=1 g/ml) and compressive strength (right) of brushite with TEOS as a reference for brushite-based silica composites with variation of silica-sol compositions.

The first composites were prepared with a TEOS substitution of 5%. 1,2-Bis(triethoxysilyl)ethane was chosen because it is still very similar to TEOS, but already has 2 more alkoxy groups and a small ethane spacer in the middle. The results (**Figure 39**) showed a slight tendency towards bimodal pore distribution, and the strength values increase with higher PLR, but the absolute values are worse than the cement reference except for PLR=1 g/ml.

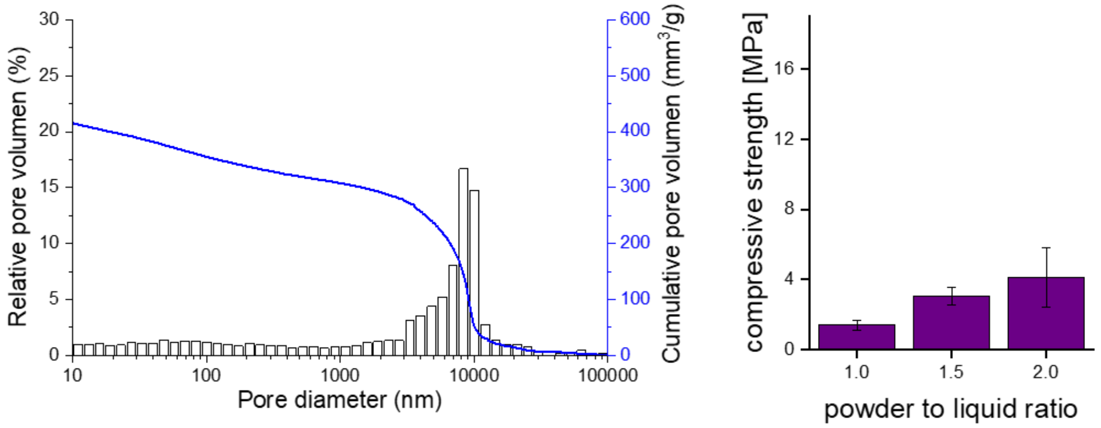

Figure 39: Pore size distribution (left, PLR=1 g/ml) and compressive strength (right) of composites of brushite with 95% TEOS and 5% 1,2-bis(triethoxysilyl)ethane.

Using a larger octane spacer with 1,2-bis(triethoxysilyl)octane, the bimodal pore distribution is again more pronounced and a significant increase in strength can be observed (**Figure 40**). This exceeds the TEOS-Brushite reference in any PLR and especially at PLR=1 g/ml this property is strongly improved.

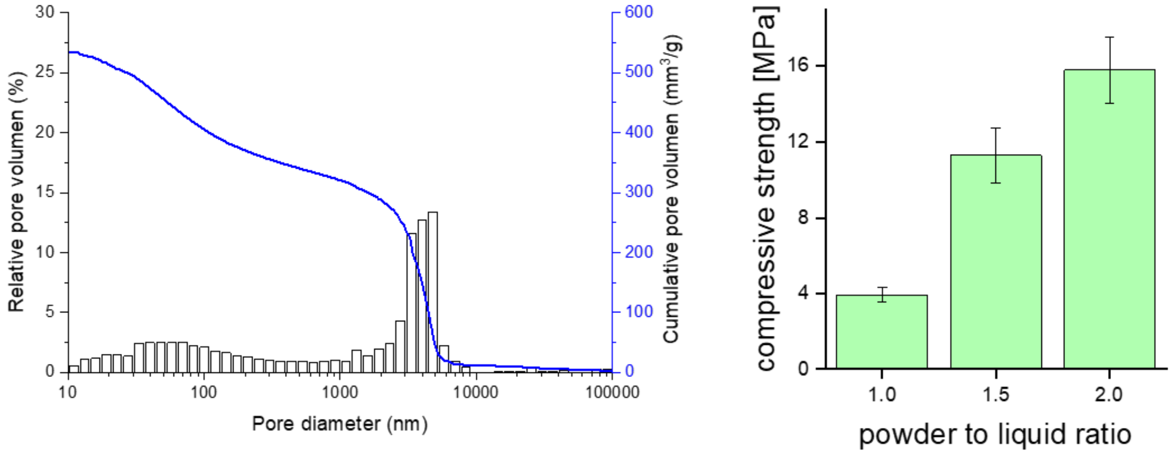

Figure 40: Pore size distribution (left, PLR=1 g/ml) and compressive strength (right) of composites of brushite with 95% TEOS and 5% 1,2-bis(triethoxysilyl)octane.

The influence of the silica molecules on the material should be further improved, which is why a comparably large precursor, P1, was used, which has a certain polarity due to two carbamate groups in the middle and thus has better hydrophilic properties compared to an octane core. The composites with 5% substitution by P1 show a pronounced bimodal pore size distribution and strongly increased strength values, as in **Figure 41**.

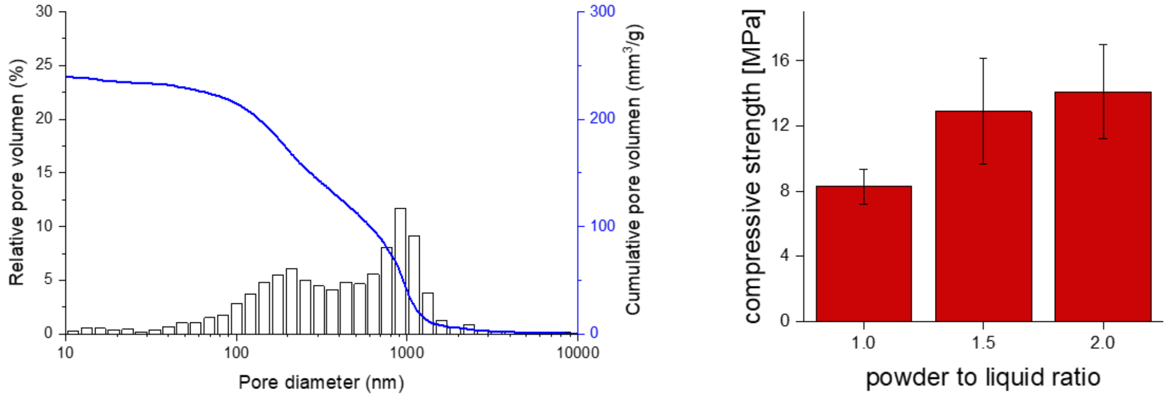

Figure 41: Pore size distribution (left, PLR=1 g/ml) and compressive strength (right) of composites of brushite with 95% TEOS and 5% P1.

The higher network density in the silica precursor leads to changes in the composite properties. In particular, the porosity in the nm-range was strongly influenced. With the increased ratio of new silica precursors, the total pore volume of the composites decreased. In addition, the combination of these two networks resulted in a significant higher compressive strength at PLR ≤ 2.0 g/ml.

Figure 42 shows the results of the brushite composites with TEOS substituted in sol by 40 mol% of the corresponding precursors. It is interesting to note that at these higher levels of sol modification, no strong tendency in pore variation is observed. Therefore, for the following study with baghdadite as cement system, the degree of substitution of TEOS by the precursors P1, P2 and P3 was set to 20mol %.

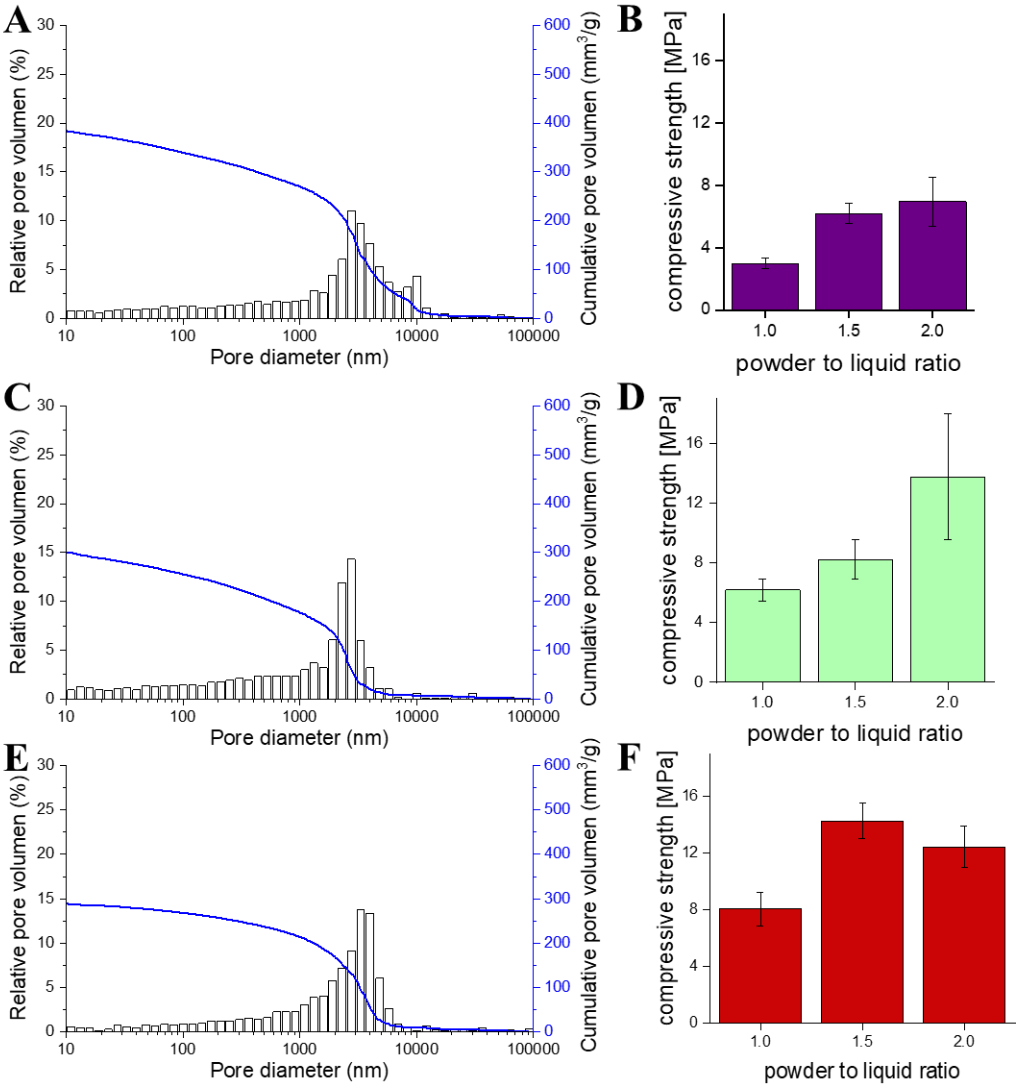

Figure 42: Pore size distribution (**A**, PLR=1 g/ml) and compressive strength (**B**) of composites of brushite with 60% TEOS and 40% 1,2-bis(triethoxysilyl)ethane. Pore size distribution (**C**, PLR=1 g/ml) and compressive strength (**D**) of composites of brushite with 60% TEOS and 40% 1,2-bis(triethoxysilyl)octane. Pore size distribution (**E**, PLR=1 g/ml) and compressive strength (**F**) of composites of brushite with 60% TEOS and 40% P1.

6.3 Silica sol variations combined with baghdadite cements

The sol for the dual-setting silica-baghdadite composites was prepared via the alkoxide pathway. In addition to the otherwise used aqueous pathway, this variant has the option of being initiated acidically or basicly. Important here is the presence of alkoxy silicates, such as the four ethoxy groups of TEOS. To modify the silicone network in the hybrid material, the sol precursor must be changed before gelation. For this purpose, three different precursors were prepared (**Figure 43**) which differ considerably in their complexity. Those precursors are a variation to TEOS, since they are larger, have more silica linkage points and have higher degree of branching. In addition, the newly used precursors are leading to carbamate groups after condensation which influence the properties of the sol and the resulting network even more.

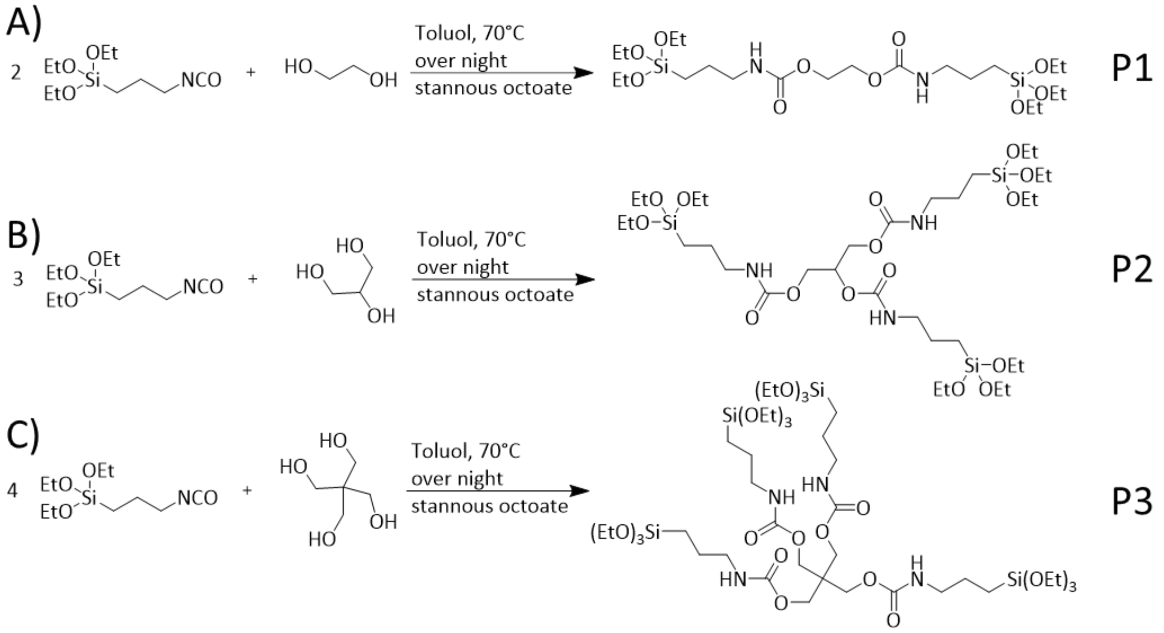

Figure 43: Synthesis scheme of branched silica precursors with ethyleneglycol (A, P1), glycerine (B, P2) and pentaerythrit (C, P3) as core molecule.

FT-IR spectroscopy was used to monitor the precursor synthesis and all spectra are shown in **Figure 44**. Comparing the reactant IR measurements with the respective product spectra, the shifts of relevant signals can be seen what concludes to be the result of successful reactions. The characteristic absorption peak at 2274 cm^{-1} of the asymmetric stretching vibration of the -NCO group is clearly visible for the isocyanate reactant, but this signal does not appear in the product, indicating that this reactant is fully reacted. In addition, the very large and broad peak from 3000 cm^{-1} to 3700 cm^{-1}, which can be assigned to an -OH group of the varying core reactant, disappears. In contrast, only a small signal around 3400 cm^{-1} is measured in the product spectrum, which can be assigned to the -NH group. In addition, after the reaction, a signal at 1640-1690 cm^{-1} arises which is caused by the carbonyl existent which is located in the newly formed carbamate group.

The remaining signals above the fingerprint region indicate CH_2/-CH_3 groups. these peaks appear in the range of 2960 cm^{-1} 2850 cm^{-1}. These observations can be applied to all three different precursor reactions.

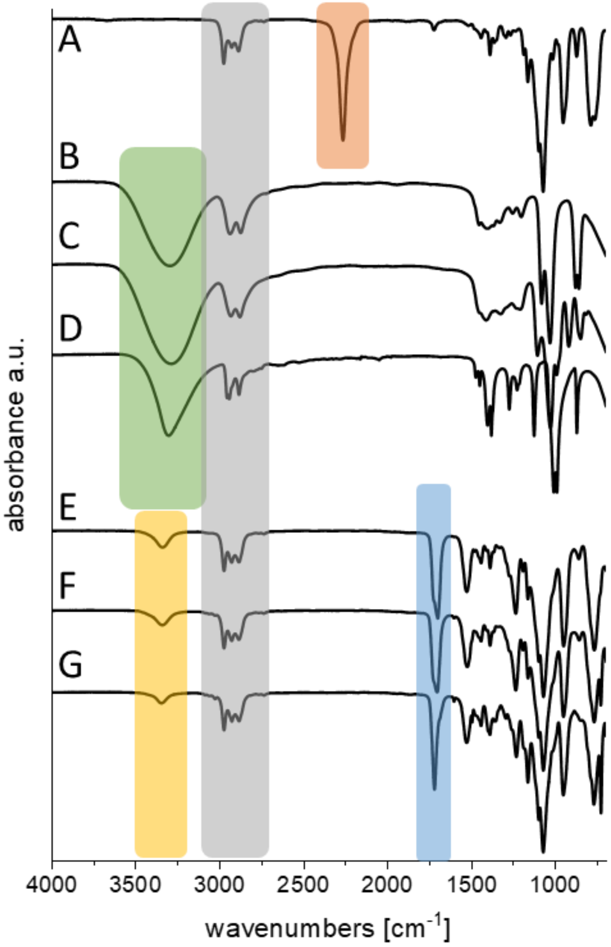

Figure 44: FT-IR spectra of the educts (A: 3-(Triethoxysilyl)-propylisocyanat, B: Ethyleneglycol, C: Glycerine, D: Pethtaerythrit) and products (E: P1, F: P2, G: P3) of the silica precursor synthesis (**Figure 43**).

Regardless of which precursors are used for the composites, the sol production follows a specific sequence. First, hydrolysis takes place at the alkoxy groups to form Si-OH groups which leads afterwards to silicone bonds (Si-O-Si) via a condensation reaction. The TEOS sol was modified by substitution with precursors P1, P2, and P3. Since the handling of a sol consisting of pure P1, P2 or P3 was not feasible, only a certain amount of TEOS was substituted. In these experiments, 20 mol-% of TEOS were replaced by the corresponding precursors.

The branched precursors with higher crosslinking capabilities were more difficult to handle in the mixing process right before setting. The dual-setting composites solidified very quickly and could therefore only be processed for a short time. The addition of citric acid monohydrate (2 wt%) to baghdadite powder prior to the reaction helped to some extent to solve this problem. The variation of powder to liquid ratio was limited, so that PLR 1 g/ml, 1.5 g/ml and 2 g/ml were investigated. For PLR 2.5 g/ml and higher, it was not possible to produce dual-setting test specimens.

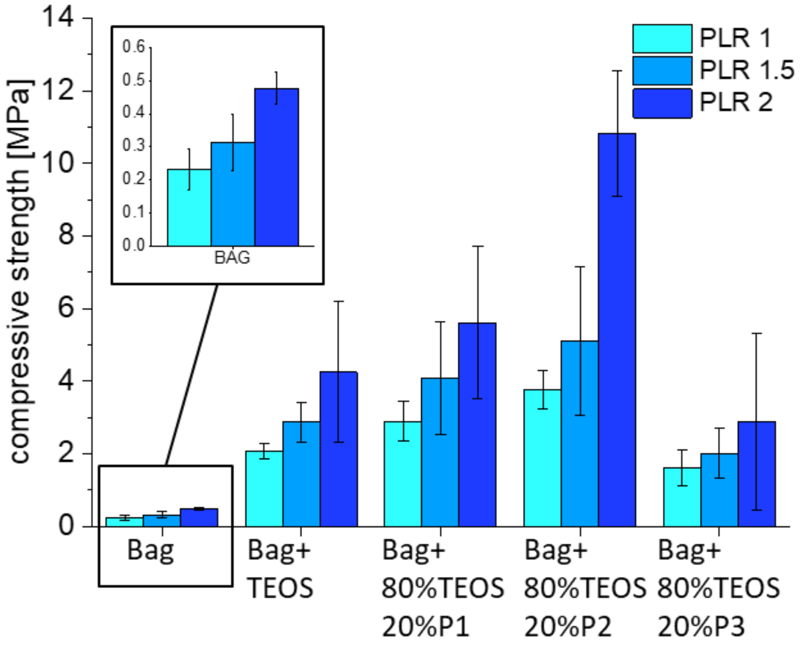

Figure 45: Compressive strength of baghdadite and TEOS dual-set composite. Also measurements with of composites with 20% of TEOS substitution with novel precursors (P1, P2, P3) were carried out. PL ratios were 1 g/ml,1.5 g/ml and 2 g/ml.

Mechanical testing (**Figure 45**) for compressive strength determination was carried out with the composites as well as pure baghdadite, which was mixed with distilled water only, and baghdadite, mixed with TEOS-Sol. This study was aimed at the initial problem of weak mechanical properties of pure baghdadite as a cement, and the results showed well the possibility of the immense influence of a second network. With the different PLRs of the baghdadite reference, no strength values above 1 MPa could be obtained. The trend of an increased strength with higher PLR could be verified.

For the baghdadite silica composites, positive reinforcing effects can be observed. Comparing the values of the modified sol compositions, the most branched precursor P3 with the highest number of binding sites, has the worst strength. For a TEOS substitution of 20% by P3, the sol suffers from the attempted optimization and it is difficult to process. This leads to a minor beneficial effect and the selected precursor P3 is not a viable option for further investigation. In contrast, very comparable compressive strength results to the dual-setting reference were obtained for P1 and P2 in each substitution variant. For further analysis of the samples only specimen with a PLR of 1.5 g/ml were used.

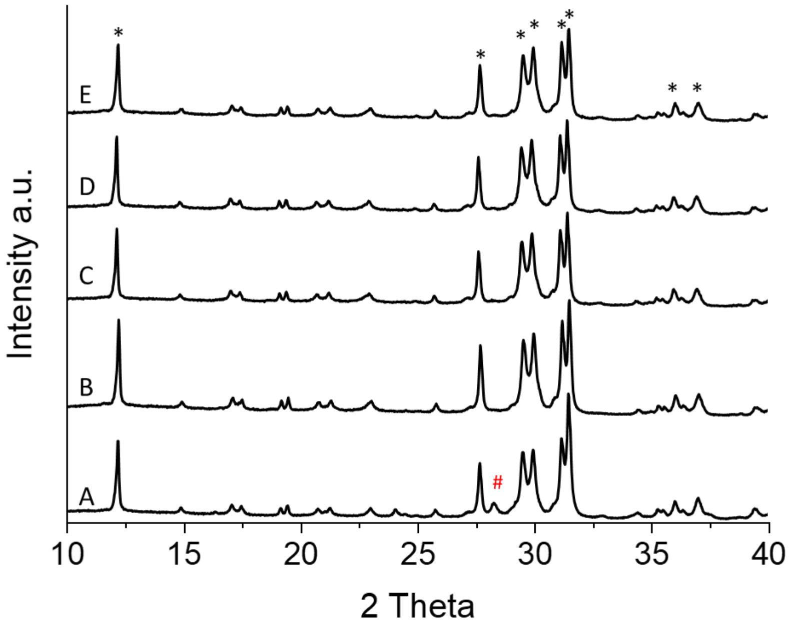

Figure 46: X- ray diffractograms of A) BAG, B) BAG+TEOS, C) BAG + 80%TEOS/ 20%-P1, D) BAG + 80%TEOS/ 20% P2 and E) BAG + 80%TEOS/ 20%-P3. Each sample was prepared at a PLR = 1.5 g/ml. (* = Baghdadite, # = Baddeleyite).

For the evaluation of the X-ray diffractograms (**Figure 46**), it should be emphasized that all composites gave a similar diffractogram with same signals. In each case, a baghdadite content of >95% of the crystallite content was calculated by Rietveld analysis. A more detailed overview for the calculate crystalline phases as well as the amorphous phases can be seen in **Table 7**.

The baddeleyite (ZrO_2, monoklin) signal only appears in the baghdadite reference measurement. This suggests that due to the addition of silica sol, the corresponding cement phase is prevented from forming in the composite. The cubic ZrO_2 Phase is not affected by the presence of the silica matrices.

Table 7: Phase composition of bag and bag-silica composites with calculated amorphous content.

	Baghdadite	ZrO$_2$	Baddeleyite	C2S	Amorphous
BAG	49%	1%	2%		48%
BAG+TEOS	55%	1%			44%
BAG + 80%TEOS/ 20%-P1	45%				54%
BAG + 80%TEOS/ 20% P2	47%	1%		1%	51%
BAG + 80%TEO/S 20%-P3	48%	1%			50%

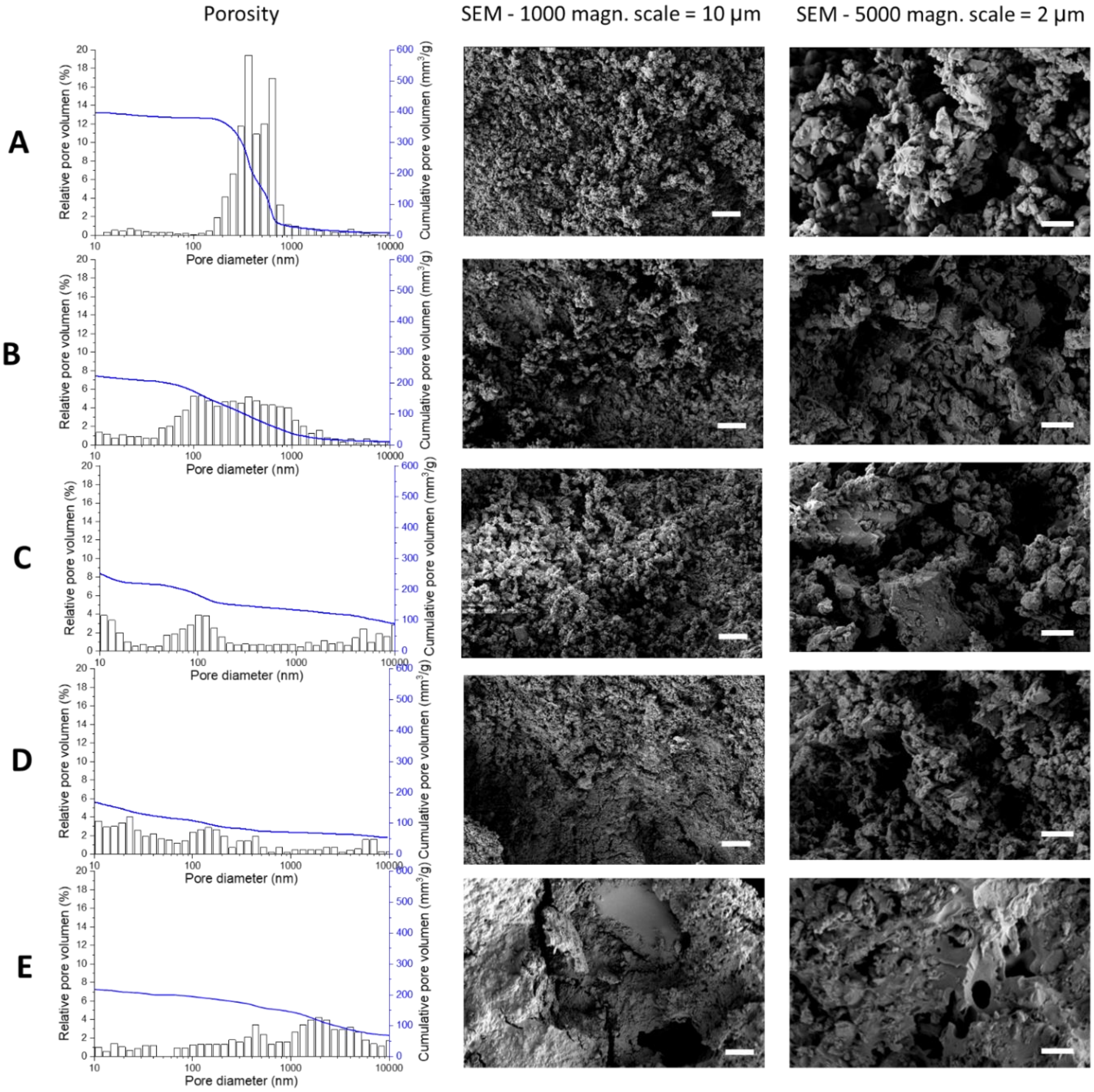

Figure 47: Porosity and SEM images of A) BAG, B) BAG+TEOS, C) BAG + 80%TEOS/ 20%-P1, D) BAG + 80%TEOS/ 20% P2 and E) BAG + 80%TEOS/ 20%-P3. Each sample was prepared at a PLR = 1.5 g/ml.

Mechanical properties are also dependent on the porosity of the material. The distribution of their pores is shown in **Figure 47** together with associated SEM images at two different magnitudes. The BAG reference has a monomodal pore size distribution in the range of (300-400 nm), but the distribution changes with the different BAG-silica composites to a more diffuse distribution whereby a clear trend is difficult to identify. The silica matrix influences the material to smaller pores and a ~ 50% decreased total porosity. The SEM images in **Figure 47** show a homogeneous morphology for all samples. Only the surface of BAG + 80%TEOS /20%-P3 is more cracked and shows some glass like areas. These are consequences of the high silica content in the material what leads to a more pronounced aging.

The porosity can also qualify materials for an application as drug delivery scaffolds. Drug release can be based on diffusion and the kinetics is controlled via the pore distribution in the material. This local application of the medication prevents the patient to be treated systemically. That way lower doses can be used, reducing the chance of side effects. Since baghdadite can be used as a bone graft, it should be considered to use drug loaded baghdadite cements. However, it can be assumed that, as with other cements, a burst release of the drug occurs with untreated baghdadite cement. It is known from the literature that a dual setting approach can overcome the problem of burst release. To investigate this assumption, the glycopeptide antibiotic vancomycin was used as model drug. Drug loading of the composites was achieved by adding vancomycin (5wt%) powder to baghdadite powder prior to the dual-setting process. The mixing of the solid phase together with the sol was noticeably liquefied by the additive and was much easier to process than without. No release profile could be observed for the drug loaded baghdadite, since the cement had already broken down after one hour. The silica composites, on the other hand, retained their shape well. With a network composed only of TEOS monomers, a slowdown of the burst release can be observed, as expected. The composites with silica networks consisting of several precursors have a release profile that deviates strongly from the standard saturation model and shifts to a more linear release. A massive inhibition of the initial drug release is observed for the composites. For the 10 mol% P2, 20 mol% P2 and 30 mol% P2 series of experiments, the overall release is more inhibited with increasing branched precursor content.

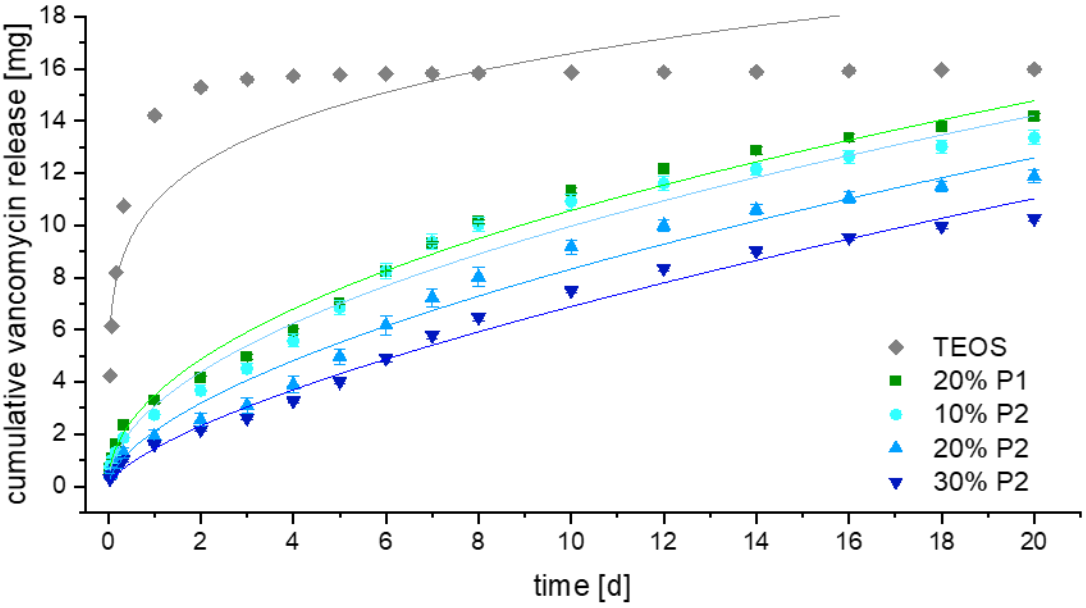

Figure 48: Vancomycin release profile of drug loaded composites for a time period of 20 d. The discrepancy between the experimental data and the fit curves results from the validity limited to 60% of the cumulative release amount of the Korsmeyer-Peppas model.[365]

Based on Fick's diffusion laws, Higuchi in 1961 developed a model, which describes the release of active ingredients from planar matrices with homogeneously dispersed drug or suspension ointments. The Higuchi model (Eq. 17) assumes that the drug concentration in the matrix must be significantly greater than the saturation solubility of the active ingredient in the solvent. In addition, for the determination of a constant diffusion coefficient, it is necessary that the matrix is inert and the structure does not change during release.

$$Q = K_H t^{1/2} \qquad \text{Eq. 17}$$

Q = cumulative release quantity

k = kinetic constant

t = release time

Based on the 2nd Fick's diffusion law, Korsmeyer et al. (1983) and Peppas et al. (1985) developed a semiempirical model related to release kinetics (Eq. 18). Assuming perfect sink conditions, a homogeneous initial drug loading, mass transfer depends on the concentration gradient between the loaded material and the solvent.

In contrast to the Higuchi model, Korsmeyer and Peppas consider the influence of polymer swelling and polymer degradation on drug release. Swelling systems have an effect on diffusion distance and molecular mobility, which is not relevant to this study.

$$M_t/M_\infty = kt^n \qquad \text{Eq. 18}$$

M_t = cumulative mass released at time t (in mol)

M_∞ = cumulative mass released at time $t \rightarrow \infty$ (in mol),

k = kinetic constant (in s^{-n})

n = release exponent.

The release exponent n characterizes the different release mechanisms depending on the geometry of the specimen. A distinction is made in the literature[365] between thin dense, cylindrical and spherical shapes. For the evaluation, the determined release exponents were compared with those of the cylinder, since this shape corresponds most closely to the sample body. The transport mechanism is described for n= 0.45 as being diffusion controlled (Case I), for values above 0.89 the mechanism proceeds according to "non-Fickian diffusion" (Case II transport, controlled) and for $0.45 < n < 0.89$ anomalous transport is assumed. This means that the mechanism is not clearly attributable to Case I or Case II and is therefore considered to be a superposition of both mechanisms. The discrepancy between the experimental data and the fit curves results from the validity limited to 60% of the cumulative release amount of the Korsmeyer-Peppas model.

Excluding the reference measurement with TEOS, the release exponent for all measurements is in the range of 0.483 -0.679. Each measured release is therefore assigned to an anomalous drug transport. The exact evaluation and values of the kinetic constant and release exponent are listed in **Table 8**

Table 8: Kinetic constant, release exponent and R^2 determined with Eq. 18 of the release study.

	K [s^{-n}]	**n**	**R^2**
TEOS	10.85	0.184	--
20%P1	3.477 ± 0.019	0.483 ± 0.002	0.9979
10%P2	3.071 ± 0.167	0.511 ± 0.022	0.9883
20%P2	2.104 ± 0.169	0.597 ± 0.030	0.9905
30%P2	1.440 ± 0.095	0.679 ± 0.026	0.9896

Additionally, evaluation with zero-order kinetics was used for the area after the burst release (3d-8d), since this allows the time-depending continuous release to be adequately demonstrated. This model follows the linear equation model and the evaluation shows that with TEOS from day 3 onwards, an extremely low release of vancomycin with a release constant of 0.045 can be measured. The composites with varied precursors show linear kinetics in the range from 3d to 8d of release with constants between 0.77 to 1.15, and R^2 values above 0.995 in each case.

As the initial release decreases, the concentration of the absolute released drug decreases accordingly. To check whether the lower concentrations still have sufficient influence on bacteria, inhibition zone tests were carried out. The diffusible antibacterial drug can diffuse from the test body into the agar and prevent bacterial growth in this area. After an incubation time of 24 hours at 37 ° C, the zone of inhibition, i.e. the bacteria-free zone around the sample, is measured and compared to a control. For this test baghdadite, baghdadite + vancomycin, baghdadite+ TEOS+ vancomycin, baghdadite+ 80% TEOS/ 20% P1+ vancomycin and baghdadite+ 80% TEOS/ 20%P2 + vancomycin were chosen as samples and the results can be seen in **Figure 49** (A-E). The test pieces of baghdadite (**Figure 49** A) show no zones of inhibition and thus no anti-microbial effect on *Staphylococcus aureus* after the first and after the second 24 h incubation period.

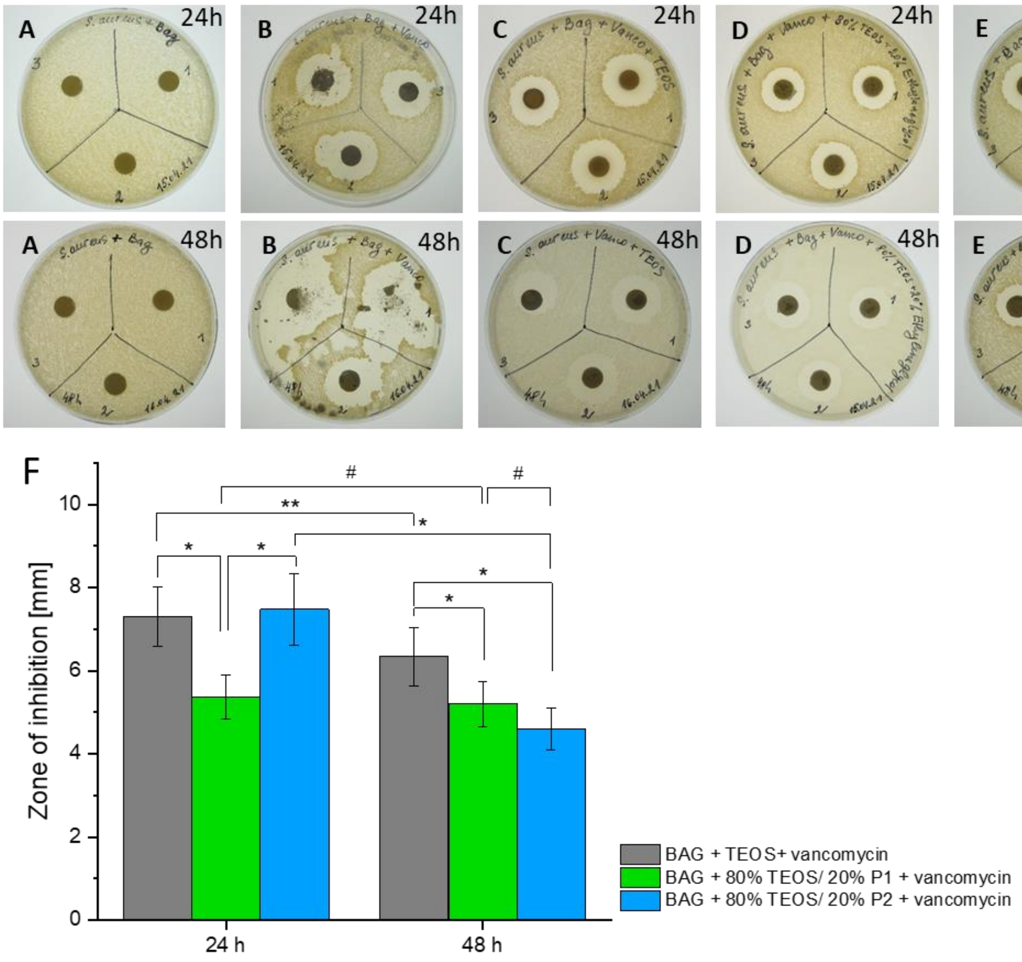

Figure 49: **A-E**:Inhibition zones of the samples A (baghdadite), B (baghdadite + Vancomycin), C (baghdadite + TEOS+ vancomycin), D (baghdadite +80% TEOS/ 20% P1+ vancomycin) and E (baghdadite + 80% TEOS/ 20%P2 + vancomycin) after 24 hours (upper row) and after 48 hours (lower row). **F**: Evaluation of the zones of inhibition of baghdadite + TEOS+ vancomycin, baghdadite + 80% TEOS/ 20% P1 + vancomycin and baghdadite + 80% TEOS/ 20% P2 + vancomycin after 24 hours and after 48 hours. * $p < 0.001$, **$p = 0.008$, # = no significant difference.

The specimens of the samples baghdadite+ TEOS+ vancomycin (**Figure 49** C), baghdadite+ 80% TEOS/ 20% P1+ vancomycin (**Figure 49** D) and baghdadite+ 80% TEOS/ 20%P2 + vancomycin **Figure 49** E) show transparent zones of inhibition as a clear anti-microbial effect on *Staphylococcus aureus* both after the first and after the second 24 h incubation period The extent of the zones of inhibition was determined by means of 4 measurements per test specimen on the original plates. The test specimens of baghdadite + vancomycin (**Figure 49** B) also show transparent areas with inhibited bacterial growth, but these test specimens fell apart crumbly during incubation in the incubator: After 24 h one of three test specimens were affected, after 48 h all 3 test specimens crumbled. Due to the lack of a clear delimitation of these test specimens, they were not taken into account in the inhibition zone calculation. All of the tested specimens, which contained the antibiotic vancomycin, inhibited bacterial growth. Samples of the cement without antibiotic did not show this effect. The area of the respective inhibition was determined semi-quantitatively by measuring the inhibition zone and comparing it with the positive controls (filter papers with different vancomycin concentrations).

Similar drug release studies with 1 wt%,3 wt% and 5 wt% of vancomycin in baghdadite ceramics have been reported by Bakhshesi-Rah et al. [213] and they could show that against *Staphylococcus aureus* the infection risk decreased with higher drug concentration. The scaffolds were produced using the space holder method and the release was observed up to 60 hours with no signs of a prolonged release.

6.4 Conclusion

This study demonstrated that dual setting composites can be produced from baghdadite and various silica precursors. Such cements showed an improved mechanical performance with compressive strength in the range 1.6 – 10.8 MPa, depending on the amount and chemical structure of the precursors. Limitations appeared regarding the fast gelation reaction of branched silica compounds which were only processible at low PLR ≤ 2 g/ml. Furthermore, the pore size distribution was altered by silica addition such that the release of vancomycin was retarded due to smaller pores, although the total porosity of these cements decreased by ~ 50%. Despite the harsh reaction conditions during cement setting, the released drug was proven to have strong antimicrobial effects against a culture of *S. aureus*.

Possible applications for these materials could be temporary fillings in infected bone bedding or for bone replicas as cancellous bone. For load-bearing tissues, it is conceivable to combine the material with established bone cements to further strengthen it.

Chapter 7

Materials and methods

This Chapter 7 includes some parts of the previously mentioned reused articles from Chapter 4 and 5 as well as some unpublished parts from the manuscript mentioned in Chapter 6.

No, Y.J.; Holzmeister, I.; Lu, Z.; Prajapati, S.; Shi, J.; Gbureck, U.; Zreiqat, H. Effect of Baghdadite Substitution on the Physicochemical Properties of Brushite Cements. Materials 2019, 12, 1719

Holzmeister, I., Weichhold, J., Groll, J., Zreiqat, H. and Gbureck, U. (2021), Hydraulic reactivity and cement formation of baghdadite. J. Am. Ceram. Soc., 104: 3554-3561.

Synthesis of brushite cement and baghdadite-substituted brushite cement

β-tricalcium phosphate (β-TCP; β-$Ca_3(PO_4)_2$) was synthesized by heating a mixture of Dicalcium phosphate anhydrous (CaHPO4, Mallinckrod-Baker, USA) and calcium carbonate (Merck, Germany) in a 2:1 ratio to 1100 °C for 5 h. The sintering cake was crushed and ball-milled for 1 h with a planetary ball-mill (PM400, Retsch, Germany) to a final medium particle size d_{50} of 14.5 µm.

Baghdadite ($Ca_3ZrSi_2O_9$,) powder was synthesized by mixing zirconium oxide (45.2 g, Sigma, Germany), calcium carbonate (122.3 g, Merck, Germany) and silica (49.3 g, Sigma, Germany) for 2 h in a ball mill (Retsch PM400, Germany). The powder mixture was sintered at 1400°C for 3 h, followed by mortar and pestle crushing and ball-milling for 30 min to obtain a particle size d_{50} of approximately 2.68 ± 0.9 µm.

Unmodified brushite cement (BC) samples were prepared by mixing equimolar amounts of β-TCP and monocalcium phosphate anhydrous ($Ca(H_2PO_4)_2$), MCPA, Budenheim, Germany; d_{50} = 21.1 µm); for the cement samples modified with baghdadite, the β-TCP reactant was subsequently replaced with baghdadite i.e. 5 wt%, 10 wt%, 20 wt%, 30wt%, 50wt% and 100wt%, and the final cements were labelled as BCB5, BCB10, BCB20, BCB30, BCB50, and BCB100, respectively, as detailed in **Table 9**. Freshly prepared 0.1 M sodium pyrophosphate (NaPP, Sigma Aldrich) solution was added to the reaction mixture as a setting retardant in order to increase the handling period without negatively affecting its cytocompatibility [302]. The powders were mixed with the NaPP solution at a powder-to-liquid ratio of 3.0 g/mL on a glass slab using a spatula, poured into appropriate moulds for cement characterization, and allowed to set at 37°C and 100% relative humidity for 24 h.

Table 9: Composition of the powder reactants per gram for each cement formulation investigated in this study.

Baghdadite/ [Baghdadite + β-TCP] (wt%)	β-TCP (g)	MCPA (g)	Baghdadite (g)	Code
0	11.04	8.31	0.000	BC
5	10.48	8.31	0.56	BCB5
10	9.92	8.31	1.12	BCB10
20	8.82	8.31	2.24	BCB20
30	7.70	8.31	3.36	BCB30
50	5.52	8.31	5.52	BCB50
100	0	8.31	11.04	BCB100

Mechanical activation of baghdadite powder

The process of mechanical activation was carried out by further high energy ball-milling of the baghdadite raw power (particle size d_{50}: 2.68 ± 0.9 µm) in isopropanol for 2, 4, 8, 16 and 24 h. Baghdadite cements were obtained by mixing the powders at different milling times with distilled water in a powder to liquid ratio (PLR) of 2 g/ml. The cement pastes were poured into rectangular silicone molds of 12 × 6 × 6 mm and left to set in 100% humidity at 37°C for 3 days.

Precursor 1 (P1) synthesis

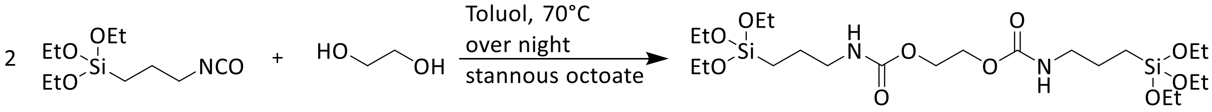

Under nitrogen atmosphere 1 ml (17.88 mmol, 3 eq) of ethyleneglycol and 8.85 ml (35.76 mmol, 6 eq) of 3-(triethoxysilyl)-propylisocyanat as well as 40 ml of dried toluene were first added to an ice-bath cooled 2-necked flask carried with a magnetic stirrer and reflux condenser. Then stannous octoate (0.2wt%) was added to the solution and heated up to 75°C and maintained heated for 24h. After being cooled to room temperature, the solvent was removed with a rotary evaporator to obtain a beige liquid with a high viscosity.

Precursor 2 (P2) synthesis

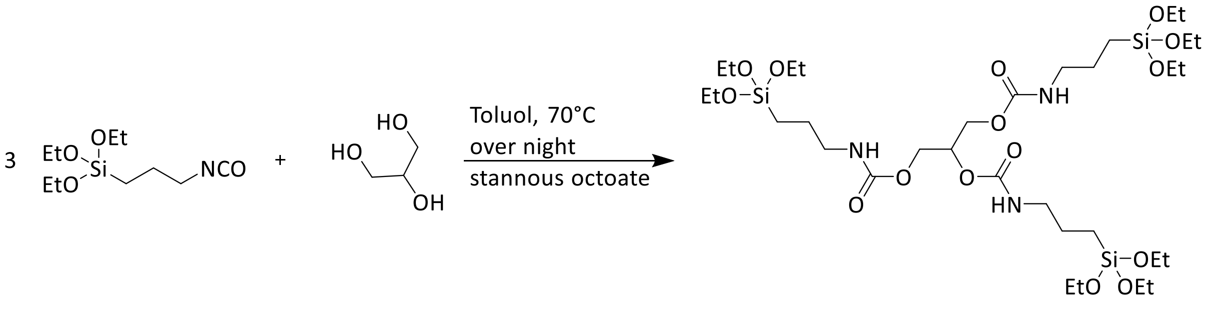

This synthesis followed the same protocol as P1-synthesis, except 2 equivalents of glycerine were used together with 6 equivalents of 3-(triethoxysilyl)-propylisocyanat.

Precursor 3 (P3) synthesis

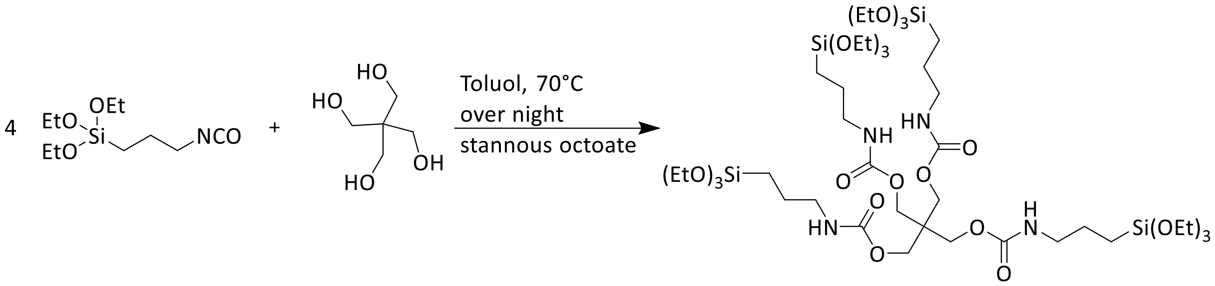

For this synthesis 3 equivalents of pentaerythrit and 12 equivalents of 3-(Triethoxysilyl)-propylisocyanat as well as 60 ml of dried toluene were processed following the P1-synthesis protocol.

Sol synthesis and composite preparation

To initiate the sol gel process, the sol precursors (TEOS, P1, P2, P3) were mixed with 0.1 M HCl and distilled water. The ratio of water to Si-OEt groups was set to 2.25. The acid catalyzed sol was mixed with baghdadite powder as soon as there was no more phase separation between the precursor phase and the water phase. The mixed pastes were poured into rectangular silicone molds of 12 × 6 × 6 mm and left to set in 100% humidity at 37°C for 3 days.

The silica precursor combinations can be seen in **Table 10**. Pure TEOS so was used with both bushite and baghdadite powder. The commercially available precursors and P1 were used as TEOS substitution of 5% as well as 40 % with brushite. The three synthesized precursors P1, P2 or P3 substituted TEOS by 20% for composites with baghdadite. The combinations of TEOS with 10%/ 30% substituted with P2 were additionally used for drug release tests in baghdadite.

Table 10: Amount of substituted precursor for corresponding cement systems.

	Substitution	**Cementphase**
1,2-Bis(triethoxysilyl)ethane	5%	Brushite
	40%	Brushite
1,2-Bis(triethoxysilyl)octane	5%	Brushite
	40%	Brushite
P1	5%	Brushite
	40%	Brushite
	20%	Baghdadite

	Substitution	Cementphase
P2	20%	Baghdadite
P3	10%	Baghdadite
	20%	Baghdadite
	30%	Baghdadite

X-ray Diffraction Analysis of Cements and Composites

X-ray diffraction measurements were performed with a D8 Advance with DaVinci design (Bruker AXS, Karlsruhe, Germany) at 40 kV and 40 mA. The measurement parameters were set to a 2Theta range of 10–70°, step size 0.02°, a scan speed of 0.5 s per step and a 0.25° divergence slit. During the measurement a sample rotation was set to 15 min^{-1}. The evaluation tool Diffrac.EVA (Bruker, Germany) was then used to qualitatively determine the phase composition of the cements. With the as obtained XRD measurements Rietveld refinements and an external standard method called the G-factor method were performed to determine the quantitative phase content [337]. The Structures of all phases (ICSD #79453 baghdadite [211], ICDD #330302 beta-C_2S , ICDD # 270997 ZnO_2 cubic, ICDD #371484 ZnO_2 monoclinic) determined with Diffrac.EVA were used together with a Chebychev polynomial of the tenth order for the background to refine the parameters scale factor, lattice parameters, crystallite size and microstrain in the Software Diffrac.TOPAS (Bruker Germany). The values obtained by this refinement were then used to calculate the true crystalline content of the present phases and the amount of amorphous content of the cement via the G-Factor method. As internal standard for these calculations, a second set of powders with the addition of 20 % crystalline alpha-corundum (Baikowski, Regular CR1) was measured.

Compressive mechanical properties

The cement pastes were poured into rectangular molds of 12 × 6 × 6 mm and set in the molds at 37 °C in 100% humidity for 3 days. A universal testing machine (Roell Z010, Zwick, Ulm, Germany) equipped with a load cell of 10 kN was used for the compressive strength measurement of the cements (n=8 – 12) at a compression rate of 1 mm/min. The compressive strength σ (MPa) was determined by dividing the maximum force F_{max} (N) by the cross-sectional area A (mm^2) of the specimens. (Eq. 19)

$$\sigma = \frac{F_{max}}{A} \qquad \text{Eq. 19}$$

The Young's modulus E (Eq. 20) can be derived from the stress-strain diagram by calculating the ratio of mechanical stress change dσ (MPa) to strain dε. Ideally, the change is linear and the E modulus accordingly represents the slope.

$$E = \frac{d\sigma}{d\varepsilon} \qquad \text{Eq. 20}$$

Microstructure and radiopacity of cements

Solid disks of set brushite and baghdadite-substituted brushite with a diameter of 20 mm and a height of 2 mm were prepared for radiopacity analysis by pouring the cement pastes into smooth silicon rubber moulds, left to set for 30 min, then removed from the molds and subsequently immersed in milliQ deionized water for 1 day at 37°C for further setting. For radiopacity, the solid cement disks with a thickness of 2.0 mm were scanned using dental X-ray machine (Heliodent DS, Sirona, Germany) at x-ray energy of 70 keV together with an aluminium stair with a stepsize ranging from 0.5-5.0 mm in 0.5 mm steps. The greyscales of the samples in the obtained images were calculated using image analysis software (ImageJ), and were compared to the greyscales of the aluminium stair to calculate the aluminium equivalent thickness according to ISO 4049. In addition, the solid cement disks were scanned using microcomputed tomography (Xradia MicroXCT-400) at x-ray energy of 70 keV. The greyscales of the samples in the obtained CT images were calculated using image analysis software (ImageJ), and were calibrated to the greyscales of air and water to obtain the Hounsfield units (HU) of each sample. According to definition, air is -1000 HU, whereas water has a value of 0 HU. For scanning electron microscopy, the hardened cement pieces from compressive strength testing were mounted onto stubs and the fracture surfaces were sputter coated with platinum, and subsequently examined under a scanning electron microscope (Zeiss CB 340, Carl Zeiss Microscopy GmbH, Oberkochen, Germany). Element maps for calcium, phosphorous, zirconium and silicon were recorded with an attached energy-dispersive X-ray spectroscope (EDS) (XMaxN, Oxford-Instruments, Wiesbaden, Germany) and evaluated with the associated software AZtec (Oxford-Instruments, Wiesbaden, Germany).

SEM / EDX Analysis

Cement fragments were coated with a 3 nm platinum layer (ACE600, Leica, Wetzlar, Germany). SEM images were taken with secondary electrons and an acceleration voltage of 2kV (Crossbeam 340, Zeiss, Oberkochen, Germany). Element maps for calcium, phosphorous, zirconium, oxygen and silicon were recorded with an energy-dispersive X-ray spectroscope (EDS) (XMaxN, Oxford-Instruments, Wiesbaden, Germany) and evaluated with the attached software AZtec (Oxford-Instruments, Wiesbaden, Germany).

Investigating primary human osteoblast cytocompatibility

These experiments were performed by the cooperation partners at the Biomaterials and Tissue Engineering Research Unit, University of Sydney. Based on the results of the previous experiments, BC, BCB5, BCB10, and BCB20 were chosen for assessment of cytocompatibility. The cytocompatibility of BC, BCB5, BCB10, and BCB20 on primary human osteoblasts (HOB) was investigated using cytotoxicity tests outlined in ISO/EN 10993-5. Permission to use discarded human tissue was granted by the Sydney Children's Hospitals Network Human Research Ethics Committee (reference code: HREC/14/SCHN/36) and informed consent was obtained. Human trabecular bone was used for isolating HOB as described previously [35]. The cells were cultured at 37 °C with 5% CO_2, and culture medium was changed every three days until cells were passaged at 80-90% confluence. All HOBs used in the experiments were at passage 2. Firstly, BC, BCB5, BCB10, and BCB20 cements were prepared, set in cylindrical moulds of 15 mm diameter and 10 mm thickness, and left to further hydrate in deionized water at 37^oC for 1 day. The set cements were then removed and crushed using mortar and pestle. The cement powders were then immersed in serum-free α-MEM culture medium at a ratio of 200 mg in 1 mL culture medium and left to incubate at 37 °C for 7 days. After incubation, the mixture was centrifuged to separate the culture medium and the cement powders. The extracted culture media were then sterilized by filtration (0.22 μm), and 10 v/v% of fetal bovine serum and 1 v/v% penicillin/streptomycin solution were added to make complete media and used for the HOB culture. The pH of the conditioned media was then obtained by isolating 5 mL of each conditioned media and recording its pH using a pH electrode, and the ionic content of the conditioned culture media was collected and analysed using inductively coupled plasma atomic emission spectroscopy (ICP-AES; Perkin Elmer, Optima 3000DV, USA).

HOB were seeded at a density of 1.0×10^3 cells cm^{-2} into 48-well plates and incubated in 200 μl of prepared media for 24 h. Cells were then incubated at 37 °C in 5% CO_2 for 1 and 7 days. Viable cell numbers were evaluated at appropriate time intervals using the MTS assay (Promega, Madison, WI) according to the manufacturer's instructions. At the predetermined time point, the culture medium was removed, and then 100 μl of MTS assay solution was added to each well and was incubated for 4 h at 37 °C. The MTS assay produces an insoluble compound called formazan proportional to the number of live viable cells. The absorbance of the formazan was read at 492 nm using a microplate reader and graphed in Microsoft Excel. Four samples were used for each time point per cement group.

Particle size distribution

For each sample three independent measurements were taken from the different powders to determine the particle size by laser diffraction (LA 300, Horiba, Kyoto, Japan). All powders were suspended in isopropanol and placed for 5 minutes into an ultrasonic bath prior measurement.

Differential thermal analysis (DTA) & thermogravimetry (TG) measurements

For DTA&TG measurement, the powder was placed in platinum crucibles and measured under an N_2 protective gas atmosphere at a flow of 70 ml/min (STA 449 F5 Jupiter Netzsch, Selb, Germany). Data was obtained for a temperature range of 30-1000 °C with a heating rate of 10°C/min. The DTA uses characteristic energy conversion during the phase transition for qualitative and quantitative analysis. The measurement is based on a comparison of the temperatures of the sample and a reference substance (magnesium oxide) in a second chamber. With constant heating, the temperature is measured via sensors and the difference is recorded. In the case of phase transitions, temperature difference appears, and conclusions about the composition of the sample can be drawn.

For TG the mass of the sample is recorded continuously during the measurement. The mass change can then be plotted as a function against temperature or time.

Porosity and pore size distribution

Porosity size distribution was measured on hardened cement fragments by mercury porosimetry (Mercury Intrusion Porosimeters Pascal 140 and 440 Thermo Fisher Scientific, Italy), These cement samples were placed in a dilatometer, and after evacuation, it was filled with mercury and gradually applied a pressure range of 0.01 to 400 kPa. In the second measuring cycle, the same mercury-filled dilatometer is used, and a higher-pressure range was applied (0.1 to 400 MPa). Subsequently, the two individual measurements were combined with the associated software "Solid" to obtain a complete pore size distribution range from 10 nm to 10000 nm.

^{29}Si-NMR measurements

Additionally, ^{29}Si-NMR measurements were performed on both powder and cement samples using a NMR spectrometer (Advance NEO WB 400 MHz, Bruker AXS, Karlsruhe, Germany). The scans where performed with a recycle delay of 120sec and a 30°-pulse to shorten the waiting time until the magnetization builds up again. The acquisitions time was set to 40ms. The evaluation and deconvolution of the data was done by the Topspin 4.0.8 (Bruker, Germany) software.

ICP-MS measurements

Ion concentrations (Ca, Si and Zr) in the used media (milliQ water & cell culture) were determined using inductively coupled plasma mass spectrometry (iCAP RQ ICP-MS, ThermoFisher Scientific, Waltham, USA). Quantitative results for all ions of interest were obtained by measuring against standard solutions with defined concentrations of 5 and 10 mg/l (Merck, Darmstadt, Germany).

Ultraviolet–visible spectroscopy (UV/Vis)

Vancomycin drug release was measured with a Thermo Scientific GENESYS 10S UV-Vis Spectrophotometer. Loaded sample pieces (rectangular shape, 12 × 6 × 6 mm) were stored in 5 ml PBS at 37 ° C with constant shaking for certain time intervals. Initially, the PBS solution was changed more frequent (after incubation time of 1h, 1h, 2h, 4h, 16h), then it was changed every 24h. The reference point for the measurement was the absorption maximum at 281 nm. The concentrations were calculated for each solution using a calibration line.

Fourier transform infrared spectroscopy (FT- IR)

FT-IR measurements were carried out via a Nicolet iS10 with Smart iTR with diamond ATR unit from Thermo Scientific. The scan range covers 4200 -650 cm^{-1}.

Test for antimicrobial effect (inhibition zone testing)

The test specimens (round, 1 cm diameter, 3-4 mm high) were sterilized by means of gamma irradiation. The used petri dishes had a diameter of 10 cm and were approx. 0.5 cm high filled with a heated solution of 1% agar in LB (lysogeny broth) medium. After the agar has hardened in the dish, bacteria (*Staphylococcus aureus* ATCC 6538) are evenly plated and three samples are distributed on it. The zones of inhibition were measured after an incubation time of 24 hours at 37 °C. This process was repeated with the used samples to measure the zones of inhibition after 48 hours.

Statistical Analysis.

All data in Chapter Chapter 4 are expressed as mean ± standard deviation (SD). For statistical analysis, Levene's test was performed to determine the homogeneity of variance of data, and then either Tukey's HSD or Tamhane's post hoc tests were used. SPSS software (IBM) was used for all statistical analyses and differences were considered as significant if $p < 0.05$.

The statistical analysis for the data in Chapter 6.3was carried out with a different software. SigmaPlot® (Systat Software Inc., San Jose, USA) was used to calculate with a one-way analysis of variance followed by Tukey’s post hoc test the data for statistical analyses. All data values are expressed as mean ± SD. The benchmark for significantly differences was at $p< 0.05$.

Data evaluation

OriginLab software (version 2018) was used to create all diagrams.

Chapter 8

Summary/Zusammenfassung

8.1 Summary

Mineral biocements are brittle materials, which usually results in catastrophic failure during mechanical loading. Here, previous works demonstrated the feasibility of reducing brittleness by a dual-setting approach, in which a silica sol was simultaneously gelled during the setting of a brushite forming cement. The current thesis aimed at further improving this concept by both using a novel silicate based cement matrix for an enhanced bonding between cement and silica matrix as well as multifunctional silica precursors to increase the network density of the gel. Due to its well-known biocompatibility and osteogenic regeneration capacity, baghdadite was chosen as mineral component of such composites. This required in a first approach the conversion of baghdadite ceramics into self-setting cement formulations. This was investigated initially by using baghdadite as reactive filler in a brushite forming cement (Chapter 4). Here, the ß-TCP component in a equimolar mixture of ß-TCP and acidic monocalcium phosphate anhydrous was subsequently replaced by baghdadite at various concentrations (0, 5, 10, 20, 30, 50, and 100 wt%) to study the influence on physicochemical cement properties such as mechanical performance, radiopacity, phase composition and microstructure. X-ray diffraction profiles demonstrated the dissolution of baghdadite during the cement reaction without affecting the crystal structure of the precipitated brushite phase. In addition, EDX analysis showed that calcium is homogeneously distributed in the cement matrix, while zirconium and silicon form cluster-like aggregates ranging in size from a few micrometers to more than 50 µm. X-ray images and µ-CT analyses indicate improved X-ray visibility with increased incorporation of baghdadite in brushite cement, with an aluminum equivalent thickness nearly doubling at a baghdadite content of 50 wt%. At the same time, the compressive strength of brushite cement increased from 12.9 ± 3.1 MPa to 21.1 ± 4.1 MPa at a baghdadite content of 10 wt%. Cell culture medium conditioned with powdered brushite cement approached physiological pH values when increasing amounts of baghdadite were added to the cement (pH = 6.47 for pure brushite, pH = 7.02 for brushite with 20 wt% baghdadite substitution). Baghdadite substitution also affected the ion content in the culture medium and thus the proliferation activity of primary human osteoblasts *in vitro*. The results demonstrated for the first time the suitability of baghdadite as a reactive cement additive for improving the radiopacity, mechanical performance, and cytocompatibility of brushite cements.

A second approach (Chapter 5) aimed to produce single component baghdadite cements by an increase of baghdadite solubility to initiate a self-setting cement reaction. For this, the material was mechanically activated by longer grinding times of up to 24h leading to both a decrease in particle and crystallite size as well as a partial amorphization of baghdadite. Baghdadite cements were formed by adding water at a powder to liquid ratio of 2.0 g/ml. Maximum compressive strengths were determined to be ~2 MPa after 3 days of setting for a 24-hour ground material. Inductively coupled plasma mass spectrometry (ICP-MS) measurements showed an incongruent dissolution profile of the set cements, with preferential dissolution of calcium and only minor release of zirconium ions. Cement formation occurs under alkaline conditions, with the unground raw powder resulting in a pH of 11.9 during setting, while prolonged grinding increases the pH to about 12.3.

Finally, mechanically activated baghdadite cements were combined with inorganic silica networks (Chapter 6) to create dual-setting cements with a further improvement of mechanical performance. While a modification of the cement pastes with a TEOS derived sol was already thought to improve strength, it was hypothesized that using multi-arm silica precursors can further enhance their mechanical performance due to a higher network density. In addition, this should also reduce pore size of both gels and cement and hence will be able to adjust the release kinetics of incorporated drugs. For this, multi-armed silica precursors were synthesized by the reaction of various multivalent alcohols (ethylene glycol, glycerine, pentaerythrit) with an isocyanate modified silica precursor. After hydrolysis under acidic conditions, the sols were mixed with baghdadite cement powders in order to allow a simultaneous gel formation and cement setting. Since the silica monomers have a high degree of linkage sites, this resulted in a branched network that interpenetrated with the growing cement crystals. In addition to minor changes in the crystalline phase composition as determined by X-ray diffraction, the novel composites exhibited improved mechanical properties with up to 20 times higher compressive strength and further benefit from an about 50% lower overall porosity than the reference pure baghdadite cement. In addition, the initial burst release of the model drug vancomycin was completely inhibited by the added silica matrix. This observation was verified by testing for the antimicrobial activity with *Staphylococcus aureus* by measuring the inhibition zones of selected samples after 24 h and 48 h, whereas the antimicrobial effectiveness of a constant vancomycin release could be demonstrated.

The current thesis clearly demonstrated the high potential of baghdadite as a cement formulation for medical application. The initially poor mechanical properties of such cements can be overcome by special processing techniques or by combination with silica networks. The achieved mechanical performance is > 10 MPa and hence suitable for bone replacement under non-load bearing conditions. The high intrinsic radiopacity as well as the alkaline pH during setting may open the way ahead to further dental applications, e.g. as root canal sealers or filler in dental composites. Here, the high pH is thought to lead to antimicrobial properties of such materials similar to commonly applied calcium hydroxide or calcium silicates, however combined with an intrinsic radiopacity for X-ray imaging. This would simplify such formulations to single component materials which are less susceptible to demixing processes during transport, storage or processing.

8.2 Zusammenfassung

Mineralische Biozemente sind spröde Materialien, die bei mechanischer Belastung in der Regel ein katastrophales Versagen zeigen. In früheren Arbeiten konnte die Sprödigkeit durch einen dual-härtenden Materialansatz verringert werden, bei dem ein dem Zement zugesetztes Kieselsol während des Aushärtens eines Bruschit-bildenden Zements simultan geliert und so die Matrix verstärkt. Die vorliegende Arbeit zielte darauf ab, dieses Konzept weiter zu verbessern, indem sowohl eine neuartige Zementmatrix auf Silikatbasis für eine verbesserte Bindung zwischen Zement und Kieselsäurematrix als auch multifunktionale Kieselsäure Precursoren zur Erhöhung der Netzwerkdichte des Gels verwendet wurden. Aufgrund der nachgewiesenen Biokompatibilität und osteogenen Regenerationsfähigkeit wurde Baghdadit als mineralischer Bestandteil solcher Komposite gewählt. Dies erforderte in einem ersten Ansatz die Umwandlung von Baghdadit-Keramik in selbsthärtende Zementformulierungen. Dies wurde zunächst durch die Verwendung von Baghdadit als reaktiver Füllstoff in einem Bruschit-bildenden Zement untersucht (Kapitel 4). Dabei wurde die β-TCP-Komponente in einem äquimolaren Gemisch aus β-TCP und saurem Monocalciumphosphat sukzessive durch Baghdadit in verschiedenen Konzentrationen (0, 5, 10, 20, 30, 50 und 100 Gew.-%) ersetzt, um den Einfluss auf die physikalisch-chemischen Zementeigenschaften, wie mechanische Festigkeit, Röntgenopazität, Phasenzusammensetzung und Mikrostruktur zu untersuchen. Röntgenbeugungsprofile zeigten die Auflösung von Baghdadit während der Zementreaktion, ohne die Kristallstruktur der ausgefällten Bruschitphase zu beeinträchtigen. Darüber hinaus zeigte die EDX-Analyse, dass Calcium homogen in der Zementmatrix verteilt ist, während Zirkon und Silizium clusterartige Aggregate mit einer Größe von einigen Mikrometern bis zu mehr als 50 µm bilden. Röntgenbilder und µ-CT-Analysen zeigen eine verbesserte Röntgensichtbarkeit bei erhöhtem Baghdadit-Anteil im Bruschit-Zement, wobei sich die Aluminium-Äquivalentdicke bei einem Baghdadit-Gehalt von 50 Gew.-% nahezu verdoppelt. Gleichzeitig stieg die Druckfestigkeit von Bruschitzement von 12,9 ± 3,1 MPa auf 21,1 ± 4,1 MPa bei einem Baghdaditgehalt von 10 Gew.-%. Zellkulturmedium, das mit pulverförmigem Bruschitzement konditioniert wurde, näherte sich physiologischen pH-Werten an, wenn dem Zement steigende Mengen an Baghdadit zugesetzt wurden (pH = 6,47 für reinen Bruschitzement, pH = 7,02 für Bruschitzement mit 20 Gew.-% Baghdadit-Substitution). Die Baghdadit-Substitution wirkte sich auch auf den Ionengehalt im Kulturmedium und damit auf die Proliferationsaktivität von primären menschlichen Osteoblasten *in vitro* aus. Die Ergebnisse zeigten zum ersten Mal die Eignung von Baghdadit als reaktives Zementadditiv zur

Verbesserung der Röntgenopazität, der mechanischen Eigenschaften und der Zytokompatibilität von Bruschitzementen.

Ein zweiter Ansatz (Kapitel 5) zielte auf die Herstellung einkomponentiger Baghdadit-Zemente durch eine Erhöhung der Baghdadit-Löslichkeit ab, um eine Zementreaktion zu initiieren. Dazu wurde das Material durch längere Mahlung von bis zu 24 Stunden mechanisch aktiviert, was sowohl zu einer Abnahme der Partikel- und Kristallitgröße, als auch zu einer teilweisen Amorphisierung von Baghdadit führte. Baghdadit-Zemente wurden durch Zugabe von Wasser bei einem Verhältnis von Pulver zu Flüssigkeit von 2,0 g/ml erhalten. Die maximalen Druckfestigkeiten wurden mit ~2 MPa nach 3 Tagen Aushärtung für ein 24 Stunden gemahlenes Material ermittelt. Massenspektrometrische Messungen mit induktiv gekoppeltem Plasma (ICP-MS) ergaben ein inkongruentes Auflösungsprofil der abgebundenen Zemente mit einer bevorzugten Auflösung von Calcium und einer nur geringen Freisetzung von Zirkonium-Ionen. Die Zementbildung erfolgt unter alkalischen Bedingungen, wobei das ungemahlene Rohpulver während des Abbindens einen pH-Wert von 11.9 aufweist, während ein längeres Mahlen den pH-Wert auf etwa 12.3 erhöht.

Abschließend wurden mechanisch aktivierte Baghdadit-Zemente mit anorganischen Silica-Netzwerken kombiniert (Kapitel 6), um dual härtende Zemente mit einer weiteren Verbesserung der mechanischen Eigenschaften zu erhalten. Während eine Modifikation der Zementpasten mit einem TEOS-abgeleiteten Sol bereits die Festigkeit verbessern sollte, wurde angenommen, dass die Verwendung von mehrarmigen Kieselsäure-Precursoren die mechanische Festigkeit aufgrund einer höheren Netzwerkdichte weiter verbessern kann. Darüber hinaus sollte sich auch die Porengröße von Gelen und Zement verringern, so dass die Freisetzungskinetik von inkorporierten Wirkstoffen angepasst werden kann. Zu diesem Zweck wurden mehrarmige Kieselsäure-Precursoren durch die Reaktion verschiedener mehrwertiger Alkohole (Ethylenglykol, Glycerin, Pentaerythrit) mit einem isocyanatmodifizierten Kieselsäure-Precursor synthetisiert. Nach der Hydrolyse unter sauren Bedingungen wurden die Sole mit Baghdadit-Zementpulvern gemischt, um eine gleichzeitige Gelbildung und Zementabbindung zu ermöglichen. Da die Kieselsäuremonomere einen hohen Grad an Verknüpfungsstellen aufweisen, führte dies zu einem verzweigten Netzwerk, das die ausfallenden Zementkristalle durchdrang. Neben geringfügigen Veränderungen in der Zusammensetzung der durch Röntgenbeugung bestimmten kristallinen Phasen, wiesen die neuartigen Komposite verbesserte mechanische Eigenschaften mit einer bis zu 20-fach höheren Druckfestigkeit auf und profitierten außerdem von einer um etwa 50 % geringeren

Gesamtporosität als der reine Baghdadit-Referenzzement. Darüber hinaus wurde die anfängliche starke Freisetzung („burst release“) des Modellwirkstoffs Vancomycin durch die zugesetzte Silica-Matrix vollständig gehemmt. Diese Beobachtung wurde durch Prüfung der antimikrobiellen Aktivität mit *Staphylococcus aureus* durch Messung des Hemmhofs im Agar-Diffusionstest ausgewählter Proben nach 24 h und 48 h verifiziert, wobei die antimikrobielle Wirksamkeit einer konstanten Vancomycin-Freisetzung nachgewiesen werden konnte.

Die vorliegende Arbeit zeigte deutlich das hohe Potenzial von Baghdadit Zementformulierungen für medizinische Anwendungen. Die anfänglich schlechten mechanischen Eigenschaften solcher Zemente können durch spezielle Verarbeitungstechniken oder durch die Kombination mit Silicanetzwerken überwunden werden. Die erzielten mechanischen Eigenschaften liegen bei > 10 MPa und die Materialien eignen sich daher für den Knochenersatz unter nicht-lasttragenden Bedingungen. Die hohe intrinsische Röntgenopazität sowie der alkalische pH-Wert während der Aushärtung könnten den Weg für weitere dentale Anwendungen öffnen, z. B. als Wurzelkanal-Zemente oder Füllstoff in Dentalkompositen. Hier ist davon auszugehen, dass der hohe pH-Wert zu antimikrobiellen Eigenschaften solcher Materialien führt, ähnlich wie bei den üblicherweise verwendeten Calciumhydroxiden oder Calciumsilikaten, jedoch in Kombination mit einer intrinsischen Röntgenopazität. Dies würde solche Formulierungen zu einkomponentigen Systemen vereinfachen, die weniger anfällig für Entmischungsprozesse während Transport, Lagerung oder Verarbeitung sind.

8.3 Outlook

This thesis aimed to produce silica modified baghdadite cements for biomedical applications. With the dual-setting approach it was possible to produce materials that meet clinically required properties regarding the setting behavior, mechanical performance and biological properties. The variation of the established TEOS precursor by branched precursors was successful not only in terms of improving the mechanical performance of the composite, but was also beneficial to adjust the release kinetics of incorporated vancomycin as model drug. Here, further works might address the use of other drug types (e.g. growth factors, chemotherapeutics, bisphosphonates) in this modified cement matrix to clarify whether the observed effect is a generic property of the nanoporous silica matrix. Another future direction could be related to the handling properties of the cement pastes as it was often not easy to apply the pastes due to a short processing time of the composites. A solution might be the use of stabilized colloidal silica nanoparticle dispersions (e.g. LEVASIL® as a commercially available compound) in combination with the branched silica precursors. The latter might be further modified with functional groups such as thiol and allyl moieties to allow a more specific cross-linking by a thiolene click-reaction or hydrophilic groups to influence the interaction between incorporated drug and silica matrix. Further research could be focused on other biocement types, e.g. hydroxyapatite cements or degradable magnesium phosphate cements with a well-known bone regeneration capacity. For the latter, the consumption of large amounts of water during precipitation of highly hydrated phases might also lead to an additional reduction in pore sizes of the gels. This concept not only can find an application in biocement, but might also help to improve the properties of civil engineering Portland cements, e.g. to prevent bleeding, for segregation control or to promote robustness as cohesion promoter.

As it was possible to already transfer baghdadite cement pastes into two different application forms (scaffolds with aligned porosity, spherical granules), future works can address further processing techniques. Here, additive manufacturing approaches should be clearly in the focus as this would allow to fabricate patient specific implant geometries. A prominent example is 3D powder printing, in which a binder liquid is locally applied to a thin layer of powder leading to a fast solidification. [366, 367] Transferring baghdadite cement powder to this process would require both suitable particle sizes for printing (approx. 10-15 µm) as well as a high reactivity for rapid hardening. If the latter is not fulfilled by the hydraulic setting reaction of the baghdadite cements, swellable polymeric particles can serve as suitable additives as described also for other bioceramics.[26, 366]

Chapter 9 References

1. Peters, F., K. Schwarz, and M. Epple, *The structure of bone studied with synchrotron X-ray diffraction, X-ray absorption spectroscopy and thermal analysis.* Thermochimica Acta, 2000. **361**(1-2): p. 131-138.
2. Kitaura, H., et al., *Osteocyte-Related Cytokines Regulate Osteoclast Formation and Bone Resorption.* International Journal of Molecular Sciences, 2020. **21**(14).
3. Sheikh, Z., et al., *Mechanisms of in Vivo Degradation and Resorption of Calcium Phosphate Based Biomaterials.* Materials, 2015. **8**(11): p. 7913-7925.
4. Shu, Y.T., et al., *Surface microcracks signal osteoblasts to regulate alignment and bone formation.* Materials Science & Engineering C-Materials for Biological Applications, 2014. **44**: p. 191-200.
5. Aaboe, M., E.M. Pinholt, and E. Hjortinghansen, *Healing of experimentally created defects - a review.* British Journal of Oral & Maxillofacial Surgery, 1995. **33**(5): p. 312-318.
6. Etienne, G., P.S. Ragland, and M.A. Mont, *Use of cancellous bone chips and demineralized bone matrix in the treatment of acetabular osteolysis: Preliminary 2-year follow-up.* Orthopedics, 2004. **27**(1): p. S123-S126.
7. Hervas, I., et al., *Microvascularized fibular graft for mandibular reconstruction - Detection of viability by bone scintigraphy and SPECT.* Clinical Nuclear Medicine, 2001. **26**(3): p. 225-229.
8. Heinemann, S., et al., *Resorbable bone substitution materials: An overview of commercially available materials and new approaches in the field of composites.* Orthopade, 2011. **40**(9): p. 761-73.
9. Bernhardt, A., M. Schumacher, and M. Gelinsky, *Formation of Osteoclasts on Calcium Phosphate Bone Cements and Polystyrene Depends on Monocyte Isolation Conditions.* Tissue Engineering Part C-Methods, 2015. **21**(2): p. 160-170.
10. Tamimi, F., Z. Sheikh, and J. Barralet, *Dicalcium phosphate cements: Brushite and monetite.* Acta Biomaterialia, 2012. **8**(2): p. 474-487.
11. Mangano, C., et al., *Dense hydroxyapatite inserted into postextraction sockets: A histologic and histomorphometric 20-year case report.* Journal of Periodontology, 2008. **79**(5): p. 929-933.
12. Den Hollander, W., et al., *Macroporous calcium phosphate ceramics for bone substitution a tracer study on biodegradation with calcium-45 tracer.* Biomaterials, 1991. **12**(6): p. 569-573.
13. Clokie, C.M.L., et al., *Closure of critical sized defects with allogenic and alloplastic bone substitutes.* Journal of Craniofacial Surgery, 2002. **13**(1): p. 111-121.
14. von Rechenberg, B., et al., *Evaluation of four biodegradable, injectable bone cements in an experimental drill hole model in sheep.* European Journal of Pharmaceutics and Biopharmaceutics, 2013. **85**(1): p. 130-138.
15. Nabiyouni, M., et al., *Magnesium-based bioceramics in orthopedic applications.* Acta Biomaterialia, 2018. **66**: p. 23-43.
16. Mohammadi, H., et al., *Bioinorganics in Bioactive Calcium Silicate Ceramics for Bone Tissue Repair: Bioactivity and Biological Properties.* Journal of Ceramic Science and Technology, 2014. **5**(1): p. 1-12.
17. Habibovic, P. and J.E. Barralet, *Bioinorganics and biomaterials: Bone repair.* Acta Biomaterialia, 2011. **7**(8): p. 3013-3026.
18. Moseke, C., et al., *Chemical characterization of hydroxyapatite obtained by wet chemistry in the presence of V, Co, and Cu ions.* Materials Science & Engineering C-Materials for Biological Applications, 2013. **33**(3): p. 1654-1661.
19. Geffers, M., J. Groll, and U. Gbureck, *Reinforcement Strategies for Load-Bearing Calcium Phosphate Biocements.* Materials, 2015. **8**(5): p. 2700-2717.
20. Sohail, M.G., et al., *Advancements in Concrete Mix Designs: High-Performance and Ultrahigh-Performance Concretes from 1970 to 2016.* Journal of Materials in Civil Engineering, 2018. **30**(3).
21. Barralet, J.E., et al., *Effect of porosity reduction by compaction on compressive strength and microstructure of calcium phosphate cement.* Journal of Biomedical Materials Research, 2002. **63**(1): p. 1-9.

22. Barralet, J.E., et al., *High-strength apatitic cement by modification with alpha-hydroxy acid salts.* Advanced Materials, 2003. **15**(24): p. 2091-+.
23. Barralet, J.E., et al., *High-Strength Apatitic Cement by Modification with α-Hydroxy Acid Salts.* Adv. Mater., 2003. **15**(24): p. 2091-2094.
24. Kruger, R. and J. Groll, *Fiber reinforced calcium phosphate cements - On the way to degradable load bearing bone substitutes?* Biomaterials, 2012. **33**(25): p. 5887-5900.
25. dos Santos, L.A., et al., *Dual-setting calcium phosphate cement modified with ammonium polyacrylate.* Artificial Organs, 2003. **27**(5): p. 412-418.
26. Christel, T., et al., *Dual setting alpha-tricalcium phosphate cements.* Journal of Materials Science-Materials in Medicine, 2013. **24**(3): p. 573-581.
27. Schamel, M., J. Groll, and U. Gbureck, *Simultaneous formation and mineralization of star-P(EO-stat-PO) hydrogels.* Materials science & engineering. C, Materials for biological applications, 2017. **75**: p. 471-477.
28. Schamel, M., et al., *Intrinsic 3D Prestressing: A New Route for Increasing Strength and Improving Toughness of Hybrid Inorganic Biocements.* Advanced Materials 2017. **29**: p. 1701035.
29. Geffers, M., et al., *Dual-setting brushite-silica gel cements.* Acta Biomaterialia, 2015. **11**: p. 467-76.
30. Lewis, G., *Injectable bone cements for use in vertebroplasty and kyphoplasty: State-of-the-art review.* Journal of Biomedical Materials Research Part B-Applied Biomaterials, 2006. **76B**(2): p. 456-468.
31. Lewis, G., *Viscoelastic properties of injectable bone cements for orthopaedic applications: State-of-the-art review.* Journal of Biomedical Materials Research Part B-Applied Biomaterials, 2011. **98B**(1): p. 171-191.
32. Dorozhkin, S.V., *Calcium Orthophosphate Cements and Concretes.* Materials, 2009. **2**(1): p. 221-291.
33. Ginebra, M.P., et al., *New processing approaches in calcium phosphate cements and their applications in regenerative medicine.* Acta Biomaterialia, 2010. **6**(8): p. 2863-2873.
34. Zhang, J.T., et al., *Calcium phosphate cements for bone substitution: Chemistry, handling and mechanical properties.* Acta Biomater., 2014. **10**(3): p. 1035-1049.
35. Ostrowski, N., A. Roy, and P.N. Kumta, *Magnesium Phosphate Cement Systems for Hard Tissue Applications: A Review.* ACS Biomater. Sci. & Engin., 2016. **2**(7): p. 1067-1083.
36. Liu, X., et al., *Minimally Invasive Injectable Graft X3 (MIIGX3) Calcium Sulfate Bone Cement Fills Bone Defects After Removal of Benign Subchondral Lesions and Reduction of Cartilage Defects.* Journal of Biomaterials and Tissue Engineering, 2020. **10**(11): p. 1686-1692.
37. Smirnov, V.V., et al., *Bone cements in the calcium phosphate-calcium sulfate system.* Doklady Chemistry, 2016. **467**: p. 136-139.
38. Engqvist, H., et al., *In vitro mechanical properties of a calcium silicate based bone void filler*, in *Bioceramics 18, Pts 1 and 2*, T. Nakamura, K. Yamashita, and M. Neo, Editors. 2006. p. 829-832.
39. Ma, B., et al., *Preparation and in vivo evaluation of a silicate-based composite bone cement.* Journal of Biomaterials Applications, 2017. **32**(2): p. 257-264.
40. Hughes, E., et al., *Inorganic cements for biomedical application: calcium phosphate, calcium sulphate and calcium silicate.* Advances in Applied Ceramics, 2015. **114**(2): p. 65-76.
41. Bohner, M., *Design of ceramic based cements and putties for bone graft substitution.* Eur. Cells & Mater, 2010. **20**: p. 1-12.
42. Wilke, H.-J., et al., *Biomechanical evaluation of vertebroplasty and kyphoplasty with polymethyl methacrylate or calcium phosphate cement under cyclic loading.* Spine, 2006. **31**(25): p. 2934-2941.
43. Gbureck, U., et al., *Rheological enhancement of mechanically activated alpha-tricalcium phosphate cements.* Journal of Biomedical Materials Research Part B-Applied Biomaterials, 2005. **73B**(1): p. 1-6.
44. Maenz, S., et al., *Enhanced mechanical properties of a novel, injectable, fiber-reinforced brushite cement.* Journal of the Mechanical Behavior of Biomedical Materials, 2014. **39**: p. 328-338.

45. Boehm, A.V., et al., *Self-healing capacity of fiber-reinforced calcium phosphate cements.* Scientific reports, 2020. **10**(1): p. 9430-9430.
46. Cameron, F.K. and J.M. Bell, *The phosphates of calcium, III; Superphosphates.* Journal of the American Chemical Society, 1906. **28**: p. 1222-1229.
47. Cameron, F.K. and A. Seidell, *The Phosphates of Calcium. I.* Journal of the American Chemical Society, 1905. **27**(12): p. 1503-1512.
48. Cameron, F.K. and J.M. Bell, *The Phosphates of Calcium. II.* Journal of the American Chemical Society, 1905. **27**(12): p. 1512-1514.
49. Cameron, F.K. and J.M. Bell, *The phosphates of calcium. IV.* Journal of the American Chemical Society, 1910. **32**: p. 869-873.
50. Bassett Jr, H., *Beiträge zum Studium der Calciumphosphate. I. Die Hydrate der Calcium-Hydroorthophosphate.* Zeitschrift für anorganische Chemie, 1907. **53**(1): p. 34-48.
51. Bassett Jr, H., *Beiträge zum Studium der Calciumphosphate. II. Die Einwirkung von Ammoniakgas auf Calcium-Hydroorthophosphate.* Zeitschrift für anorganische Chemie, 1907. **53**(1): p. 49-62.
52. Bassett jr, H., *Beiträge zum Studium der Calciumphosphate. III. Das System CaO□ P2O5□ H2O.* Zeitschrift für anorganische Chemie, 1908. **59**(1): p. 1-55.
53. Bassett, H., *LVI.—The phosphates of calcium. Part IV. The basic phosphates.* Journal of the Chemical Society, Transactions, 1917. **111**: p. 620-642.
54. Lide, D.R., *CRC handbook of chemistry and physics*. 2005, CRC Press, Boca Raton, FL. p. p.2544.
55. Cantelar, E., et al., *Optical characterisation of rare earths in natural fluorapatite.* Journal of Alloys and Compounds, 2001. **323**: p. 851-854.
56. Ribeiro, H.B., et al., *About the blue and green colours in natural fluorapatite.* physica status solidi (c), 2005. **2**(1): p. 720-723.
57. LeGeros, R.Z., *Calcium phosphates in oral biology and medicine.* Monographs in oral sciences, 1991: p. p. 201.
58. Elliot, J., *Structure and chemistry of the apatites and other calcium orthophosphates. Stud.* Inorg. Chem, 1994. **18**: p. 389-398.
59. Köster, K., H. Heide, and R. König, *Resorbierbare Calciumphosphatkeramik im Tierexperiment unter Belastung.* Langenbecks Archiv für Chirurgie, 1977. **343**(3): p. 173-181.
60. Bermudez, O., et al., *Development of some calcium phosphate cements from combinations of α-TCP, MCPM and CaO.* Journal of Materials Science: Materials in Medicine, 1994. **5**(3): p. 160-163.
61. Bermúdez, O., et al., *Optimization of a calcium orthophosphate cement formulation occurring in the combination of monocalcium phosphate monohydrate with calcium oxide.* Journal of Materials Science: Materials in Medicine, 1994. **5**(2): p. 67-71.
62. Driessens, F., et al., *Effective formulations for the preparation of calcium phosphate bone cements.* Journal of Materials Science: Materials in Medicine, 1994. **5**(3): p. 164-170.
63. Huan, Z. and J. Chang, *Novel bioactive composite bone cements based on the β-tricalcium phosphate–monocalcium phosphate monohydrate composite cement system.* Acta Biomaterialia, 2009. **5**(4): p. 1253-1264.
64. Karaffa, L.S., *The Merck index: an encyclopedia of chemicals, drugs, and biologicals*. 2013: RSC Publishing.
65. O'neill, W., *The fallacy of the calcium-phosphorus product.* Kidney international, 2007. **72**(7): p. 792-796.
66. LeGeros, R., *Formation and transformation of calcium phosphates: relevance to vascular calcification.* Zeitschrift für Kardiologie, 2001. **90**(3): p. 116-124.
67. Becker, A., et al., *A comparative study of clinically well-characterized human atherosclerotic plaques with histological, chemical, and ultrastructural methods.* Journal of inorganic biochemistry, 2004. **98**(12): p. 2032-2038.
68. Kurashina, K., et al., *In vivo study of calcium phosphate cements: implantation of an α-tricalcium phosphate/dicalcium phosphate dibasic/tetracalcium phosphate monoxide cement paste.* Biomaterials, 1997. **18**(7): p. 539-543.
69. Driessens, F., et al., *Osteotransductive bone cements.* Proceedings of the Institution of Mechanical Engineers, Part H: Journal of Engineering in Medicine, 1998. **212**(6): p. 427-435.

70. Takagi, S., L. Chow, and K. Ishikawa, *Formation of hydroxyapatite in new calcium phosphate cements.* Biomaterials, 1998. **19**(17): p. 1593-1599.
71. Yamamoto, H., et al., *Mechanical strength of calcium phosphate cement in vivo and in vitro.* Biomaterials, 1998. **19**(17): p. 1587-1591.
72. Fukase, Y., et al., *Setting reactions and compressive strengths of calcium phosphate cements.* Journal of dental research, 1990. **69**(12): p. 1852-1856.
73. TenHuisen, K. and P. Brown, *The formation of hydroxyapatite-ionomer cements at 38 C.* Journal of dental research, 1994. **73**(3): p. 598-606.
74. Fernandez, E., et al., *Kinetic study of the setting reaction of a calcium phosphate bone cement.* Journal of Biomedical Materials Research: An Official Journal of The Society for Biomaterials and The Japanese Society for Biomaterials, 1996. **32**(3): p. 367-374.
75. Fernandez, E., et al., *The cement setting reaction in the CaHPO4-α-Ca3 (PO4) 2 system: An X-ray diffraction study.* Journal of Biomedical Materials Research: An Official Journal of The Society for Biomaterials, The Japanese Society for Biomaterials, and the Australian Society for Biomaterials, 1998. **42**(3): p. 403-406.
76. Fernandez, E., et al., *Production and characterization of new calcium phosphate bone cements in the CaHPO4-alpha-Ca3 (PO4) 2 system: pH, workability and setting times.* Journal of materials science. Materials in medicine, 1999. **10**(4): p. 223-230.
77. Kuroda, K. and M. Okido, *Hydroxyapatite coating of titanium implants using hydroprocessing and evaluation of their osteoconductivity.* Bioinorganic chemistry and applications, 2012. **2012**.
78. Yin, X., M. Stott, and A. Rubio, *α-and β-tricalcium phosphate: A density functional study.* Physical Review B, 2003. **68**(20): p. 205205.
79. Constantz, B.R., et al., *Skeletal repair by in situ formation of the mineral phase of bone.* Science, 1995. **267**(5205): p. 1796-1799.
80. Oda, M., et al., *Effects of liquid phase on basic properties of α-tricalcium phosphate-based apatite cement.* Dental materials journal, 2008. **27**(5): p. 672-677.
81. Mirtchi, A.A., J. Lemaître, and E. Munting, *Calcium phosphate cements: effect of fluorides on the setting and hardening of β-tricalcium phosphate-dicalcium phosphate-calcite cements.* Biomaterials, 1991. **12**(5): p. 505-510.
82. Mirtchi, A.A., J. Lemaître, and E. Munting, *Calcium phosphate cements: study of the β-tricalcium phosphate—dicalcium phosphate—calcite cements.* Biomaterials, 1990. **11**(2): p. 83-88.
83. Lemaitre, J., E. Munting, and A. Mirtchi, *Setting, hardening and resorption of calcium phosphate hydraulic cements.* Revue de Stomatologie et de Chirurgie Maxillo-faciale, 1992. **93**(3): p. 163-165.
84. Ohura, K., et al., *Resorption of, and bone formation from, new β-tricalcium phosphate-monocalcium phosphate cements: An in vivo study.* Journal of Biomedical Materials Research: An Official Journal of The Society for Biomaterials and The Japanese Society for Biomaterials, 1996. **30**(2): p. 193-200.
85. Lecomte, A., et al., *Biphasic calcium phosphate: a comparative study of interconnected porosity in two ceramics.* Journal of Biomedical Materials Research Part B: Applied Biomaterials, 2008. **84**(1): p. 1-6.
86. Tancret, F., et al., *Modelling the mechanical properties of microporous and macroporous biphasic calcium phosphate bioceramics.* Journal of the European Ceramic Society, 2006. **26**(16): p. 3647-3656.
87. Bouler, J.M., et al., *Macroporous biphasic calcium phosphate ceramics: influence of five synthesis parameters on compressive strength.* Journal of Biomedical Materials Research: An Official Journal of The Society for Biomaterials and The Japanese Society for Biomaterials, 1996. **32**(4): p. 603-609.
88. Wang, J., et al., *Biological evaluation of biphasic calcium phosphate ceramic vertebral laminae.* Biomaterials, 1998. **19**(15): p. 1387-1392.
89. Daculsi, G., *Biphasic calcium phosphate concept applied to artificial bone, implant coating and injectable bone substitute.* Biomaterials, 1998. **19**(16): p. 1473-1478.
90. Daculsi, G., et al., *Biphasic calcium phosphate/hydrosoluble polymer composites: a new concept for bone and dental substitution biomaterials.* Bone, 1999. **25**(2): p. 59S-61S.

91. Daculsi, G., et al., *Current state of the art of biphasic calcium phosphate bioceramics.* J Mater Sci Mater Med, 2003. **14**(3): p. 195-200.
92. LeGeros, R., et al., *Biphasic calcium phosphate bioceramics: preparation, properties and applications.* Journal of materials science: Materials in Medicine, 2003. **14**(3): p. 201-209.
93. Alam, M.I., et al., *Comparative study of biphasic calcium phosphate ceramics impregnated with rhBMP-2 as bone substitutes.* Journal of Biomedical Materials Research: An Official Journal of The Society for Biomaterials and The Japanese Society for Biomaterials, 2001. **54**(1): p. 129-138.
94. Daculsi, G. *Biphasic calcium phosphate granules concept for injectable and mouldable bone substitute*. in *Advances in science and technology*. 2006. Trans Tech Publ.
95. Moseke, C. and U. Gbureck, *Tetracalcium phosphate: Synthesis, properties and biomedical applications.* Acta Biomaterialia, 2010. **6**(10): p. 3815-3823.
96. Kay, M.I., R. Young, and A. Posner, *Crystal structure of hydroxyapatite.* Nature, 1964. **204**(4963): p. 1050-1052.
97. Kingery, W.D., *Fundamental study of phosphate bnding in refractories. 1. Literature review.* J. Am. Ceram. Soc., 1950. **33**(8): p. 239-241.
98. Legeros, R.Z., A. Chohayeb, and A. Schulman, *Apatitic Calcium Phosphates possible Dental restorative Materials.* Journal of Dental Research, 1982. **61**(SPEC. ISSUE): p. 343-343.
99. Brown, W.E. and L.C. Chow, *A new Calcium-Phosphate setting Cement.* Journal of Dental Research, 1983. **62**: p. 672-672.
100. Sahin, E. and M. Ciftcioglu, *Monetite promoting effect of NaCl on brushite cement setting kinetics.* Journal of Materials Chemistry B, 2013. **1**(23): p. 2943-2950.
101. Bermudez, O., et al., *Development of an Octocalcium Phosphate Cement.* Journal of Materials Science-Materials in Medicine, 1994. **5**(3): p. 144-146.
102. Gbureck, U., et al., *Mechanical activation and cement formation of beta-tricalcium phosphate.* Biomaterials, 2003. **24**(23): p. 4123-4131.
103. Gbureck, U., et al., *Mechanical activation of tetracalcium phosphate.* J Am Ceram Soc, 2004. **87**(2): p. 311-313.
104. Gbureck, U., et al., *Amorphous alpha-tricalcium phosphate: Preparation and aqueous setting reaction.* Journal of the American Ceramic Society, 2004. **87**(6): p. 1126-1132.
105. Otsuka, M., et al., *A novel skeletal drug-delivery system using self-setting calcium-phosphate cement .6. Effect of particle-size of metastabile calcium phosphates on mechanical strength of a novel self-setting bioactive calcium-phosphate cement.* Journal of Biomedical Materials Research, 1995. **29**(1): p. 25-32.
106. ., H.M., *Physikalische Charakterisierung von Calciumphosphat-Pulvern zur Einstellung von Prozessparametern für die Herstellung von Knochenzement.* PhD Thesis, University of Wuerzburg, 2003.
107. Zawacki, S.J., et al., *The growth of calcium phosphates.* Acs Symposium Series, 1986. **323**: p. 650-662.
108. Hassan KAR. The microelectrophoretic behaviour of sparingly soluble salts. MS thesis. Suny, B., 1984. .
109. Meininger, S., et al., *Phytic acid as alternative setting retarder enhanced biological performance of dicalcium phosphate cement in vitro.* Sci. Rep., 2017. **7**.
110. Barralet, J.E., L.M. Grover, and U. Gbureck, *Ionic modification of calcium phosphate cement viscosity. Part II: hypodermic injection and strength improvement of brushite cement.* Biomaterials, 2004. **25**(11): p. 2197-2203.
111. Yang, N., et al., *Research progresses in magnesium phosphate cement–based materials.* Journal of Materials in Civil Engineering, 2014. **26**(10): p. 04014071.
112. Wang, A.-j., et al., *Effect of liquid-to-solid ratios on the properties of magnesium phosphate chemically bonded ceramics.* Materials Science and Engineering: C, 2013. **33**(5): p. 2508-2512.
113. Ostrowski, N., et al., *Systematic assessment of synthesized tri-magnesium phosphate powders (amorphous, semi-crystalline and crystalline) and cements for ceramic bone cement applications.* Journal of Materials Science & Technology, 2015. **31**(5): p. 437-444.
114. Mestres, G. and M.-P. Ginebra, *Novel magnesium phosphate cements with high early strength and antibacterial properties.* Acta biomaterialia, 2011. **7**(4): p. 1853-1861.

115. Wu, F., et al., *Self-setting bioactive calcium–magnesium phosphate cement with high strength and degradability for bone regeneration.* Acta biomaterialia, 2008. **4**(6): p. 1873-1884.

116. Mestres, G., et al., *Antimicrobial properties and dentin bonding strength of magnesium phosphate cements.* Acta biomaterialia, 2013. **9**(9): p. 8384-8393.

117. Mestres, G., et al., *Magnesium phosphate cements for endodontic applications with improved long-term sealing ability.* International endodontic journal, 2014. **47**(2): p. 127-139.

118. Yang, G., et al., *Bioactive calcium sulfate/magnesium phosphate cement for bone substitute applications.* Materials Science and Engineering: C, 2014. **35**: p. 70-76.

119. Kanter, B., et al., *Control of in vivo mineral bone cement degradation.* Acta Biomater., 2014. **10**(7): p. 3279-3287.

120. Großardt, C., et al., *Passive and active in vitro resorption of calcium and magnesium phosphate cements by osteoclastic cells.* Tissue Engineering Part A, 2010. **16**(12): p. 3687-3695.

121. Moseke, C., V. Saratsis, and U. Gbureck, *Injectability and mechanical properties of magnesium phosphate cements.* Journal of Materials Science: Materials in Medicine, 2011. **22**(12): p. 2591-2598.

122. Vorndran, E., et al., *Formation and properties of magnesium–ammonium–phosphate hexahydrate biocements in the Ca–Mg–PO 4 system.* Journal of Materials Science: Materials in Medicine, 2011. **22**(3): p. 429-436.

123. Ewald, A., et al., *Effect of cold-setting calcium-and magnesium phosphate matrices on protein expression in osteoblastic cells.* Journal of Biomedical Materials Research Part B: Applied Biomaterials, 2011. **96**(2): p. 326-332.

124. Zhou, H., et al., *Microwave assisted preparation of magnesium phosphate cement (MPC) for orthopedic applications: a novel solution to the exothermicity problem.* Materials Science and Engineering: C, 2013. **33**(7): p. 4288-4294.

125. Yang, J. and C. Qian, *Effect of borax on hydration and hardening properties of magnesium and pottassium phosphate cement pastes.* Journal of Wuhan University of Technology-Mater. Sci. Ed., 2010. **25**(4): p. 613-618.

126. Ding, Z., et al., *Cementing mechanism of potassium phosphate based magnesium phosphate cement.* Ceramics international, 2012. **38**(8): p. 6281-6288.

127. Yang, Q. and X. Wu, *Factors influencing properties of phosphate cement-based binder for rapid repair of concrete.* Cement and concrete research, 1999. **29**(3): p. 389-396.

128. Ribeiro, D.V. and M.R. Morelli, *Performance analysis of magnesium phosphate cement mortar containing grinding dust.* Materials Research, 2009. **12**(1): p. 51-56.

129. Walling, S.A. and J.L. Provis, *Magnesia-based cements: a journey of 150 years, and cements for the future?* Chemical reviews, 2016. **116**(7): p. 4170-4204.

130. Sarkar, A., *Hydration/dehydration characteristics of struvite and dittmarite pertaining to magnesium ammonium phosphate cement systems.* Journal of materials science, 1991. **26**(9): p. 2514-2518.

131. Frazier, A.W., J.R. Lehr, and J.P. Smith, *The magnesium phosphates hannayite, schertelite and bobierrite.* American Mineralogist: Journal of Earth and Planetary Materials, 1963. **48**(5-6): p. 635-641.

132. Wang, A.-j., et al., *Effect of raw material ratios on the compressive strength of magnesium potassium phosphate chemically bonded ceramics.* Materials Science and Engineering: C, 2013. **33**(8): p. 5058-5063.

133. Ostrowski, N., A. Roy, and P.N. Kumta, *Magnesium phosphate cement systems for hard tissue applications: a review.* ACS Biomaterials Science & Engineering, 2016. **2**(7): p. 1067-1083.

134. Tamimi, F., et al., *Biocompatibility of magnesium phosphate minerals and their stability under physiological conditions.* Acta biomaterialia, 2011. **7**(6): p. 2678-2685.

135. Abdelrazig, B., J. Sharp, and B. El-Jazairi, *The microstructure and mechanical properties of mortars made from magnesia-phosphate cement.* Cement and Concrete Research, 1989. **19**(2): p. 247-258.

136. Abdelrazig, B., J. Sharp, and B. El-Jazairi, *The chemical composition of mortars made from magnesia-phosphate cement.* Cement and concrete research, 1988. **18**(3): p. 415-425.

137. Waselau, M., et al., *Effects of a magnesium adhesive cement on bone stability and healing following a metatarsal osteotomy in horses.* American journal of veterinary research, 2007. **68**(4): p. 370-378.

138. Haque, M.A. and B. Chen, *Research progresses on magnesium phosphate cement: A review.* Construction and Building Materials, 2019. **211**: p. 885-898.

139. Yu, Y., et al., *Evaluation of inherent toxicology and biocompatibility of magnesium phosphate bone cement.* Colloids and Surfaces B: Biointerfaces, 2010. **76**(2): p. 496-504.

140. Xia, Y., et al., *Degradability, biocompatibility, and osteogenesis of biocomposite scaffolds containing nano magnesium phosphate and wheat protein both in vitro and in vivo for bone regeneration.* International journal of nanomedicine, 2016. **11**: p. 3435.

141. Wang, W. and K.W. Yeung, *Bone grafts and biomaterials substitutes for bone defect repair: A review.* Bioactive materials, 2017. **2**(4): p. 224-247.

142. Glimcher, M.J., *The nature of the mineral phase in bone: biological and clinical implications*, in *Metabolic bone disease and clinically related disorders*. 1998, Elsevier. p. 23-52e.

143. Wolf, F.I. and V. Trapani, *Cell (patho) physiology of magnesium.* Clinical science, 2008. **114**(1): p. 27-35.

144. Neuman, W. and M. Neuman, *The nature of the mineral phase of bone.* Chemical Reviews, 1953. **53**(1): p. 1-45.

145. Yoshizawa, S., et al., *Role of magnesium ions on osteogenic response in bone marrow stromal cells.* Connective tissue research, 2014. **55**(sup1): p. 155-159.

146. Yoshizawa, S., et al., *Magnesium ion stimulation of bone marrow stromal cells enhances osteogenic activity, simulating the effect of magnesium alloy degradation.* Acta biomaterialia, 2014. **10**(6): p. 2834-2842.

147. Liu, W., et al., *Novel tricalcium silicate/magnesium phosphate composite bone cement having high compressive strength, in vitro bioactivity and cytocompatibility.* Acta biomaterialia, 2015. **21**: p. 217-227.

148. Wu, F., et al., *Injectable bioactive calcium–magnesium phosphate cement for bone regeneration.* Biomedical Materials, 2008. **3**(4): p. 044105.

149. Gou, Z., et al., *Study on the self-setting property and the in vitro bioactivity of β-Ca2SiO4.* Journal of Biomedical Materials Research Part B: Applied Biomaterials, 2005. **73B**(2): p. 244-251.

150. Liu, W., J. Chang, and Z. Yue, *Physicochemical properties and biocompatibility of tricalcium and dicalcium silicate composite cements after hydration.* International Journal of Applied Ceramic Technology, 2011. **8**(3): p. 560-565.

151. Zhao, W., et al., *The self-setting properties and in vitro bioactivity of tricalcium silicate.* Biomaterials, 2005. **26**(31): p. 6113-6121.

152. Ishida, H., et al., *Highly Reactive β-Dicalcium Silicate: IV, Ball-Milling and Static Hydration at Room Temperature.* Journal of the American Ceramic Society, 1992. **75**(10): p. 2779-2784.

153. Hong, S.H. and J.F. Young, *Hydration kinetics and phase stability of dicalcium silicate synthesized by the Pechini process.* Journal of the American Ceramic Society, 1999. **82**(7): p. 1681-1686.

154. Camilleri, J., *Characterization and hydration kinetics of tricalcium silicate cement for use as a dental biomaterial.* Dental materials, 2011. **27**(8): p. 836-844.

155. Liu, W. and J. Chang, *In vitro evaluation of gentamicin release from a bioactive tricalcium silicate bone cement.* Materials Science and Engineering: C, 2009. **29**(8): p. 2486-2492.

156. Huan, Z. and J. Chang, *Effect of sodium carbonate solution on self-setting properties of tricalcium silicate bone cement.* Journal of biomaterials applications, 2008. **23**(3): p. 247-262.

157. Aza, D. and D. Aza, *Morphological and structural study of pseudowollastonite implants in bone.* Journal of Microscopy, 2000. **197**(1): p. 60-67.

158. De Aza, P., et al., *Transmission electron microscopy of the interface between bone and pseudowollastonite implant.* Journal of microscopy, 2001. **201**(1): p. 33-43.

159. Zhang, N., et al., *Effects of pseudowollastonite (CaSiO3) bioceramic on in vitro activity of human mesenchymal stem cells.* Biomaterials, 2010. **31**(30): p. 7653-7665.

160. Carrodeguas, R., et al., *Assessment of natural and synthetic wollastonite as source for bioceramics preparation.* Journal of Biomedical Materials Research Part A: An Official Journal of The Society for Biomaterials, The Japanese Society for Biomaterials, and The Australian Society for Biomaterials and the Korean Society for Biomaterials, 2007. **83**(2): p. 484-495.

161. Lin, Q., et al., *The reactivity of nano silica with calcium hydroxide.* Journal of Biomedical Materials Research Part B: Applied Biomaterials, 2011. **99**(2): p. 239-246.
162. Wu, C., et al., *The effect of strontium incorporation into CaSiO3 ceramics on their physical and biological properties.* Biomaterials, 2007. **28**(21): p. 3171-3181.
163. Wu, C., et al., *In vitro bioactivity of akermanite ceramics.* Journal of Biomedical Materials Research Part A: An Official Journal of The Society for Biomaterials, The Japanese Society for Biomaterials, and The Australian Society for Biomaterials and the Korean Society for Biomaterials, 2006. **76**(1): p. 73-80.
164. Wu, C., et al., *Preparation and characteristics of a calcium magnesium silicate (bredigite) bioactive ceramic.* Biomaterials, 2005. **26**(16): p. 2925-2931.
165. Wu, C.T. and J. Chang, *Synthesis and in vitro bioactivity of bredigite powders.* Journal of Biomaterials Applications, 2007. **21**(3): p. 251-263.
166. Wu, C., et al., *A novel bioactive porous bredigite (Ca 7 MgSi 4 O 16) scaffold with biomimetic apatite layer for bone tissue engineering.* Journal of Materials Science: Materials in Medicine, 2007. **18**(5): p. 857-864.
167. Hu, S., et al., *Antibacterial activity of silicate bioceramics.* Journal of Wuhan University of Technology-Mater. Sci. Ed., 2011. **26**(2): p. 226-230.
168. Srinath, P., P. Abdul Azeem, and K. Venugopal Reddy, *Review on calcium silicate-based bioceramics in bone tissue engineering.* International Journal of Applied Ceramic Technology, 2020. **17**(5): p. 2450-2464.
169. Iwata, N.Y., et al., *Sintering behavior and apatite formation of diopside prepared by coprecipitation process.* colloids and surfaces B: Biointerfaces, 2004. **34**(4): p. 239-245.
170. Nonami, T. and S. Tsutsumi, *Study of diopside ceramics for biomaterials.* Journal of Materials Science: Materials in Medicine, 1999. **10**(8): p. 475-479.
171. Arcos, D., D. Greenspan, and M. Vallet-Regí, *A new quantitative method to evaluate the in vitro bioactivity of melt and sol-gel-derived silicate glasses.* Journal of Biomedical Materials Research Part A: An Official Journal of The Society for Biomaterials, The Japanese Society for Biomaterials, and The Australian Society for Biomaterials and the Korean Society for Biomaterials, 2003. **65**(3): p. 344-351.
172. Nakajima, S., *Experimental studies of healing process on reinforcement ceramic implantation in rabbit mandible.* Shika gakuho. Dental science reports, 1990. **90**(4): p. 525-553.
173. Nakajima, S., et al., *Physicochemical characteristics of new reinforcement ceramic implant.* Shika gakuho. Dental science reports, 1989. **89**(11): p. 1709-1717.
174. De Aza, P.N., Z.B. Luklinska, and M. Anseau, *Bioactivity of diopside ceramic in human parotid saliva.* Journal of Biomedical Materials Research Part B: Applied Biomaterials: An Official Journal of The Society for Biomaterials, The Japanese Society for Biomaterials, and The Australian Society for Biomaterials and the Korean Society for Biomaterials, 2005. **73**(1): p. 54-60.
175. Toya, T., et al., *Preparation and properties of glass-ceramics from wastes (Kira) of silica sand and kaolin clay refining.* Journal of the European Ceramic Society, 2004. **24**(8): p. 2367-2372.
176. Chandrasekaran, V., R. Taggart, and D. Polonis, *The influence of constitution and microstructure on the temperature coefficient of resistivity in Ti-base alloys.* Journal of Materials Science, 1974. **9**(6): p. 961-968.
177. Xue, W., et al., *Plasma-sprayed diopside coatings for biomedical applications.* Surface and coatings technology, 2004. **185**(2-3): p. 340-345.
178. Kamitakahara, M., et al., *Preparation of Porous Glass-Ceramics Containing Whitlockite and Diopside for Bone Repair.* Journal of the Ceramic Society of Japan, 2006. **114**(1325): p. 82-86.
179. Wu, C. and J. Chang, *Degradation, bioactivity, and cytocompatibility of diopside, akermanite, and bredigite ceramics.* Journal of Biomedical Materials Research Part B-Applied Biomaterials, 2007. **83B**(1): p. 153-160.
180. Iwata, N.Y., et al., *Preparation of diopside with apatite-forming ability by sol–gel process using metal alkoxide and metal salts.* Colloids and Surfaces B: Biointerfaces, 2004. **33**(1): p. 1-6.
181. Zhai, W.Y., et al., *Stimulatory effects of the ionic products from Ca-Mg-Si bioceramics on both osteogenesis and angiogenesis in vitro.* Acta Biomaterialia, 2013. **9**(8): p. 8004-8014.

182. Liu, N., et al., *The interactions of Mg2+/Zn2+-containing silicate materials with stem cells and bacteria.* Materials letters, 2013. **112**: p. 105-108.
183. Wu, C. and H. Zreiqat, *Porous bioactive diopside (CaMgSi2O6) ceramic microspheres for drug delivery.* Acta biomaterialia, 2010. **6**(3): p. 820-829.
184. Ou, J., et al. *Preparation of Merwinite with apatite-forming ability by sol-gel process*. in *Key Engineering Materials*. 2007. Trans Tech Publ.
185. Hafezi-Ardakani, M., et al., *Synthesis and characterization of nanocrystalline merwinite (Ca3Mg (SiO4) 2) via sol–gel method.* Ceramics International, 2011. **37**(1): p. 175-180.
186. Hafezi, M., et al., *Histological analysis of bone repair in rat femur via nanostructured merwinite granules.* Ceramics International, 2013. **39**(4): p. 4575-4580.
187. Liu, Q., et al., *A comparative study of proliferation and osteogenic differentiation of adipose-derived stem cells on akermanite and β-TCP ceramics.* Biomaterials, 2008. **29**(36): p. 4792-4799.
188. Gu, H., et al., *The stimulation of osteogenic differentiation of human adipose-derived stem cells by ionic products from akermanite dissolution via activation of the ERK pathway.* Biomaterials, 2011. **32**(29): p. 7023-7033.
189. Sun, H., et al., *Proliferation and osteoblastic differentiation of human bone marrow-derived stromal cells on akermanite-bioactive ceramics.* Biomaterials, 2006. **27**(33): p. 5651-5657.
190. Huang, Y., et al., *In vitro and in vivo evaluation of akermanite bioceramics for bone regeneration.* Biomaterials, 2009. **30**(28): p. 5041-5048.
191. Xia, L., et al., *Proliferation and osteogenic differentiation of human periodontal ligament cells on akermanite and β-TCP bioceramics.* Eur Cell Mater, 2011. **22**(68): p. e82.
192. Anselme, K., *Osteoblast adhesion on biomaterials.* Biomaterials, 2000. **21**(7): p. 667-681.
193. Wu, C. and J. Chang, *Synthesis and apatite-formation ability of akermanite.* Materials Letters, 2004. **58**(19): p. 2415-2417.
194. Zhai, W., et al., *Silicate bioceramics induce angiogenesis during bone regeneration.* Acta Biomaterialia, 2012. **8**(1): p. 341-349.
195. Chen, X., et al., *Synthesis and characteristics of monticellite bioactive ceramic.* Journal of Materials Science: Materials in Medicine, 2008. **19**(3): p. 1257-1263.
196. Ou, J., et al., *Preparation and in vitro bioactivity of novel merwinite ceramic.* Biomedical Materials, 2008. **3**(1): p. 015015.
197. Wu, C., et al., *The effect of Zn contents on phase composition, chemical stability and cellular bioactivity in Zn–Ca–Si system ceramics.* Journal of Biomedical Materials Research Part B: Applied Biomaterials: An Official Journal of The Society for Biomaterials, The Japanese Society for Biomaterials, and The Australian Society for Biomaterials and the Korean Society for Biomaterials, 2008. **87**(2): p. 346-353.
198. Zreiqat, H., et al., *The incorporation of strontium and zinc into a calcium–silicon ceramic for bone tissue engineering.* Biomaterials, 2010. **31**(12): p. 3175-3184.
199. Lin, K., et al., *Study of the mechanical property and in vitro biocompatibility of CaSiO3 ceramics.* Ceramics International, 2005. **31**(2): p. 323-326.
200. Kobayashi, T., et al., *Osteogenic cell cytotoxicity and biomechanical strength of the new ceramic diopside.* Journal of Biomedical Materials Research: An Official Journal of The Society for Biomaterials and The Japanese Society for Biomaterials, 1997. **37**(1): p. 100-107.
201. Wu, C. and J. Chang, *A novel akermanite bioceramic: preparation and characteristics.* Journal of biomaterials applications, 2006. **21**(2): p. 119-129.
202. Wu, C., J. Chang, and W. Zhai, *A novel hardystonite bioceramic: preparation and characteristics.* Ceramics international, 2005. **31**(1): p. 27-31.
203. Sadeghzade, S., R. Emadi, and S. Labbaf, *Formation mechanism of nano-hardystonite powder prepared by mechanochemical synthesis.* Advanced Powder Technology, 2016. **27**(5): p. 2238-2244.
204. Schumacher, T.C., et al., *Mechanical evaluation of calcium-zirconium-silicate (baghdadite) obtained by a direct solid-state synthesis route.* J Mech Behav Biomed Mater, 2014. **34**: p. 294-301.
205. Henkel, J., et al., *Bone regeneration based on tissue engineering conceptions—a 21st century perspective.* Bone research, 2013. **1**(1): p. 216-248.

206. Johnson, A.J.W. and B.A. Herschler, *A review of the mechanical behavior of CaP and CaP/polymer composites for applications in bone replacement and repair.* Acta biomaterialia, 2011. **7**(1): p. 16-30.
207. Gerhardt, L.-C. and A.R. Boccaccini, *Bioactive glass and glass-ceramic scaffolds for bone tissue engineering.* Materials, 2010. **3**(7): p. 3867-3910.
208. Fu, Q., et al., *Bioactive glass scaffolds for bone tissue engineering: state of the art and future perspectives.* Materials Science and Engineering: C, 2011. **31**(7): p. 1245-1256.
209. Al-Hermezi, H.M., D. McKie, and A.J. Hall, *Baghdadite, a new calcium zirconium silicate mineral from Iraq.* Mineralogical Magazine, 1986. **50**(355): p. 119-123.
210. Biagioni, C., et al., *Single crystal refinement of the structure of baghdadite from Fuka (Okayama Prefecture, Japan).* 2010.
211. Plaister, J.R., et al., *Structure Determination of Ca3HfSi2O9 and Ca3ZrSi2O9 from Powder Diffraction.* Journal of Solid State Chemistry, 1995. **115**(2): p. 464-468.
212. Arefpour, A., et al., *Baghdadite/Polycaprolactone nanocomposite scaffolds: preparation, characterisation, and in vitro biological responses of human osteoblast-like cells (Saos-2 cell line).* Materials Technology, 2020. **35**(7): p. 421-432.
213. Bakhsheshi-Rad, H.R., et al., *Novel nanostructured baghdadite-vancomycin scaffolds: In-vitro drug release, antibacterial activity and biocompatibility.* Materials Letters, 2017. **209**: p. 369-372.
214. Abbasian, V., R. Emadi, and M. Kharaziha, *Biomimetic nylon 6-baghdadite nanocomposite scaffold for bone tissue engineering.* Materials Science and Engineering: C, 2020. **109**: p. 110549.
215. Sadeghzade, S., et al., *In vitro evaluation of diopside/baghdadite bioceramic scaffolds modified by polycaprolactone fumarate polymer coating.* Materials Science and Engineering: C, 2020. **106**: p. 110176.
216. Ramaswamy, Y., et al., *The responses of osteoblasts, osteoclasts and endothelial cells to zirconium modified calcium-silicate-based ceramic.* Biomaterials, 2008. **29**(33): p. 4392-4402.
217. Roohani-Esfahani, S.I., et al., *Repairing a critical-sized bone defect with highly porous modified and unmodified baghdadite scaffolds.* Acta Biomaterialia, 2012. **8**(11): p. 4162-4172.
218. Li, J.J., et al. *Efficacy of novel synthetic bone substitutes in the reconstruction of large segmental bone defects in sheep tibiae*. Biomedical materials (Bristol, England), 2016. **11**, 015016 DOI: 10.1088/1748-6041/11/1/015016.
219. Li, J.J., et al., *Effects of Material–Tissue Interactions on Bone Regeneration Outcomes Using Baghdadite Implants in a Large Animal Model.* Advanced Healthcare Materials, 2018. **7**(15): p. 1800218.
220. Sehgal, R.R., et al., *Nanostructured gellan and xanthan hydrogel depot integrated within a baghdadite scaffold augments bone regeneration.* Journal of Tissue Engineering and Regenerative Medicine, 2017. **11**(4): p. 1195-1211.
221. Sadeghpour, S., et al., *Fabrication of a novel nanostructured calcium zirconium silicate scaffolds prepared by a freeze-casting method for bone tissue engineering.* Ceramics International, 2014. **40**(10): p. 16107-16114.
222. Karamian, E., et al., *Fabrication of hydroxyapatite-baghdadite nanocomposite scaffolds coated by PCL/Bioglass with polyurethane polymeric sponge technique.* Nanomedicine Journal, 2017. **4**(3): p. 177-183.
223. Najafinezhad, A., et al., *A comparative study on the synthesis mechanism, bioactivity and mechanical properties of three silicate bioceramics.* Materials Science and Engineering: C, 2017. **72**: p. 259-267.
224. Liang, Y., et al., *Excellent stability of plasma-sprayed bioactive Ca3ZrSi2O9 ceramic coating on Ti–6Al–4V.* Applied Surface Science, 2010. **256**(14): p. 4677-4681.
225. Pahlevanzadeh, F., et al., *Apatite-forming ability, cytocompatibility, and mechanical properties enhancement of poly methyl methacrylate-based bone cements by incorporating of baghdadite nanoparticles.* International Journal of Applied Ceramic Technology, 2019. **16**(5): p. 2006-2019.
226. Soundrapandian, C., et al., *Porous bioactive glass scaffolds for local drug delivery in osteomyelitis: development and in vitro characterization.* Aaps Pharmscitech, 2010. **11**(4): p. 1675-1683.

227. Tavangarian, F. and R. Emadi, *Nanostructure effects on the bioactivity of forsterite bioceramic.* Materials Letters, 2011. **65**(4): p. 740-743.

228. Sadeghzade, S., et al., *Synthesis, characterization and strengthening mechanism of modified and unmodified porous diopside/baghdadite scaffolds.* Materials Chemistry and Physics, 2019. **228**: p. 89-97.

229. Luo, T., C. Wu, and Y. Zhang, *The in vivo osteogenesis of Mg or Zr-modified silicate-based bioceramic spheres.* Journal of Biomedical Materials Research Part A, 2012. **100**(9): p. 2269-2277.

230. No, Y.J., et al., *Injectable radiopaque and bioactive polycaprolactone-ceramic composites for orthopedic augmentation.* Journal of Biomedical Materials Research Part B: Applied Biomaterials, 2015. **103**(7): p. 1465-1477.

231. Avnir, D., et al., *Enzymes and Other Proteins Entrapped in Sol-Gel Materials.* Chemistry of Materials, 1994. **6**(10): p. 1605-1614.

232. Campostrini, R., et al., *Immobilization of plant cells in hybrid sol-gel materials.* Journal of Sol-Gel Science and Technology, 1996. **7**(1-2): p. 87-97.

233. Meunier, C.F., et al., *Living hybrid materials capable of energy conversion and CO2 assimilation.* Chemical Communications, 2010. **46**(22): p. 3843-3859.

234. Coiffier, A., et al., *Sol-gel encapsulation of bacteria: a comparison between alkoxide and aqueous routes.* Journal of Materials Chemistry, 2001. **11**(8): p. 2039-2044.

235. Lickiss, P.D., *The Synthesis and Structure of Organosilanols*, in *Advances in Inorganic Chemistry*, A.G. Sykes, Editor. 1995, Academic Press. p. 147-262.

236. J.D. Brinker, G.S., *The Physics and Chemistry of Sol-Gel Processing*. 1990: Academic Press.

237. Gill, I. and A. Ballesteros, *Encapsulation of Biologicals within Silicate, Siloxane, and Hybrid Sol−Gel Polymers: An Efficient and Generic Approach.* Journal of the American Chemical Society, 1998. **120**(34): p. 8587-8598.

238. Booth, N., *The denaturation of proteins: Denaturation in the presence of alcohol.* Biochemical Journal, 1930. **24**(6): p. 1699-1705.

239. Brandhuber, D., et al., *Glycol-Modified Silanes in the Synthesis of Mesoscopically Organized Silica Monoliths with Hierarchical Porosity.* Chemistry of Materials, 2005. **17**(16): p. 4262-4271.

240. Bangi, U.K.H., A. Venkateswara Rao, and A. Parvathy Rao, *A new route for preparation of sodium-silicate-based hydrophobic silica aerogels via ambient-pressure drying.* Science and Technology of Advanced Materials, 2008. **9**(3): p. 035006.

241. Schmidt, M. and F. Schwertfeger, *Applications for silica aerogel products.* Journal of Non-Crystalline Solids, 1998. **225**: p. 364-368.

242. Schwertfeger, F., D. Frank, and M. Schmidt, *Hydrophobic waterglass based aerogels without solvent exchange or supercritical drying.* Journal of Non-Crystalline Solids, 1998. **225**: p. 24-29.

243. Venton, D.L. and E. Gudipati, *Entrapment of enzymes using organo-functionalized polysiloxane copolymers.* Biochimica et Biophysica Acta (BBA) - Protein Structure and Molecular Enzymology, 1995. **1250**(2): p. 117-125.

244. Wang, J., P.V.A. Pamidi, and D.S. Park, *Screen-Printable Sol−Gel Enzyme-Containing Carbon Inks.* Analytical Chemistry, 1996. **68**(15): p. 2705-2708.

245. Wang, J., D.S. Park, and P.V.A. Pamidi, *Tailoring the macroporosity and performance of sol-gel derived carbon composite glucose sensors.* Journal of Electroanalytical Chemistry, 1997. **434**(1): p. 185-189.

246. Sampath, S., et al., *Sol-gel derived ceramic-carbon enzyme electrodes: Glucose oxidase as a test case.* Journal of Sol-Gel Science and Technology, 1996. **7**(1): p. 123-128.

247. Avnir, D., *Organic Chemistry within Ceramic Matrixes: Doped Sol-Gel Materials.* Accounts of Chemical Research, 1995. **28**(8): p. 328-334.

248. Dave, B.C., et al., *Sol-gel encapsulation methods for biosensors.* Analytical Chemistry, 1994. **66**(22): p. 1120A-1127A.

249. Lin, J. and C.W. Brown, *Sol-gel glass as a matrix for chemical and biochemical sensing.* TrAC Trends in Analytical Chemistry, 1997. **16**(4): p. 200-211.

250. Vallet-Regí, M., A.J. Salinas, and D. Arcos, *From the bioactive glasses to the star gels.* Journal of Materials Science: Materials in Medicine, 2006. **17**(11): p. 1011-1017.

251. Nam, K.-H., et al., *Condensation reaction of 3-(methacryloxypropyl)-trimethoxysilane and diisobutylsilanediol in non-hydrolytic sol-gel process.* Journal of Sol-Gel Science and Technology, 2006. **39**(3): p. 255-260.
252. Sanchez, C., et al., *Applications of hybrid organic-inorganic nanocomposites.* Journal of Materials Chemistry, 2005. **15**(35-36): p. 3559-3592.
253. Schottner, G., *Hybrid Sol−Gel-Derived Polymers: Applications of Multifunctional Materials.* Chemistry of Materials, 2001. **13**(10): p. 3422-3435.
254. Glad, M., et al., *Use of silane monomers for molecular imprinting and enzyme entrapment in polysiloxane-coated porous silica.* Journal of Chromatography A, 1985. **347**: p. 11-23.
255. Mahltig, B. and H. Böttcher, *Modified Silica Sol Coatings for Water-Repellent Textiles.* Journal of Sol-Gel Science and Technology, 2003. **27**(1): p. 43-52.
256. Gill, I., *Bio-doped Nanocomposite Polymers: Sol−Gel Bioencapsulates.* Chemistry of Materials, 2001. **13**(10): p. 3404-3421.
257. Sharp, K.G., *Star alkoxysilane molecules, gels and appreciably tough glasses.* Journal of Materials Chemistry, 2005. **15**(35-36): p. 3812-3820.
258. Textor, T. and B. Mahltig, *A sol–gel based surface treatment for preparation of water repellent antistatic textiles.* Applied Surface Science, 2010. **256**(6): p. 1668-1674.
259. Vilčnik, A., et al., *Structural Properties and Antibacterial Effects of Hydrophobic and Oleophobic Sol−Gel Coatings for Cotton Fabrics.* Langmuir, 2009. **25**(10): p. 5869-5880.
260. Sripanyakorn, S., et al., *The silicon content of beer and its bioavailability in healthy volunteers.* British Journal of Nutrition, 2004. **91**(3): p. 403-409.
261. Zhang, E., et al., *Microstructure, mechanical properties and bio-corrosion properties of Mg–Si (–Ca, Zn) alloy for biomedical application.* Acta biomaterialia, 2010. **6**(5): p. 1756-1762.
262. LeVier, R.R., *Distribution of silicon in the adult rat and rhesus monkey.* Bioinorganic Chemistry, 1975. **4**(2): p. 109-115.
263. Najda, J., J. Gmiński, and M. Dróżdż, *The action of excessive, inorganic silicon (Si) on the mineral metabolism of calcium (Ca) and magnesium (Mg).* Biological trace element research, 1993. **37**(2): p. 107-114.
264. Seaborn, C.D. and F.H. Nielsen, *Effects of germanium and silicon on bone mineralization.* Biological trace element research, 1994. **42**(2): p. 151-164.
265. Seaborn, C. and F. Nielsen, *Dietary silicon and arginine affect mineral element composition of rat femur and vertebra.* Biological trace element research, 2002. **89**(3): p. 239-250.
266. Wu, C., et al., *Porous akermanite scaffolds for bone tissue engineering: preparation, characterization, and in vitro studies.* Journal of Biomedical Materials Research Part B: Applied Biomaterials: An Official Journal of The Society for Biomaterials, The Japanese Society for Biomaterials, and The Australian Society for Biomaterials and the Korean Society for Biomaterials, 2006. **78**(1): p. 47-55.
267. Wu, C., et al., *Incorporation of titanium into calcium silicate improved their chemical stability and biological properties.* Journal of Biomedical Materials Research Part A: An Official Journal of The Society for Biomaterials, The Japanese Society for Biomaterials, and The Australian Society for Biomaterials and the Korean Society for Biomaterials, 2008. **86**(2): p. 402-410.
268. Hench, L.L., *Bioceramics: from concept to clinic.* Journal of the american ceramic society, 1991. **74**(7): p. 1487-1510.
269. Pietak, A.M., et al., *Silicon substitution in the calcium phosphate bioceramics.* Biomaterials, 2007. **28**(28): p. 4023-4032.
270. Honda, M., et al., *Cell proliferation, morphology and differentiation of transgenic-cloned pig calvarial osteoblasts on the silicon-substituted hydorxyapatite ceramics fabricated via ultrasonic spray-pyrolysis technique.* Journal of the Australian Ceramic Society, 2011. **47**(1): p. 37-41.
271. Vallet-Regí, M. and D. Arcos, *Silicon substituted hydroxyapatites. A method to upgrade calcium phosphate based implants.* Journal of Materials chemistry, 2005. **15**(15): p. 1509-1516.
272. Reid, J., et al., *Phase formation and evolution in the silicon substituted tricalcium phosphate/apatite system.* Biomaterials, 2005. **26**(16): p. 2887-2897.

273. Gomes, P.S., et al., *Evaluation of human osteoblastic cell response to plasma-sprayed silicon-substituted hydroxyapatite coatings over titanium substrates.* Journal of Biomedical Materials Research Part B: Applied Biomaterials, 2010. **94**(2): p. 337-346.
274. Hahn, B.-D., et al., *Aerosol deposition of silicon-substituted hydroxyapatite coatings for biomedical applications.* Thin Solid Films, 2010. **518**(8): p. 2194-2199.
275. Arcos, D. and M. Vallet-Regí, *Sol–gel silica-based biomaterials and bone tissue regeneration.* Acta biomaterialia, 2010. **6**(8): p. 2874-2888.
276. Boyer, L., J. Carpena, and J. Lacout, *Synthesis of phosphate-silicate apatites at atmospheric pressure.* Solid State Ionics, 1997. **95**(1-2): p. 121-129.
277. Reid, J.W., et al., *Synthesis and characterization of single-phase silicon-substituted α-tricalcium phosphate.* Biomaterials, 2006. **27**(15): p. 2916-2925.
278. Tang, X.L., X.F. Xiao, and R.F. Liu, *Structural characterization of silicon-substituted hydroxyapatite synthesized by a hydrothermal method.* Materials Letters, 2005. **59**(29-30): p. 3841-3846.
279. Patel, N., et al., *A comparative study on the in vivo behavior of hydroxyapatite and silicon substituted hydroxyapatite granules.* Journal of Materials Science: Materials in Medicine, 2002. **13**(12): p. 1199-1206.
280. Sadjadi, M., et al., *Silica enhanced formation of hydroxyapatite nanocrystals in simulated body fluid (SBF) at 37 C.* Materials Chemistry and Physics, 2011. **130**(1-2): p. 67-71.
281. Leroux, T., B. Perez-Ordonez, and H.P. von Schroeder, *Osteolysis after the use of a silicon-stabilized tricalcium phosphate-based bone substitute in a radius fracture: a case report.* The Journal of hand surgery, 2007. **32**(4): p. 497-500.
282. Itatani, K., et al., *Effect of colloidal silica addition on the formation of porous spherical α-calcium orthophosphate agglomerates by spray pyrolysis technique.* Journal of the ceramic society of japan, 2009. **117**(1363): p. 363-368.
283. Komlev, V., et al., *Single-phase bone cement based on dicalcium phosphate dihydrate powder and sodium silicate solution.* Materials Letters, 2012. **73**: p. 115-118.
284. Su, J.-C., et al., *Study on Preparation and Properties of Self-setting Silicon Hydroxyapatite Bone Cement.* Journal of Inorganic Materials, 2011. **26**(1): p. 55-60.
285. Cao, L.-H., et al., *Study on Adulterate Sodium Silica Apatite Cement Porous Scaffolds for Bone Defect Repair.* Journal of Inorganic Materials, 2011. **26**(6): p. 591-596.
286. Morejón-Alonso, L., R.G. Carrodeguas, and L.A.d. Santos, *Effects of silica addition on the chemical, mechanical and biological properties of a new α-Tricalcium Phosphate/Tricalcium Silicate Cement.* Materials Research, 2011. **14**: p. 475-482.
287. Qian, G., et al., *Promoting bone regeneration of calcium phosphate cement by addition of PLGA microspheres and zinc silicate via synergistic effect of in-situ pore generation, bioactive ion stimulation and macrophage immunomodulation.* Applied Materials Today, 2020. **19**: p. 100615.
288. Anitha, A., et al., *Bioinspired Composite Matrix Containing Hydroxyapatite-Silica Core-Shell Nanorods for Bone Tissue Engineering.* ACS Appl Mater Interfaces, 2017. **9**(32): p. 26707-26718.
289. Motisuke, M., et al., *Apatite bone cement reinforced with calcium silicate fibers.* Journal of Materials Science: Materials in Medicine, 2014. **25**(10): p. 2357-2363.
290. Marovic, D., et al., *Effect of silanized nanosilica addition on remineralizing and mechanical properties of experimental composite materials with amorphous calcium phosphate.* Clinical oral investigations, 2014. **18**(3): p. 783-792.
291. Mehrafzoon, S., S. Hassanzadeh-Tabrizi, and A. Bigham, *Synthesis of nanoporous Baghdadite by a modified sol-gel method and its structural and controlled release properties.* Ceramics International, 2018. **44**(12): p. 13951-13958.
292. Pham, D.Q., et al., *Mechanical and chemical properties of Baghdadite coatings manufactured by atmospheric plasma spraying.* Surface and Coatings Technology, 2019. **378**.
293. Detsch, R., et al., *The resorption of nanocrystalline calcium phosphates by osteoclast-like cells.* Acta Biomaterialia, 2010. **6**(8): p. 3223-3233.
294. Theiss, F., et al., *Biocompatibility and resorption of a brushite calcium phosphate cement.* Biomaterials, 2005. **26**(21): p. 4383-4394.

295. Sheikh, Z., et al., *Mechanisms of in Vivo Degradation and Resorption of Calcium Phosphate Based Biomaterials.* Materials, 2015. **8**(11): p. 5430.
296. Alkhraisat, M., et al., *The effect of hyaluronic acid on brushite cement cohesion.* Acta biomaterialia, 2009. **5**(8): p. 3150-3156.
297. Barralet, J., L. Grover, and U. Gbureck, *Ionic modification of calcium phosphate cement viscosity. Part II: hypodermic injection and strength improvement of brushite cement.* Biomaterials, 2004. **25**(11): p. 2197-2203.
298. Bohner, M. and G. Baroud, *Injectability of calcium phosphate pastes.* Biomaterials, 2005. **26**(13): p. 1553-1563.
299. Pina, S., et al., *Influence of setting liquid composition and liquid-to-powder ratio on properties of a Mg-substituted calcium phosphate cement.* Acta Biomaterialia, 2009. **5**(4): p. 1233-1240.
300. Luo, J., H. Engqvist, and C. Persson, *A ready-to-use acidic, brushite-forming calcium phosphate cement.* Acta Biomaterialia, 2018. **81**: p. 304-314.
301. Tamimi-Mariño, F., et al., *Increase of the final setting time of brushite cements by using chondroitin 4-sulfate and silica gel.* Journal of Materials Science: Materials in Medicine, 2007. **18**(6): p. 1195-1201.
302. Meininger, S., et al., *Phytic acid as alternative setting retarder enhanced biological performance of dicalcium phosphate cement in vitro.* Scientific Reports, 2017. **7**(1): p. 558.
303. Engstrand, J., C. Persson, and H. Engqvist, *The effect of composition on mechanical properties of brushite cements.* Journal of the Mechanical Behavior of Biomedical Materials, 2014. **29**: p. 81-90.
304. Hofmann, M.P., et al., *High-strength resorbable brushite bone cement with controlled drug-releasing capabilities.* Acta Biomaterialia, 2009. **5**(1): p. 43-49.
305. Alkhraisat, M.H., et al., *Beta-tricalcium phosphate release from brushite cement surface.* Journal of Biomedical Materials Research Part A, 2008. **84A**(3): p. 710-717.
306. Mariño, F.T., et al., *Advantages of using glycolic acid as a retardant in a brushite forming cement.* Journal of Biomedical Materials Research Part B: Applied Biomaterials, 2007. **83B**(2): p. 571-579.
307. O'Neill, R., et al., *Critical review: Injectability of calcium phosphate pastes and cements.* Acta biomaterialia, 2017. **50**: p. 1-19.
308. Sheikh, Z., et al., *Biodegradable Materials for Bone Repair and Tissue Engineering Applications.* Materials, 2015. **8**(9): p. 5744-5794.
309. Bohner, M., *Reactivity of calcium phosphate cements.* Journal of Materials Chemistry, 2007. **17**(38): p. 3980-3986.
310. Bohner, M. and U. Gbureck, *Thermal reactions of brushite cements.* Journal of Biomedical Materials Research Part B-Applied Biomaterials, 2008. **84B**(2): p. 375-385.
311. Han, B., et al., *beta-TCP/MCPM-based premixed calcium phosphate cements.* Acta Biomaterialia, 2009. **5**(8): p. 3165-3177.
312. Zhang, Z., et al., *Acidic pH environment induces autophagy in osteoblasts.* Scientific Reports, 2017. **7**: p. 46161.
313. Chai, F., et al., *In vitro studies on the influence of precultural conditioning method on osteoblast reactions of a new type of injectable calcium cement material.* Journal of Biomedical Materials Research Part B: Applied Biomaterials, 2006. **77**(1): p. 104-113.
314. Jamshidi, P., et al., *Brushite cement additives inhibit attachment to cell culture beads.* Biotechnology and bioengineering, 2013. **110**(5): p. 1487-1494.
315. Hubbell, J.H. and S.M. Seltzer, *Tables of X-ray mass attenuation coefficients and mass energy-absorption coefficients 1 keV to 20 MeV for elements Z= 1 to 92 and 48 additional substances of dosimetric interest*. 1995, National Inst. of Standards and Technology-PL, Gaithersburg, MD (United States). Ionizing Radiation Div.
316. Aberg, J., et al., *In Vivo Evaluation of an Injectable Premixed Radiopaque Calcium Phosphate Cement.* International Journal of Biomaterials, 2011. **2011**.
317. Acarturk, O., et al., *Bone healing response to an injectable calcium phosphate cement with enhanced radiopacity.* Journal of Biomedical Materials Research Part B: Applied Biomaterials, 2008. **86**(1): p. 56-62.
318. Ginebra, M.P., et al., *Mechanical performance of acrylic bone cements containing different radiopacifying agents.* Biomaterials, 2002. **23**(8): p. 1873-1882.

319. Ginebra, M.-P., et al., *New processing approaches in calcium phosphate cements and their applications in regenerative medicine.* Acta biomaterialia, 2010. **6**(8): p. 2863-2873.
320. Bohner, M., et al., *Synthesis of spherical calcium phosphate particles for dental and orthopedic applications.* Biomatter, 2013. **3**(2): p. e25103.
321. Paul, W. and C. Sharma, *Development of porous spherical hydroxyapatite granules: application towards protein delivery.* Journal of Materials Science: Materials in Medicine, 1999. **10**(7): p. 383-388.
322. Bohner, M., *Calcium phosphate emulsions: possible applications.* Key Engineering Materials, 2001. **192**.
323. Moseke, C., et al., *Low temperature fabrication of spherical brushite granules by cement paste emulsion.* Journal of Materials Science: Materials in Medicine, 2012. **23**(11): p. 2631-2637.
324. Christel, T., et al., *Fabrication and cytocompatibility of spherical magnesium ammonium phosphate granules.* Materials Science and Engineering: C, 2014. **42**: p. 130-136.
325. Pina, S. and J.M. Ferreira, *Brushite-forming Mg-, Zn-and Sr-substituted bone cements for clinical applications.* Materials, 2010. **3**(1): p. 519-535.
326. Pina, S., et al., *Biological responses of brushite-forming Zn-and ZnSr-substituted beta-tricalcium phosphate bone cements.* Eur Cell Mater, 2010. **20**: p. 162-177.
327. Cabrejos-Azama, J., et al., *Magnesium substitution in brushite cements for enhanced bone tissue regeneration.* Materials Science and Engineering: C, 2014. **43**: p. 403-410.
328. Han, G., et al., *Development of calcium silicate/calcium phosphate cement for bone regeneration.* Biomedical Materials, 2007. **2**(3): p. S153.
329. Wilson, A.D. and J.W. Nicholson, *Acid-base cements: their biomedical and industrial applications*. Vol. 3. 2005: Cambridge University Press.
330. Luo, J., et al., *Compressive, diametral tensile and biaxial flexural strength of cutting-edge calcium phosphate cements.* Journal of the Mechanical Behavior of Biomedical Materials, 2016. **60**: p. 617-627.
331. Mah, P., T. Reeves, and W. McDavid, *Deriving Hounsfield units using grey levels in cone beam computed tomography.* Dentomaxillofacial Radiology, 2010. **39**(6): p. 323-335.
332. Schamel, M., et al., *In vitro ion adsorption and cytocompatibility of dicalcium phosphate ceramics.* Biomaterials research, 2017. **21**: p. 10-10.
333. No, Y.J., et al., *Effect of Baghdadite Substitution on the Physicochemical Properties of Brushite Cements.* Materials (Basel, Switzerland), 2019. **12**(10).
334. Mejdoub, R., et al., *The effect of prolonged mechanical activation duration on the reactivity of Portland cement: Effect of particle size and crystallinity changes.* Construction and Building Materials, 2017. **152**: p. 1041-1050.
335. Gbureck, U., M.P. Hofmann, and J.E. Barralet, *Thermal performance of mechanically activated tetracalcium phosphate.* Journal of the American Ceramic Society, 2005. **88**(5): p. 1327-1330.
336. Brueckner, T., et al., *Mechanical activation and cement formation of trimagnesium phosphate.* Journal of the American Ceramic Society, 2018. **101**(5): p. 1830-1834.
337. Jansen, D., et al., *Does Ordinary Portland Cement contain amorphous phase? A quantitative study using an external standard method.* Powder Diffraction, 2011. **26**(1): p. 31-38.
338. Hurle, K., et al., *Effect of amorphous phases during the hydraulic conversion of alpha-TCP into calcium-deficient hydroxyapatite.* Acta Biomaterialia, 2014. **10**(9): p. 3931-3941.
339. Kriskova, L., et al., *Hydraulic Behavior of Mechanically and Chemically Activated Synthetic Merwinite.* Journal of the American Ceramic Society, 2014. **97**(12): p. 3973-3981.
340. Gbureck, U., et al., *Nanocrystalline tetracalcium phosphate cement.* Journal of Dental Research, 2004. **83**(5): p. 425-428.
341. Gbureck, U., et al., *Antimicrobial potency of alkali ion substituted calcium phosphate cements.* Biomaterials, 2005. **26**(34): p. 6880-6886.
342. Richardson, I.G., *The calcium silicate hydrates.* Cement and Concrete Research, 2008. **38**(2): p. 137-158.
343. Beaudoin, J.J., L. Raki, and R. Alizadeh, *A 29Si MAS NMR study of modified C–S–H nanostructures.* Cement and Concrete Composites, 2009. **31**(8): p. 585-590.
344. Chen, J.J., et al., *Solubility and structure of calcium silicate hydrate.* Cement and Concrete Research, 2004. **34**(9): p. 1499-1519.

345. Cong, X. and R. James Kirkpatrick, *17O and 29Si MAS NMR study of β–C2S hydration and the structure of calcium-silicate hydrates.* Cement and Concrete Research, 1993. **23**(5): p. 1065-1077.
346. Parry-Jones, G., et al., *29Si MAS-NMR hydration and compressive strength study in cement paste.* Cement and Concrete Research, 1989. **19**(2): p. 228-234.
347. Rejmak, P., et al., *29Si NMR in Cement: A Theoretical Study on Calcium Silicate Hydrates.* The Journal of Physical Chemistry C, 2012. **116**(17): p. 9755-9761.
348. Klur, I., et al. *C-S-H Structure Evolution with Calcium Content by Multinuclear NMR*. in *Nuclear Magnetic Resonance Spectroscopy of Cement-Based Materials*. 1998. Berlin, Heidelberg: Springer Berlin Heidelberg.
349. Cong, X. and R.J. Kirkpatrick, *29Si MAS NMR study of the structure of calcium silicate hydrate.* Advanced Cement Based Materials, 1996. **3**(3): p. 144-156.
350. Okada, Y., H. Ishida, and T. Mitsuda, *29Si NMR Spectroscopy of Silicate Anions in Hydrothermally Formed C-S-H.* Journal of the American Ceramic Society, 1994. **77**(3): p. 765-768.
351. Richardson, I.G., *The nature of C-S-H in hardened cements.* Cement and Concrete Research, 1999. **29**(8): p. 1131-1147.
352. Brough, A.R., et al., *Application of Selective 29Si Isotopic Enrichment to Studies of the Structure of Calcium Silicate Hydrate (C-S-H) Gels.* Journal of the American Ceramic Society, 1994. **77**(2): p. 593-596.
353. Seifert, A., et al., *Morphological Control of Freeze-Structured Scaffolds by Selective Temperature and Material Control in the Ice-Templating Process.* Advanced Engineering Materials, 2021.
354. Seifert, A., et al., *Phase Conversion of Ice-Templated α-Tricalcium Phosphate Scaffolds into Low-Temperature Calcium Phosphates with Anisotropic Open Porosity.* Advanced Engineering Materials, 2021. **23**(5): p. 2001417.
355. Brunette, D., *Spreading and orientation of epithelial cells on grooved substrata.* Experimental cell research, 1986. **167**(1): p. 203-217.
356. Wang, J.H.-C., et al., *Alignment and proliferation of MC3T3-E1 osteoblasts in microgrooved silicone substrata subjected to cyclic stretching.* Journal of Biomechanics, 2000. **33**(6): p. 729-735.
357. Monsees, T.K., et al., *Effects of different titanium alloys and nanosize surface patterning on adhesion, differentiation, and orientation of osteoblast-like cells.* Cells Tissues Organs, 2005. **180**(2): p. 81-95.
358. Green, A.M., et al., *Fibroblast response to microtextured silicone surfaces: texture orientation into or out of the surface.* Journal of biomedical materials research, 1994. **28**(5): p. 647-653.
359. Walboomers, X., et al., *Growth behavior of fibroblasts on microgrooved polystyrene.* Biomaterials, 1998. **19**(20): p. 1861-1868.
360. Matsuzaka, K., et al., *Effect of microgrooved poly-l-lactic (PLA) surfaces on proliferation, cytoskeletal organization, and mineralized matrix formation of rat bone marrow cells.* Clinical oral implants research, 2000. **11**(4): p. 325-333.
361. Schmidt, J. and A. Von Recum, *Texturing of polymer surfaces at the cellular level.* Biomaterials, 1991. **12**(4): p. 385-389.
362. Christel, T., et al., *Dual setting alpha-tricalcium phosphate cements.* J Mater Sci Mater Med, 2013. **24**(3): p. 573-81.
363. Schamel, M., J. Groll, and U. Gbureck, *Simultaneous formation and mineralization of star-P(EO-stat-PO) hydrogels.* Mater Sci Eng C Mater Biol Appl, 2017. **75**: p. 471-477.
364. Geffers, M., et al., *Dual-setting brushite–silica gel cements.* Acta Biomaterialia, 2015. **11**: p. 467-476.
365. Siepmann, J. and N.A. Peppas, *Modeling of drug release from delivery systems based on hydroxypropyl methylcellulose (HPMC).* Advanced drug delivery reviews, 2012. **64**: p. 163-174.
366. Vorndran, E., et al., *3D powder printing of β-tricalcium phosphate ceramics using different strategies.* Advanced Engineering Materials, 2008. **10**(12): p. B67-B71.
367. Peters, F., et al., *Comparative study of patient individual implants from β-tricalcium phosphate made by different techniques based on CT data.* Materialwissenschaft und Werkstofftechnik:

Entwicklung, Fertigung, Prüfung, Eigenschaften und Anwendungen technischer Werkstoffe, 2006. **37**(6): p. 457-461.

Chapter 10 Appendix

10.1 List of Figures

10.2 List of Tables

10.3 List of Publications

- Holzmeister I.; Schamel M.; Gbureck U.; Vorndran E. *Acta Biomaterialia* **2018**, 74, 17-35.

- No Y.J.; Holzmeister I.; Lu Z.; Prajapati S.; Shi J.; Gbureck U.; Zreiqat H. *Materials* **2019**, 12, 1719.

- Holzmeister I.; Weichhold J.; Groll J.; Zreiqat H.; Gbureck U. *Journal of the American Ceramic Society* **2021**, 104, 3554-3561.

Danksagung

An dieser Stelle möchte ich mich bei den Personen bedanken, die zum Gelingen dieser Arbeit beigetragen haben und mit denen ich dieses Kapitel in meinem Leben gestalten durfte.

Herrn Prof. Dr. Uwe Gbureck danke ich für die Möglichkeit, meine Dissertation am Lehrstuhl für Funktionswerkstoffe der Medizin und Zahnheilkunde durchzuführen. Danke, Uwe, dass du mich in deine Arbeitsgruppe aufgenommen hast. Danke für deine Betreuung und für deine motivierenden Worte. Danke für deine Geduld und Geselligkeit. Ich freue mich schon auf die Tage, wenn wir uns wiedersehen.

Herrn Prof. Dr. Jürgen Groll möchte ich für all die Chancen danken, die durch seine Leitung am FMZ möglich gemacht werden. Danke für die fachliche Expertise und die persönliche Entwicklungsmöglichkeit. Sei es durch den Prozess der Promotion selbst oder Kommunikationsseminare.

Herrn Prof. Dr. Torsten Blunk danke ich für die Begutachtung meiner Dissertation.

Bei Jörg und Andrea möchte ich mich dafür bedanken, dass ich jederzeit an deren Türe klopfen konnte um mir Rat zu holen.

Ein herzliches Dankeschön geht an Tanja und Birgit für eure Unterstützung bei allem Organisatorischen. Mit welchem Anliegen ich auch zu euch gekommen bin, ihr habt mich immer mit einem Lächeln empfangen, das sich durch eure freundlichen Wesen stets auf mich übertragen hat.

Im Zuge dessen möchte ich Isabell meinen Dank aussprechen. Du bist immer bereit mit Rat und Tat zu helfen oder mit ein paar flotten Sprüchen dem Arbeitsklima gut zu tun.

Auch Harald und Toni möchte ich für ihre kompetente Hilfe in den unterschiedlichsten Situationen danken. Ihr findet einfach immer eine Lösung für jedes Problem.

Außerdem danke ich dem gesamten FMZ. Es war angenehm dort zusammen mit den vielen verschiedenen Kollegen arbeiten zu dürfen. Das Institut war ein kollegiales und schönes Umfeld an das ich mich immer gerne erinnern werde. Danke an Csaba, Franzi, Ilona, Jessi, Johanna, Jun, Leo, Manuel, Matze, Michael, Moataz, Philipp und Sandra für eine schöne Zeit.

Bei den „Zementies“ möchte ich mich herzlich bedanken. Auch wenn die Konstellation mit Studenten und Praktikanten variierte, blieb das miteinander stets harmonisch. Danke Annika, für die gemeinsame Zeit am FMZ die wir seit der Masterarbeit hatten.

Mein besonderer Dank geht and die Bürokollegen, Jan und Friederike. Für die schöne Zeit in der wir uns kennengelernt haben und zu Freunden wurden und für die gemeinsamen Stunden auch außerhalb des Instituts. Danke Friederike für dein offenes Ohr, auch wenn mal keine Kaffeepause eingeplant war. Und Jan, ich danke dir für den Einklang zwischen uns. Ob wir uns wortlos zunicken oder viel erzählen, ich fühle mich von dir verstanden.

Bei Flo möchte ich mich für mehr als nur eine gute Zeit bedanken, denn ohne dich wäre ich niemals an diesen Lehrstuhl gekommen. Die entstandene Routine zur Mittagspause war einmalig und deine Art Gespräche zu führen beflügelte unsere Diskussionen jedes Mal. Du bist für mich ein Vorbild und ich möchte dich daher zitieren: „Danke dir, dass du dazu beigetragen hast, meine Zeit am FMZ noch um ein Erhebliches schöner zu gestalten!“

Ein paar wunderbare Menschen, die mich seit dem Studium und/oder darüber hinaus begleitet haben möchte ich an dieser Stelle noch nennen. In den unterschiedlichsten Situationen haben sie mich motiviert und inspiriert. Sei es bei Sport, auf Reisen, tiefgründigen Gesprächen oder durch andere Lebensweisheiten; Danke Pasu, Sebbie, Frani, Franzi, Agnes, Alina, Brian, Loew, Kiki und Loris.

Abschließend möchte ich mich bei meiner Familie bedanken, die es stets gut mit mir meint und mich unterstützt. Danke Phil für deine Hilfe bei allen Fragen die ich so habe. Es macht mich stolz dich als meinen Bruder zu haben. Danke Mama und Papa, dass ihr mir das Studium ermöglicht habt und immer für mich da seid.